

TECHNISCHE UNIVERSITÄT MÜNCHEN

Lehrstuhl II für Technische Chemie

## **Reductive cleavage of aromatic ethers by supported metal catalysts**

Meng Wang

Vollständiger Abdruck der von der Fakultät für Chemie der Technischen Universität  
München zur Erlangung des akademischen Grades eines

**Doktors der Naturwissenschaften (Dr. rer. nat.)**

genehmigten Dissertation.

Vorsitzender: Univ.-Prof. Dr. Tom Nilges

Prüfer der Dissertation:

1. Univ.-Prof. Dr. techn. Johannes A. Lercher
2. Prof. Ph.D. Gary L. Haller (Yale University, New Haven, CT, USA)
3. Univ.-Prof. Dr. Roland A. Fischer

Die Dissertation wurde am 07.08.2018 bei der Technischen Universität München eingereicht  
und durch die Fakultät für Chemie am 10.09.2018 angenommen.

大哉一诚天下动，如鼎三足兮，曰知、曰仁、曰勇。

— 江谦 (1876—1942)

*The good I stand on is my truth and honesty.*

— *William Shakespeare (1564 — 1616)*

*'Henry VIII', Act 5, Scene 1*



## Acknowledgement

First and foremost I would like to express my sincerest appreciation to my thesis advisor, Prof. Johannes A. Lercher, for offering me the opportunity to work in his group and the endless support throughout my Ph.D., especially for a Chinese student who is working in the US and getting the degree from Germany. I am incredibly fortunate to have been able to work at the Pacific Northwest National Laboratory (PNNL) and enlightened by his guidance, patience, trust and profound knowledge. Being a “stubborn” student, I gained a lot of knowledge from our invaluable scientific group discussion that will help both my scientific and personal growth.

I would also like to express my deep appreciation to my mentor Dr. Donald M. Camaioni for guiding me to think and work scientifically and efficiently in PNNL. He is the best go to person I ever had and his thoughtful guidance, warm encouragement and high degree of attention to even the smallest details helped my growth in research. I am greatly grateful for the time and efforts Don has spent to coach me. Then I would like to express a sincere gratitude to my mentor Dr. Oliver Y. Gutierrez for the discussions we had, and for the suggestions he gave me. Thank you for your uncountable assistance in the laboratory and my graduation.

I am deeply grateful to Prof. Mirosław A. Derewinski for his suggestions, encouragement and unfailing assistance in a variety of ways not only about science. I am full of gratitude to John Fulton, with whom I learned XAFS (X-ray absorption fine structure) during our APS (Advanced Photon Source) trips and data analysis. Don, Mirek, John and Oliver have broadened my horizons in and outside the lab and let me have an enriched life in the Pacific Northwest.

My heartfelt gratitude to Dr. Jian Zhi Hu for his kind guidance and assistance, the resources I have got and the discussions we have made helped me know the lab regulations and understand how to efficiently make use of characterizations for catalysis. I deeply appreciate the help of Dr. Donghai Mei and his students, Zhibo Ren and Yuntao Zhao, about the theoretical calculations. My sincere thanks go to Dr. John Linehan and Dr. Sarah Burton for their valuable advice and great help. I am also utmost grateful to the people at PNNL who helped me in the field of catalysis and characterization. Especially, the great help of Dr. Abhi Karkamkar, Dr. Mark Bowden, Dr. Molly O’Hagan and Dr. Libor Kovarik is highly appreciated. I am also

incredibly grateful to Dr. Wendy Shaw and Dr. Aaron Appel, who were my managers at PNNL, as well as to the PNNL administrative staff.

Next, I would like to thank my lab mates Dr. Hui Shi, Dr. Zizwe Chase, Dr. Aleksei Vjunov, Dr. Sebastian Proding, Dr. Jian Zheng and Dr. Feng Chen who have always supported me during my research. Especially the extensive help from Hui Shi at the beginning of my study. My sincere appreciation also goes to Dr. Nianhua Xue, Dr. Yifeng Zhu, Dr. Bo Peng, Dr. Manish Shetty, Dr. Udishnu Sanyal, Dr. Katherine Koh, Laura Meyer, thank all of you for your kind help not only in science.

Furthermore, I would like to thank our senior scientists and administrative staff in TCII at TUM, Prof. Andreas Jentys, Dr. Yue Liu, Stefanie Seibold, Kateryna Kryvko, Bettina Federmann and Ulrike Sanwald, who all helped me for my stay at TUM. Moreover, I would like to thank all following colleagues in TUM, Dr. Yuanshuai Liu, Xi Chen, Guanhua Cheng, Takaaki Ikuno, Insu Lee, Wanqiu Luo, Ferdinand Vogelgsang, Manuel Wagenhofer, Yang Zhang and Ruixue Zhao. Thank you for your support and help.

Particularly, I would like to thank Prof. Gary L. Haller for the help on my thesis.

Finally, I am great indebted to my family, relatives and friends who loved me and I loved. Especially thank my wife Huifang for building our life together and thank our parents' endless support.

Meng Wang

July 2018.

**Abstract**

The catalytic hydrolysis and hydrogenolysis of aromatic ethers have been explored on supported metal catalysts. Palladium is highly selective for reductive hydrolysis and transesterification in water and alcohols, respectively. Partial hydrogenation of one aromatic ring prior to the insertion of H<sub>2</sub>O or alcohol has been identified. Kinetic analysis suggests that hydrogenolysis is catalyzed via a (concerted) addition of hydrogen, cleavage of the C-O bond and formation of a phenoxy group, the critical step has being aided by a strong interaction of the ether oxygen with the metal.

**Kurzzusammenfassung**

Die katalytische Hydrolyse und Hydrogenolyse von aromatischen Ethern wurden an geträgerten Metallkatalysatoren untersucht. Palladium ist hochselektiv für die reduktive Hydrolyse bzw. Umätherung in Wasser und Alkoholen. Die partielle Hydrierung eines aromatischen Rings vor dem Einbringen von H<sub>2</sub>O oder Alkohol wurde identifiziert. Die kinetische Analyse deutet, dass die Hydrogenolyse durch (konzertierte) Zugabe von Wasserstoff, Spaltung der C-O-Bindung und Bildung einer Phenoxygruppe katalysiert wird. Der geschwindigkeitsbestimmende Schritt wird durch eine starke Wechselwirkung des Äthersauerstoffs mit dem Metall unterstützt.





## Table of Contents

Acknowledgement .....	i
Abstract .....	iii
Kurzzusammenfassung .....	iii
Table of Contents .....	v
<b>Chapter 1 Introduction</b> .....	<b>1</b>
1.1 General background .....	2
1.2 Importance of the cleavage of aromatic C-O bonds .....	5
1.2.1 Depolymerization of lignin .....	5
1.2.2 Activation of carbon oxygen bond .....	8
1.3 Reaction routes of reductive conversion of aryl ethers .....	9
1.3.1 Hydrogenolysis .....	11
1.3.2 Hydrolysis .....	14
1.3.3 Hydrogenation .....	15
1.3.4 Reactions of phenols .....	16
1.4 Mechanistic studies .....	20
1.5 Scope of this thesis .....	22
1.6 References .....	24
<b>Chapter 2 Palladium Catalyzed Hydrolytic Cleavage of Aromatic C-O Bonds</b> .....	<b>29</b>
2.1 Introduction .....	30
2.2 Experimental .....	31
2.2.1 Chemicals and commercial catalysts .....	31
2.2.2 Catalyst testing .....	31
2.3 Result and discussion .....	32
2.3.1 Kinetic studies of supported palladium catalysts .....	32

2.3.2 Control experiments of 1-phenoxy cyclohexene.....	37
2.3.3 Hypothesis of the reaction mechanism of reductive hydrolysis.....	38
2.3.4 Isotope labelling experiments by H <sub>2</sub> <sup>18</sup> O.....	39
2.4 Conclusions.....	42
2.5 Acknowledgements.....	43
2.6 Appendix.....	43
2.6.1 Derivation of rate equations .....	43
2.7 References.....	47
<b>Chapter 3 Palladium Catalyzed Reductive Insertion of Alcohols in Aryl Ether Bonds</b> .....	<b>49</b>
3.1 Introduction.....	50
3.2 Experimental .....	51
3.2.1 Chemicals and commercial catalysts .....	51
3.2.2 Catalyst testing.....	52
3.3 Result and discussion.....	52
3.3.1 Reactions of diphenyl ether and related compounds on Pd/C in methanol.....	52
3.3.2 Control experiments for 1-phenoxy cyclohexene .....	56
3.3.3 Control experiments for cyclohexanone .....	58
3.3.4 Reaction of higher alcohols and other ethers .....	60
3.4 Conclusions.....	62
3.5 Acknowledgements.....	63
3.6 Appendix.....	63
3.6.1 Equilibrium between cyclohexanone, methoxycyclohexene and dimethoxycyclohexane ..	63
3.7 References.....	64
<b>Chapter 4 Mechanistic Studies of Hydrogenolysis of Aryl Ethers Catalyzed by Nickel Nanoparticles</b> .....	<b>66</b>
4.1 Introduction.....	67
4.2 Experimental .....	67

---

4.2.1 Chemicals and commercial catalysts .....	67
4.2.2 Catalyst tests .....	68
4.2.3 DFT calculations .....	68
4.3 Result and discussion .....	69
4.3.1 Reactions of diphenyl ether over Ni catalyst in water and decalin .....	69
4.3.2 Isotopic experiments of diphenyl ether .....	75
4.3.3 Comparison between diphenyl ether and benzyl phenyl ether .....	78
4.3.4 Hypothesis for reaction mechanism of hydrogenolysis and DFT calculations .....	81
4.4 Conclusions .....	84
4.5 Acknowledgements .....	84
4.6 Appendix .....	84
4.6.1 Analysis of D incorporation in the chemicals by MS .....	84
4.6.2 Derivation of rate equations .....	85
4.6.3 Discussion about diffusion limitation .....	87
4.7 References .....	89
<b>Chapter 5 Catalytic Reductive Cleavage of Diphenyl Ether over Noble Metal Catalysts .....</b>	<b>91</b>
5.1 Introduction .....	92
5.2 Experimental .....	94
5.2.1 Chemicals and commercial catalysts .....	94
5.2.2 Catalyst tests .....	94
5.2.3 Catalyst characterizations .....	95
5.3 Result and discussion .....	95
5.3.1 Reactions in decalin .....	95
5.3.2 Reactions in water .....	100
5.3.3 Discussion .....	104
5.4 Conclusions .....	105
5.5 Acknowledgements .....	106

5.6 Appendix.....	106
5.6.1 Particle size and dispersion of supported metal nanoparticles.....	106
5.6.2 Reaction details in decalin .....	108
5.6.2 Reaction details in water .....	112
5.7 References.....	116
<b>Chapter 6 Summary.....</b>	<b>119</b>
Curriculum Vitae .....	122
List of Publications .....	123
List of Presentations.....	126
Contribution of collaborators .....	127

## **Chapter 1 Introduction**

## 1.1 General background

Primary energy, energy in nature that has not been subjected to any human engineered conversion or transformation process, can be non-renewable or renewable. Non-renewable energy resources do not renew themselves at sufficient rates for sustainable extraction in meaningful human time-frames, such as fossil fuels (coal, petroleum, natural gas). These are also called finite resources. Renewable energy, in contrast, is naturally replenished on a human timescale, such as sunlight, wind, rain, biomass and geothermal heat. Figure 1-1 shows the source of primary energy production in the US from 1949 to 2017. Fossil fuels still dominates the prime energy sources nowadays, while the production of renewable energy kept increasing in the past 50 years.<sup>1</sup>

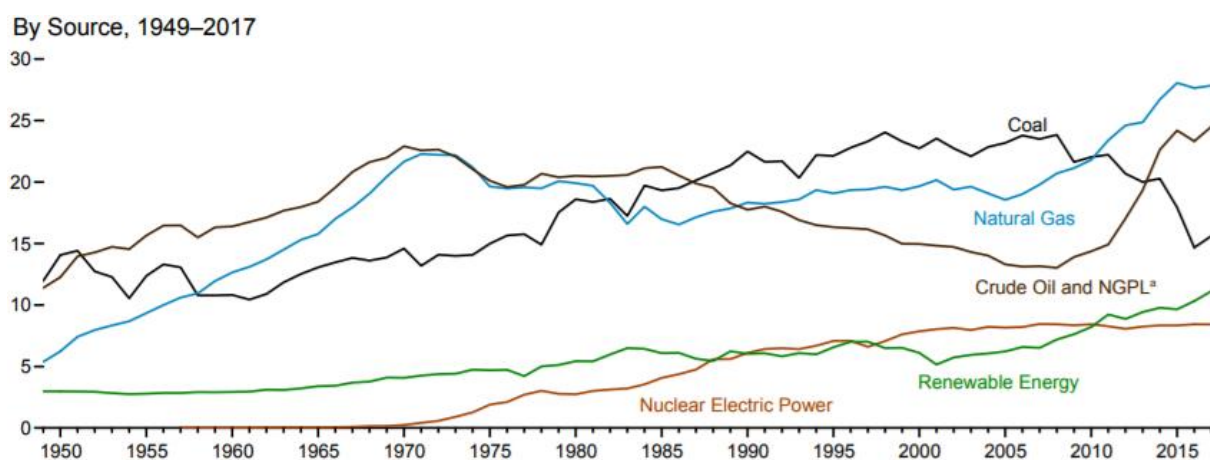


**Figure 1-1. Primary energy production (Quadrillion BTU) of the US.**

Source: U.S. Energy Information Administration (Monthly Energy Review April 2018)<sup>1</sup>

Due to the growth of global economy and population, restricted fossil fuels (finite resources) will not meet the needs of the world's energy growth. Renewable energy from clean sources, with low environmental impact, will be much more important in the future. According to the World Energy Outlook of 2017 (Figure 1-2)<sup>2</sup> from the International Renewable Energy Agency, renewables capture two-thirds of global investment in power plants to 2040 as they become, for many countries, the least-cost source of new generation. The Energy Roadmap for 2050 from the European Commission also indicates that renewable energy will have a very high share in gross final energy consumption (75 % in 2050) and in electricity consumption (reaching 97 % in 2050).<sup>3</sup> The Annual Energy Outlook 2018 from the U.S. Energy Information Administration gave the renewable growth projections of 1.78 billion metric tons in 2050.<sup>4</sup>

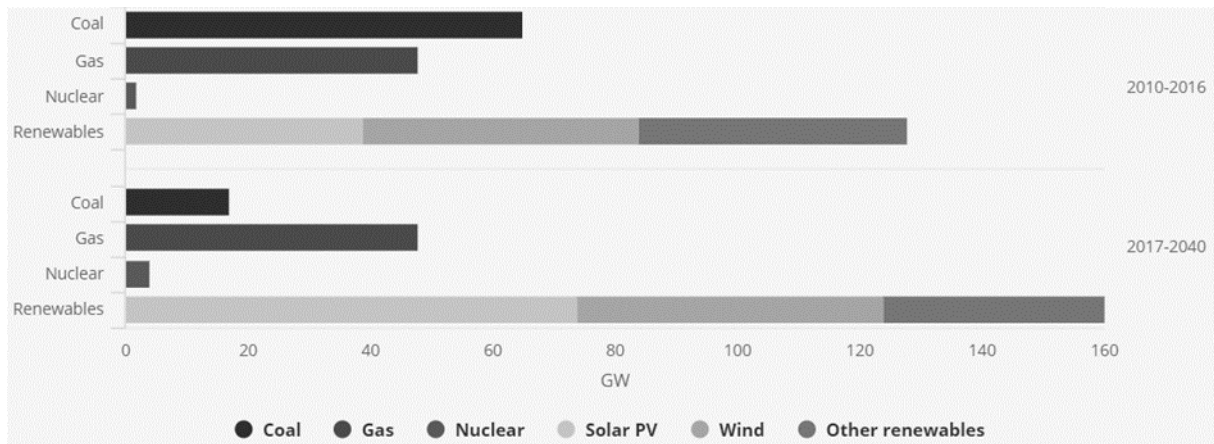


**Figure 1-2. Global average annual net capacity additions by type.**

Source: International Renewable Energy Agency (World Energy Outlook 2017).<sup>2</sup>

Renewable energies are continually replenished by nature and derived directly (such as thermal, photo-chemical, and photo-electric) or indirectly (such as wind, hydropower, and photosynthetic energy stored in biomass) from the sun, or from other natural movements and mechanisms of the environment (such as geothermal and tidal energy).<sup>5</sup> These natural energy sources are turned into usable forms of energy, such as electricity, heat and fuels, by renewable energy technologies.<sup>6</sup> Biomass, the term used for all organic material originating from plants, trees and crops, is one of the main sources of renewable energy (Figure 1-3). It will be the key to the energy transition until 2030 and beyond, especially for applications that are not easily converted to electricity or other technologies in the short and medium term (e.g. high temperature processes in industry, advanced biofuels for road freight, etc.).<sup>7</sup>

**Major Sources, 1949–2017**

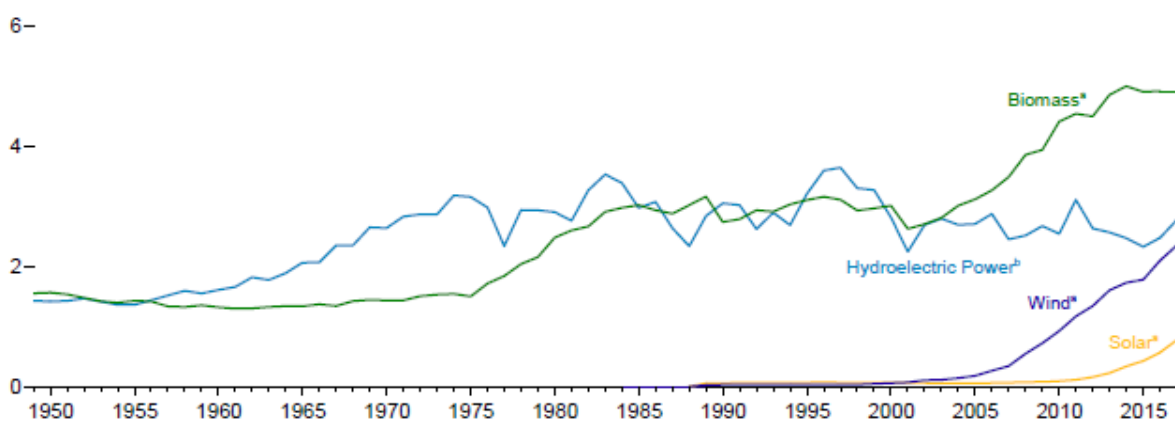


**Figure 1-3. Renewable Energy Consumption of the US (Quadrillion Btu)**

Source: U.S. Energy Information Administration (Annual Energy Outlook 2018).<sup>4</sup>

In addition to the many benefits of renewable energy, biomass is particularly attractive because it is the only current renewable source of liquid transportation fuel, and the only renewable organic carbon

resource in nature which gives it unique advantage in producing value-added products.<sup>8-9</sup> The ideal biomass growth and manufacturing scheme is shown in Figure 1-4. The inputs for biofuel production are CO<sub>2</sub>, H<sub>2</sub>O, light, air, and nutrients. And the outputs are energy to power transportation vehicles and food. The three main technologies necessary for a carbohydrate economy are (1) growth of the biomass feedstock, (2) biomass conversion into fuel, and (3) fuel utilization. We will focus on the conversion of biomass.

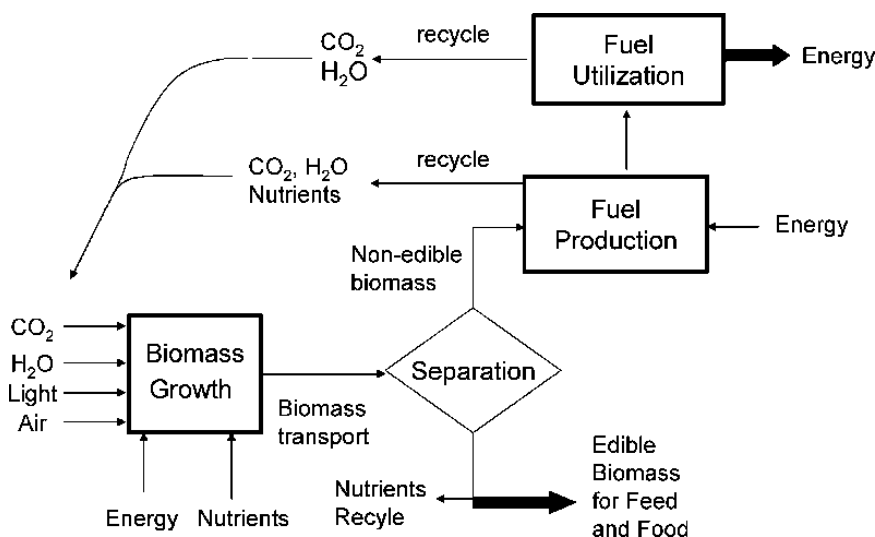


**Figure 1-4. Sustainable production of transportation fuels from biomass in an integrated biomass production-conversion system.<sup>8</sup> (Reprinted with permission from reference 8. Copyright © 2006, American Chemical Society.)**

Lignocellulosic biomass is composed of three main fractions, as shown in Figure 1-5, cellulose (comprises 40 – 80 % of lignocellulosic biomass feedstock), hemicellulose (15 – 30 %), and lignin (10 – 25 %).<sup>10-11</sup> Cellulose consists of a linear polysaccharide with  $\beta$ -1,4 linkages of D-glucopyranose monomers, and the degree of polymerization of cellulose is approximately 10000 to 15000 glucopyranose monomer units in wood and cotton, respectively.<sup>8, 12</sup> Unlike cellulose, hemicellulose is a polymer of five different sugars.<sup>12</sup> Since cellulose and hemicellulose have been studied for a long time, well-rounded utilization technologies have been industrially applied for the production of biofuels and important chemicals from these sources.<sup>12-17</sup> Lignin is a highly branched, substituted, mononuclear aromatic polymer found in the cell walls, and the structure and composition of lignin depend strongly on the type of biomass and even on the part of the plant, so they are relatively intractable.<sup>18</sup> Nowadays, only 5% of lignin is used in low-value commercial applications, as a low-grade fuel for heat and power applications, or as concrete additive, because direct use of lignin required long pressing time and high processing temperature due to its extremely low reactivity.<sup>18-19</sup> While over the last 20 -30 years, there has been an explosion of research into, and commercialization of, lignin-based products and processes which add significant value to the material that has been labelled as waste.<sup>20-22</sup> From an energy point of view, the depolymerization of lignin to aromatics as an alternative to the petrochemical industry is probably the most promising way to sustainable utilization of lignin.<sup>23</sup> With its unique structure and



chemical properties, a wide variety of bulk and fine chemicals, particularly aromatic compounds, are also potentially obtainable from lignin conversion.<sup>24-26</sup>

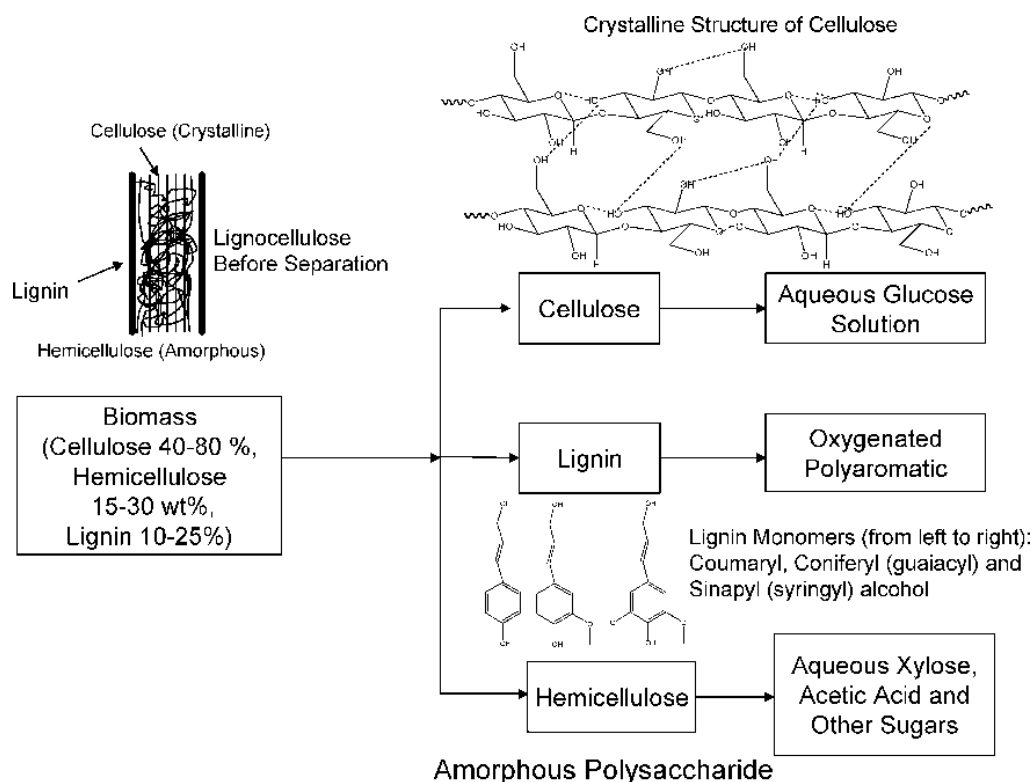


**Figure 1-5.** Structures of different biomass fractions (lignocellulose, cellulose, lignin and hemicellulose) before and after reactions.<sup>8</sup> (Reprinted with permission from reference 8. Copyright © 2006, American Chemical Society.)

## 1.2 Importance of the cleavage of aromatic C-O bonds

### 1.2.1 Depolymerization of lignin

Lignin is a class of amorphous tridimensional biopolymer built of three cinnamyl alcohol monomers: sinapyl alcohol (S), coniferyl alcohol (G) and p-coumaryl alcohol (H), which are linked via C-C and C-O bonds.<sup>26-27</sup> The units and a representative structure of lignin are shown in Figure 1-6. Because lignin contains much less oxygen than cellulose and hemicellulose, it is ideally a more promising feedstock for transformation.<sup>28-29</sup> The catalyzed conversion of lignin to alkane energy carriers requires a cascade of reactions for deconstructing and reducing the polymeric and highly oxyfunctionalized material. Through a variety of depolymerization treatments, *e.g.* pyrolysis, thermolysis, hydrogenolysis, gasification, hydrolysis and chemical oxidation, the monomer of aromatics and phenolics could be obtained by breaking the linkages between the building blocks.<sup>30</sup> Because lignin and the derived smaller structural units have high boiling points, significant energy input is required for catalytic upgrading in the gas phase. Thus, in order to depolymerize the structures and enable further upgrading at lower

temperatures, these transformations need to be conducted in the liquid phase. Basically, lignin consists of a variety of linkages irregularly connecting various aryl ethers, and the proportion of these linkages varies according to the type of wood, typically more than two-thirds of the linkages in lignin are ether linkages.<sup>31</sup> For example, birch, a kind of hardwood, the proportions of  $\beta$ -O-4-aryl ether,  $\alpha$ -O-4-aryl ether, 4-O-5-diaryl ether,  $\beta$ -5-phenylcoumaran, 5-5-biphenyl,  $\beta$ -1-(1,2-diarylpropane) and  $\beta$ - $\beta$ -(resinol) are 60 %, 6-8 %, 6.5 %, 6 %, 4.5 %, 7 % and 3 %, respectively.<sup>31</sup>

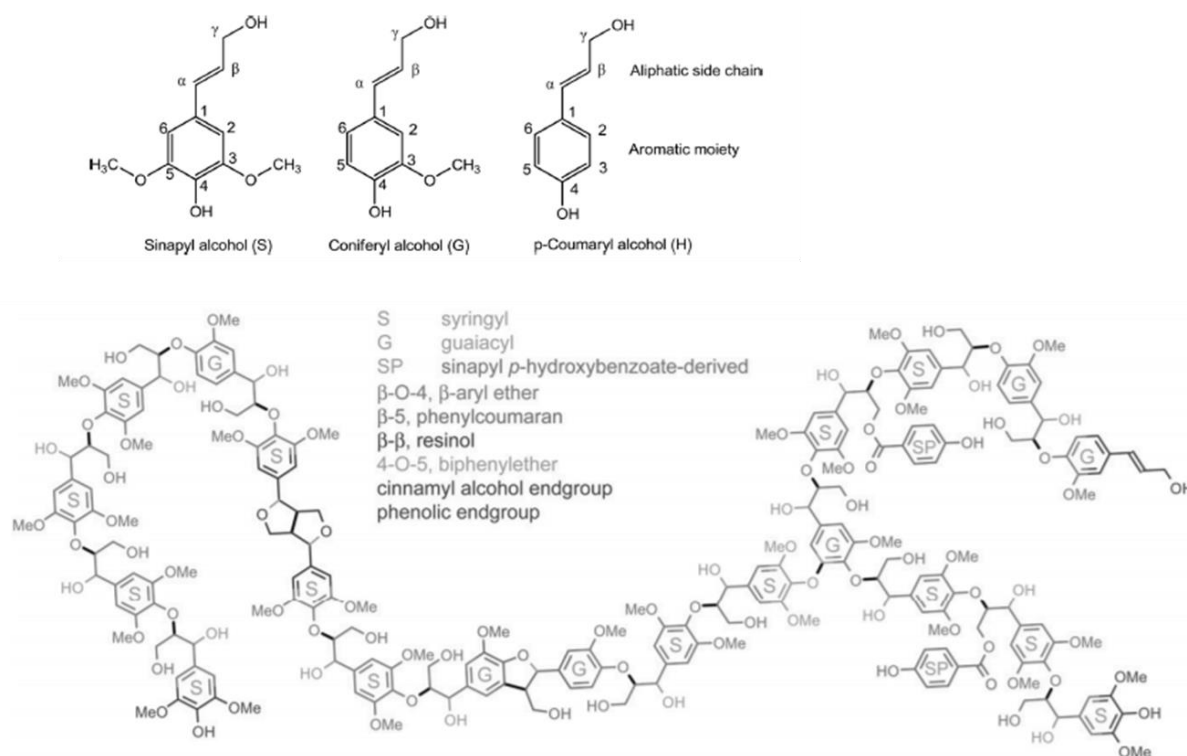


**Figure 1-6. Structures of, the primary building blocks of lignin and a representative structure of lignin.<sup>27</sup> (Reprinted with permission from reference 27. Copyright by the American Society of Plant Biologists.)**

In order to convert lignin into aromatic monomeric compounds, catalytic depolymerization process has been developed over various kinds of catalysts. More than seventy years ago, copper-chromium oxide catalysts and Raney Ni were used as a catalyst for the conversion of soft wood, with propyl cyclohexanol, syringol and guaiacol components isolated as main products from the process.<sup>32-34</sup> Although the process is effective and many different catalysts have been developed, such as Pd/C, Rh/C, Ru/C, Rh/Al<sub>2</sub>O<sub>3</sub>, Ru/Al<sub>2</sub>O<sub>3</sub>, zeolite-supported metal catalysts, etc,<sup>35-37</sup> reductive pyrolysis is highly energy consuming.<sup>38</sup> For lignin valorization, the alternative strategy is based on the deconstruction of lignin into low-molecular-weight feedstocks followed by sequential upgrading to form useful chemicals and fuels.<sup>26</sup> The depolymerization step is a major challenge. Because of the complexity and variability of lignin, several simpler, low-molecular weight lignin model compounds have been applied for the fundamental study of lignin valorization.<sup>26</sup> The use of lignin model compounds serves several primary

purposes for the depolymerization of lignin. They contain linkages that resemble those found in the lignin polymer, such as  $\beta$ -O-4-linkage ( $\beta$ -O-4-aryl ether),  $\alpha$ -O-4-linkage ( $\alpha$ -O-4-aryl ether), 4-O-5-linkage (diaryl ether),  $\beta$ -5-linkage (phenylcoumaran),  $\alpha$ -I-linkage (diphenylmethane), etc. Thus their conversion provides insight into the degradation and reactivity of the lignin structure as a whole. And because the model molecules are often found in lignin degradation streams after depolymerization, upgrading these compounds to high-value chemicals is therefore important. These model compounds contain only one type of linkage usually, so the analysis of the reaction paths and catalytic performance are simplified relative to the complicated lignin.<sup>38</sup>

As mentioned in Figure 1-6, linkages ( $\beta$ -O-4,  $\alpha$ -O-4 and 4-O-5) which contain C-O bond are the most abundant and important linkages in lignin polymer structure. The aromatic components can also be directly linked by C-C bonds, as in 4-methoxy biphenyl and diphenyl methane. So the cleavage of the model compounds is divided into three different bond cleavages: carbon-carbon bonds, phenyl alkyl ether bonds and aryl-aryl ether bonds.<sup>39</sup> Some examples for the cleavage of the  $\beta$ -O-4 model compound, containing carbon-carbon bond, phenyl alkyl ether bond and aryl-aryl ether bond, are listed in Figure 1-7. The carbon-carbon bonds in lignin are some of the most difficult bonds to break, and the aliphatic ether bond is relatively easy to cleave.<sup>40</sup> The C-C bond dissociation energy in the linkage of lignin is as high as 384 kJ/mol, so devising a strategy to selectively cleave the C-O bond (bond dissociation energy: 218–314 kJ/mol) in the linkages can be more efficient.<sup>41</sup> Because the bond strength of the aliphatic C-O bond is much lower than the aromatic C-O bond, the cleavage of aromatic C-O bond is much more challenging. Since the aliphatic C-O bond is usually selectively cleaved in the model compounds which contain these two kinds of C-O bonds, such as  $\beta$ -O-4 and  $\alpha$ -O-4 model compounds,<sup>42-44</sup> aromatic C-O bond cleavage is usually relevant in aryl-methyl ethers and diaryl ethers which are relatively difficult to be upgraded.

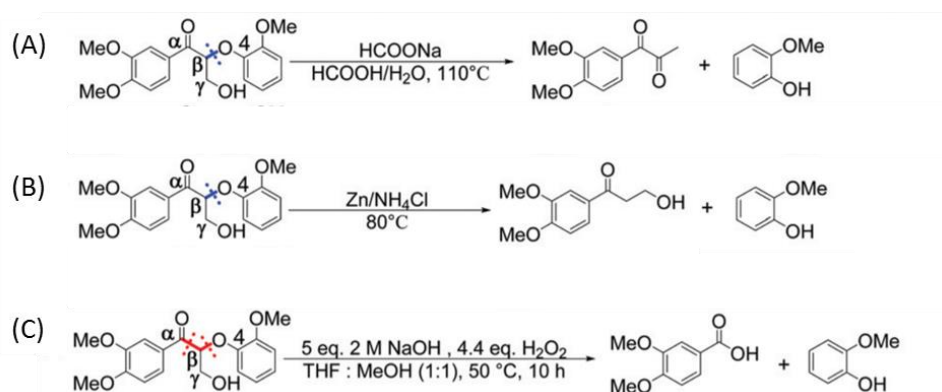


Figure 1-7. C  $\beta$ -O bond and C-C bond cleavage of  $\beta$ -O-4 model compound.<sup>45-50</sup> (Adapted with permission from reference 50. Copyright © 2017, Royal Society of Chemistry.)

Alkyl-aryl ethers usually undergo C<sub>alkyl</sub>-O bond cleavage except anisole, and aryl-aryl ethers only undergo C<sub>aryl</sub>-O bond cleavage under hydrogenolysis conditions (Figure 1-8).<sup>42</sup> And the relative reactivity of ether substrates is Aryl-OAryl > Ar-OMethyl.<sup>51</sup> Considering that anisole is not a model motif of the structure in the lignin polymer and that we would like to focus on the fundamental investigation of the cleavage of aromatic C-O bond in lignin model compounds, diphenyl ether is the most suitable compound to work with.

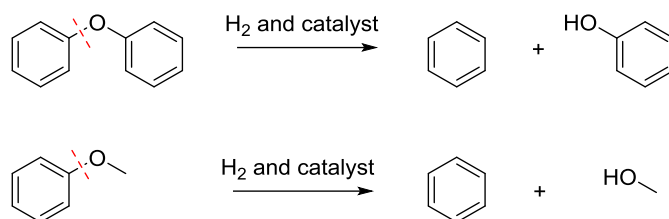


Figure 1-8. Hydrogenolysis of diphenyl ether and anisole.<sup>51-52</sup>

### 1.2.2 Activation of carbon oxygen bond

The catalytic cleavage of aromatic C-O ether bond can be tracked back to the work published in 1979.<sup>53</sup> In this report, the cleavage of aromatic C-O bond was initiated by nickel insertion, then a nickel alkoxide intermediate was formed, and it resulted in C-C coupling by reacting with a Grignard's reagent (transmetalation and reductive elimination).<sup>53</sup> The activation of aromatic ether bond is not only important in the depolymerization of lignin, but also could potentially open up new possibilities in the cross coupling while changing logics in organic synthesis with little generation of waste (Figure 1-9).<sup>54</sup> Due to the high activation barrier for effecting aromatic C-O bond cleavage and the site-selectivity in the presence of multiple C-O bonds (as we mentioned in the previous section), this cleavage is still a difficult synthetic problem.<sup>57-59</sup>

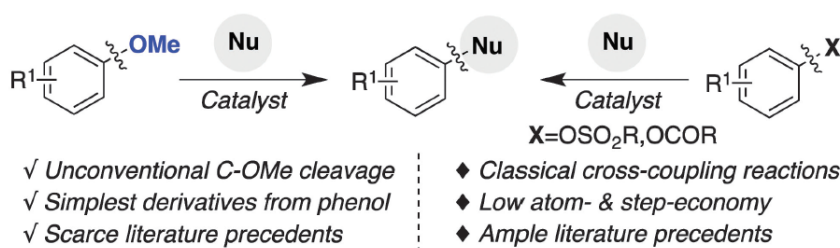
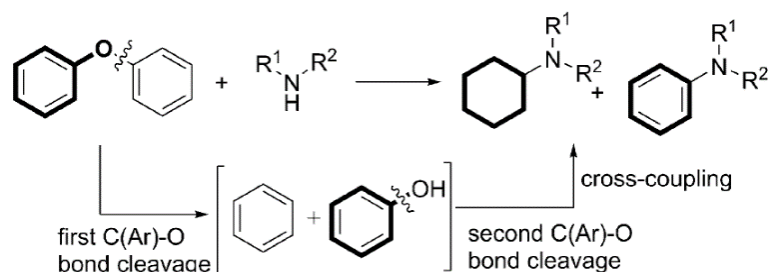


Figure 1-9. Catalytic functionalization of aryl alkyl ethers vs. “classical” C-O electrophiles.<sup>54</sup>(Adapted with permission from reference 54. Copyright © 2014, Royal Society of Chemistry.)

There are many seminal works in homogeneous metal-catalyzed activation of C-O bonds in aryl ether derivatives, as well as in C-C, C-N, and C-H (hydrogenolysis) bond-formation.<sup>54-55, 57</sup> Mechanistic insights have also been provided in the past years.<sup>60-62</sup> Although significant contributions have been described in a stoichiometric fashion of heterogeneous catalysis, fewer examples for novel reactions

and mechanistic studies are found in heterogeneous catalysis. Based on the understanding of elementary steps for the cleavage of aryl ethers in the heterogeneous catalytic system, new reactions and mechanisms can be discovered. Here is an example, as shown in Figure 1-10, based on the knowledge from palladium-catalyzed formal cross-coupling of phenols with amine<sup>63-64</sup>, the authors reported heterogeneous palladium-catalyzed cross coupling of diphenyl ether with amines.<sup>65</sup>



**Figure 1-10. Palladium-catalyzed formal cross-coupling of diaryl ethers with amines.<sup>65</sup> (Reprinted and adapted with permission from reference 65. Copyright © 2018, John Wiley and Sons.)**

### 1.3 Reaction routes of reductive conversion of aryl ethers

Several attempts have been made in order to develop suitable catalysts and processes for the breakdown/conversion of diphenyl ether as the model compound. Generally, the cleavage of the C–O bond in diphenyl ether needs harsh reaction conditions, which yield poor selectivity. Figure 1-11 represents the common reaction pathways, hydrogenolysis, hydrolysis and hydrogenation, of the conversion of diphenyl ether in liquid phase reactions. Secondary reactions usually happen at the same time under reductive conditions. The products from hydrogenolysis and hydrolysis are hydrogenated afterward, and the initial hydronation product, cyclohexyl phenyl ether, can be converted via hydrogenolysis, hydrolysis and hydrogenation.<sup>44, 66</sup>

Hydrogenolysis of diphenyl ether produces equimolar concentrations of phenol and benzene which are then hydrogenated to cyclohexanone/cyclohexanol and cyclohexane, respectively. For the products, if there is no dehydration/deoxygenation of oxygenates, the molar ratio between hydrocarbons and oxygenates will be 1:1 via hydrogenolysis. Hydrolysis of diphenyl ether forms 2 moles of phenol which will be converted to cyclohexanone and cyclohexanol via further hydrogenation. Hydrogenation of diphenyl ether results in one aromatic ring hydronation product: cyclohexyl phenyl ether. When the cleavage of aromatic/aliphatic C–OH is nonexistent and the cleavage of hydrogenated products, cyclohexyl phenyl ether and dicyclohexyl ether is carefully determined, we can calculate the selectivity of different pathways by analyzing the products distribution. The carbon-based selectivity to hydrogenolysis is twice the sum of the selectivities to benzene and cyclohexane. The selectivity to hydrolysis is calculated by subtracting the selectivities of benzene and cyclohexane from the sum of those of phenol, cyclohexanone and cyclohexanol.

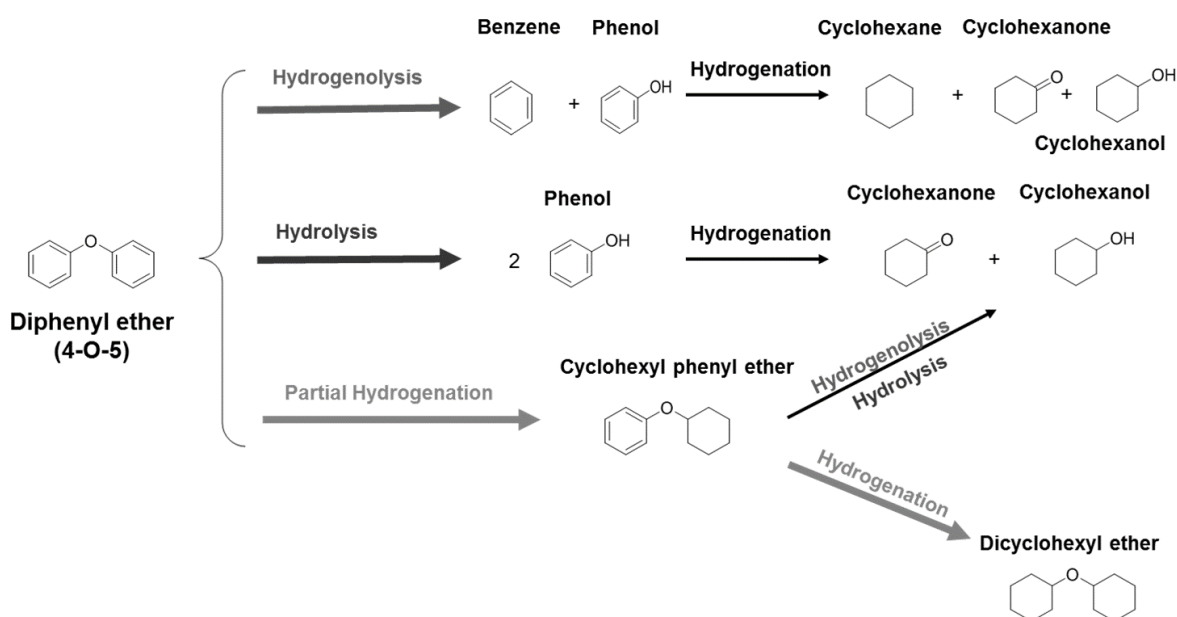


**Figure 1-11. Reaction routes of diphenyl ether and the secondary reactions.**

Our group reported the conversion of diphenyl ether over nickel nanoparticles under  $H_2$  in the aqueous phase (Figure 1-12). The work showed that the three reactions (hydrogenation, hydrogenolysis and hydrolysis) occurred in parallel.<sup>44, 67</sup> Cyclohexanol and benzene are the major products, and more oxygenates are generated than the hydrocarbons from cleavage. This indicates that the major reactions are hydrogenolysis and hydrolysis. Cyclohexanol is formed by parallel hydrogenolysis–hydrogenation and hydrolysis–hydrogenation pathways because phenol is rapidly hydrogenated under the reaction conditions. Since the initial yield ratio of cyclohexanol to benzene was 7:3 and the initial selectivity of cyclohexyl phenyl ether was about 13 %, the selectivities to hydrogenolysis, hydrolysis and hydrogenation of diphenyl ether were determined to be 52 %, 35 % and 13 %, respectively.<sup>44, 67</sup> Hydrogenolysis and hydrolysis were hypothesized to occur via a C-O bond breaking and recombination mechanism. The Ar-OAr bond is cleaved into Ar· and ·OAr fragments at first, for hydrogenolysis, the abundant dissociated H· atoms on the Ni surface are added to benzene and phenol; for hydrolysis, subsequent addition of H· and ·OH (from water dissociation) produces two phenols (Figure 1-13).<sup>44</sup>

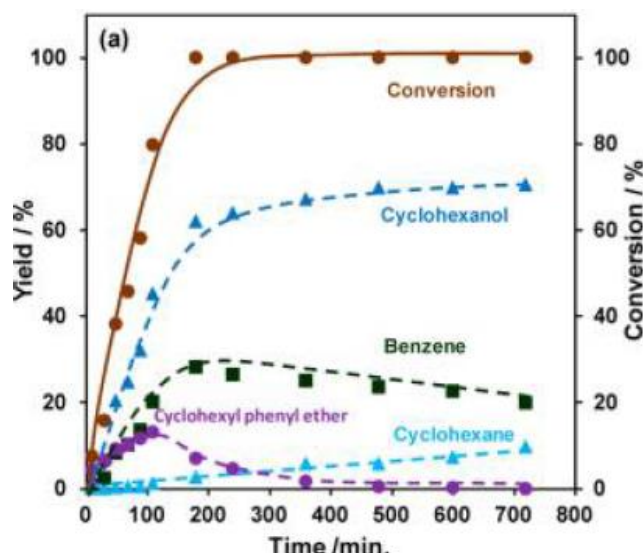


**Figure 1-12.** Product distributions for the conversion of diphenyl ether over Ni/SiO<sub>2</sub> as functions of time.<sup>44</sup> (Reprinted and adapted with permission from reference 44. Copyright © 2012, American Chemical Society.)

Conditions: diphenyl ether (1.70 g), 57 wt % Ni/SiO<sub>2</sub> (0.30 g), 120 °C, 6 bar H<sub>2</sub>, stirring at 700 rpm.



**Figure 1-13.** Cleavage of diphenyl ether over Ni catalyst.<sup>44</sup> (Reprinted and adapted with permission from reference 44. Copyright © 2012, American Chemical Society.)

### 1.3.1 Hydrogenolysis

Diphenyl ether is one of the simplest and strongest aromatic ethers, it is stable in supercritical water,<sup>68-69</sup> nevertheless it can be cleaved by catalytic hydrogenolysis if hydrogen and an appropriate metal catalyst are used.<sup>70</sup> The hydrogenolysis of C-O bonds in aryl ethers requires high temperatures and pressures and normally occurs with poor selectivities of aromatics.<sup>26, 70</sup> Some remarkable works of Hartwig's group revealed a new strategy to the hydrogenolysis of aryl C-O bond using homogeneous nickel (Figure 1-14A) and heterogeneous nickel catalysts (Figure 1-14B) in the presence of NaOBu as base. Under just one bar of hydrogen at temperatures of 80 to 120 °C, products from hydrogenolysis, benzene and phenol, are generated without further hydrogenation even at full conversion.<sup>71</sup>

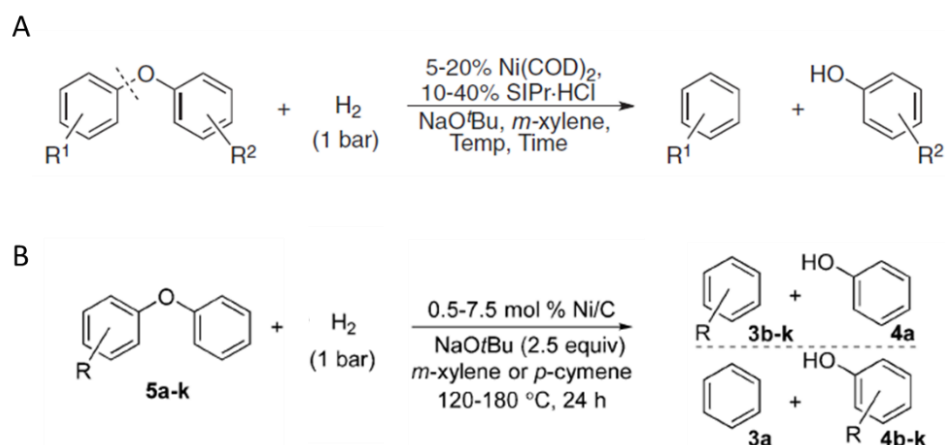


**Figure 1-14.** Hydrogenolysis of diaryl ethers under the catalysis of nickel complex (A) and particles supported on carbon (B).<sup>51, 71</sup> (Adapted with permission from reference 51 and 71. Copyright © 2011, American Association for the Advancement of Science and Copyright © 2015, John Wiley and Sons.)

Raney Ni has also been found as a considerably highly chemoselective catalyst for transferring hydrogenolysis of diaryl ethers.<sup>72-73</sup> Because it is an extremely active catalyst for hydrogen transfer reactions, hydrogen gas is no longer needed during the hydrogenolysis when isopropanol is added into the system as a hydrogen source (Figure 1-15). Phenol was easily hydrogenated to cyclohexanone and cyclohexanol under the reaction condition, so benzene and cyclohexanol are the major products from hydrogenolysis of diphenyl ether (Figure 1-15A).<sup>72</sup> When acid catalyst (H-BEA-35 zeolite) was co-added into the system, benzene was the only major product without the formation of saturated products by the catalytic tandem reactions (Figure 1-15B).<sup>73</sup>

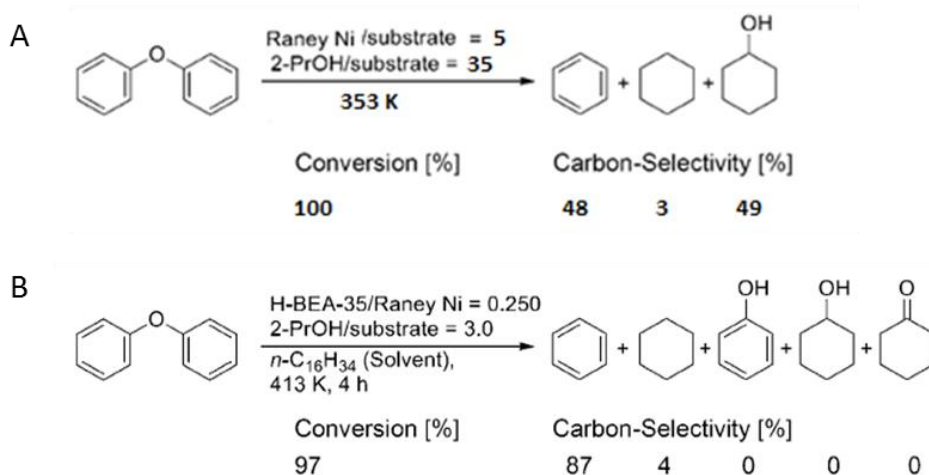


**Figure 1-15.** Transfer hydrogenolysis of diphenyl ether over Raney Ni in the absence (A) and presence (B) of acid catalyst.<sup>72-73</sup> (Adapted with permission from reference 73. Copyright © 2013, John Wiley and Sons.)

A non-metal catalyst was also discovered for the hydrogenolysis under mild reaction conditions. With 5 equiv. of  $\text{Et}_3\text{SiH}$  and 2 equiv. of  $\text{KOt-Bu}$ , the diaryl ethers underwent C–O cleavage with good to excellent efficiencies (Figure 1-16).<sup>74</sup> The alkyl organosilicates might be the key reactive species involved during the reaction, but the detailed mechanism is unclear.



$$\text{Ar}_1\text{-O-Ar}_2 \xrightarrow[165\text{ }^\circ\text{C, 20 h, Mes}]{\text{Et}_3\text{SiH (3); KOt-Bu (3)}} \text{Ar}_{1,2}\text{-H} + \text{Ar}_{1,2}\text{-OH}$$

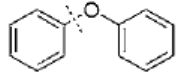
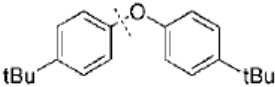
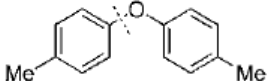
Entry	Diaryl ether	Conv. (%)	Ar <sub>1</sub> -H	Ar <sub>1</sub> -OH
			Ar <sub>2</sub> -H	Ar <sub>2</sub> -OH
1		96	64	65
2		100	76	98
3		100	52	84

Figure 1-16. Catalytic hydrogenolysis of diaryl ethers by triethylsilane.<sup>74</sup> (Adapted with permission from reference 74. Copyright © 2013, Royal Society of Chemistry.)

A highly selective protocol for C-O hydrogenolysis not accompanied by hydrogenation of aromatic rings in appreciable amounts, was partially achieved in the presence of homogeneous nickel and ruthenium catalysts,<sup>51, 75</sup> unsupported nickel nanoparticles,<sup>76</sup> Raney Nickel<sup>72-73</sup>, supported nickel nanoparticles<sup>71</sup> or a Lewis-base<sup>74</sup> under reductive conditions. Nickel-based catalysts have been widely used,<sup>77-79</sup> and a base has been sometimes involved to improve the selectivity towards monomeric aromatics.<sup>51, 76</sup> Different metal catalysts have also been investigated, such as copper,<sup>80-81</sup> ruthenium<sup>82-83</sup> and rhodium.<sup>66</sup> And nickel-based bimetallic catalysts, NiM (M = Ru, Rh, Pd and Au), have been tested for the hydrogenolysis of aryl ethers too.<sup>77, 84</sup> The reactions have been performed in organic solvents, but water has also been used.<sup>44, 77</sup> An example for the aqueous phase reaction with presence of base is shown in Figure 1-17, and the conversion is catalyzed by NiAu bimetallic catalysts under hydrogen.<sup>84</sup>

$$\text{Diphenyl ether} \xrightarrow[100\text{ }^\circ\text{C, H}_2\text{O}]{10\text{ mol\% Ni}_7\text{Au}_3, 0/2.7\text{ eq. NaOH, 10 bar H}_2} \text{Ph-OH} + \text{Cyclohex-OH} + \text{Cyclohex-O-Ph} + \text{Cyclohex-O-Cyclohex}$$

Entry	NaOH [eq.]	t [h]	Conversion [%]	15 [%]	16 [%]	23 [%]	24 [%]
1	0	5	33.7	0.2	17.3	2.2	0.5
2	2.7	5	22.8	4.1	5.4	0.8	0.1
3	2.7	15	37.2	6.5	12.3	1.4	0.2

Figure 1-17. Conversion and main products yield of the hydrogenolysis of diphenyl ether over Ni<sub>7</sub>Au<sub>3</sub> as a function of the pH amount.<sup>84</sup> (Adapted with permission from reference 84. Copyright © 2015, Elsevier Ltd.) Reaction conditions: 10 mol % Ni<sub>7</sub>Au<sub>3</sub>, NaOH, 10 bar H<sub>2</sub>, H<sub>2</sub>O, 100 °C.

### 1.3.2 Hydrolysis

As we mentioned before, diphenyl ether is stable in supercritical water.<sup>68-69</sup> By adding an acid or base, diphenyl ether can be converted to phenol via hydrolysis at 460 °C.<sup>85-86</sup> Figure 1-18 shows the acid and base catalyzed mechanisms. For base, on the left of Figure 1-18, the mechanism starts with a nucleophilic attack of a hydroxide anion on the diphenyl ether to provide the intermediate. By eliminating a phenol molecule, the intermediate decomposes to phenolate which is subsequently protonated to form the next phenol molecule. For Brønsted acid, such as H<sub>3</sub>PO<sub>4</sub><sup>85</sup> or the proton initially generated by the dissociation of water<sup>69</sup>, the protonation of diphenyl ether initiates the reaction, then the intermediate converts to phenol and phenyl cation by decomposition, the phenyl cation reacts with water forming a second phenol molecule and a proton afterward. Lewis acids, such as NaCl or Ni(BF<sub>4</sub>)<sub>2</sub> have also been used in supercritical water for the hydrolysis of diphenyl ether.<sup>87-88</sup> Because of the positive influence of the high salt concentrations, the reaction route for Lewis acid was proposed that H<sup>+</sup> and OH<sup>-</sup> ions in the outer hydration shells of the water clusters were generated from the charge transfer in the water, and the ions were active species for the diphenyl ether hydrolysis.<sup>87</sup>

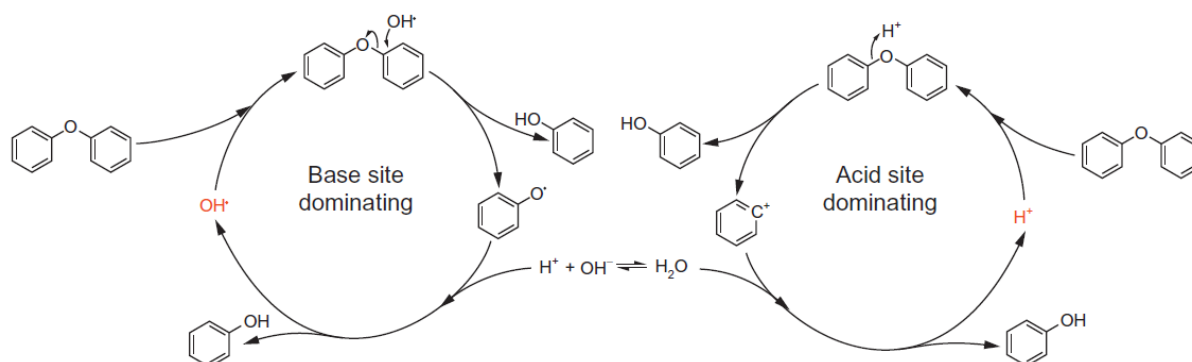


**Figure 1-18.** The reaction mechanism of acid- and base-catalyzed hydrolysis of ether bonds.<sup>89</sup> (Reprinted and adapted with permission from reference 89. Copyright © 2010, John Wiley and Sons.)

Another reaction mechanism, a radical pathway, was also suggested for the conversion of diphenyl ether in supercritical water. The ether bond is homolytically cleaved generating a phenoxy and a phenyl radical. Figure 1-19 shows the details of the possible routes for the radicals. These species can recombine with hydrogen to form phenol and benzene (reaction I), or recombine with themselves which lead to the formation of dimers such as 4-hydroxy biphenyl (reaction II and III) or even higher molecular compounds (e.g., phenoxy biphenyl).<sup>39, 89</sup>

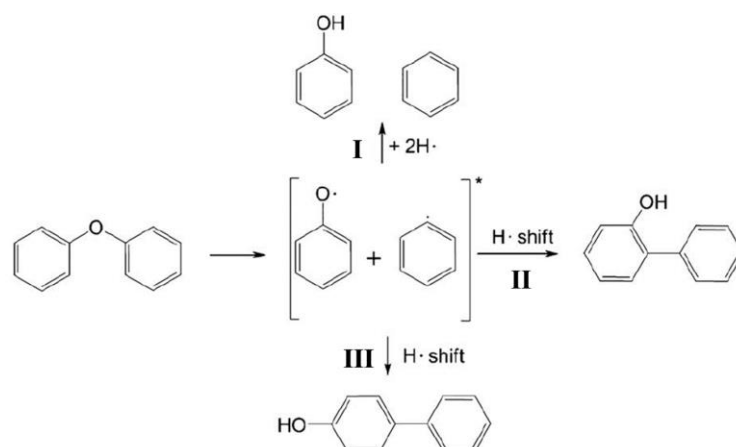


**Figure 1-19.** The reaction mechanism of radical pathway of hydrolysis of diphenyl ether.<sup>86, 89</sup> (Reprinted and adapted with permission from reference 89. Copyright © 2010, John Wiley and Sons.)

According to the theoretical calculation of the hydrolysis of diphenyl ether, the reaction should proceed completely above 120 °C at 25 MPa and water/ether ratio of 35:1, it means the reaction is thermodynamically not limited.<sup>39</sup> Our group reported an achievement for the 100 % selectivity of phenol from diphenyl ether conversion with much lower amounts of base ( $\text{K}_2\text{CO}_3$ ) supported on  $\text{ZrO}_2$ .<sup>89</sup> The phenol was generated via an ionic mechanism, show in Figure 1-20. The reaction was induced by the polarization of the ether bond by the cation. During the reaction, the dispersion and accessibility of the catalyst,  $\text{K}_2\text{CO}_3$ , was enhanced by supporting it on  $\text{ZrO}_2$ .

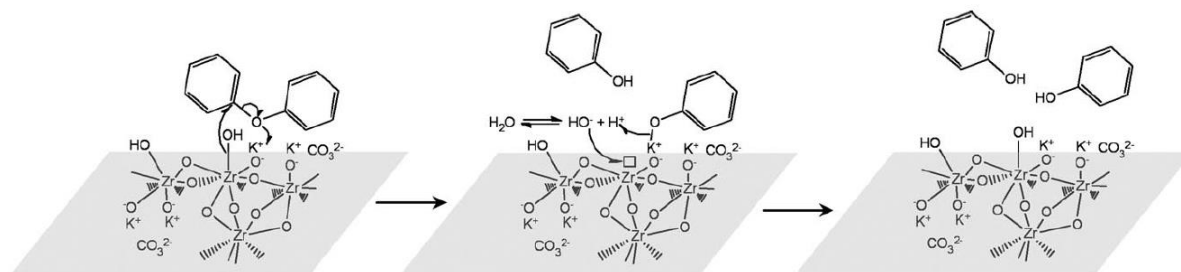


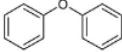
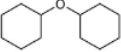
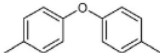
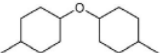
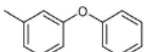
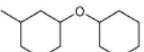
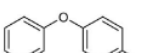
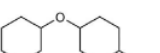
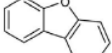
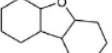
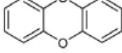
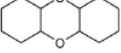
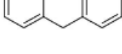
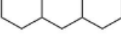
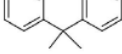
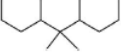
**Figure 1-20.** Mechanism for the formation of phenol from diphenyl ether in the presence of 3 wt% of 10 wt%  $\text{K}_2\text{CO}_3/\text{ZrO}_2$ .<sup>89</sup> (Reprinted and adapted with permission from reference 89. Copyright © 2010, John Wiley and Sons.)

### 1.3.3 Hydrogenation

Both heterogeneous and homogeneous catalysts have been developed for reductive C–O cleavage of diphenyl ether. Under the reductive reaction conditions, cyclohexanol and cyclohexane are the final products from the hydrogenation of the initial products (phenol and benzene). An alternative method is turning the aromatic C–O bond to aliphatic C–O bond which is weaker and easier to be broken by other catalysts. The selective hydrogenation of the aromatic rings of diphenyl ether will generate dicyclohexyl ether which is still hard to be cleaved via metal catalyst, but easy to be hydrolyzed with acid/base catalysts. Moreover, selective hydrogenation of aromatic rings plays an important role in the generation

of all kinds of aliphatic derivatives. So the selective hydrogenation of lignin-derived fragments is also important.

Heterogeneous ruthenium catalyst was chosen as an example of a selective hydrogenation catalyst in the discussion below. The Ru-based material has been proven a good catalyst in hydrogenolysis of the aromatic ether bonds,<sup>83, 90</sup> but ruthenium is also good in selective hydrogenation of aromatic rings.<sup>91</sup> The modification of the catalyst could dramatically change the performance. The Ru/C showed good selectivity for hydrogenolysis of diphenyl ether under mild reaction conditions in isopropanol.<sup>83</sup> With the modification of the support, N-doped carbon support, the diaryl ethers are hydrogenated to aliphatic ethers almost without cleavage of the C-O bonds (Figure 1-21).<sup>92</sup>

Substrate	Product	Yields (%) <sup>†</sup>
		84/86 <sup>‡</sup> (65/66 <sup>‡</sup> )
		87
		89
		85
		91
		89
		86
		81

**Figure 1-21. Selective hydrogenation of diaryl ethers.**<sup>92</sup> (Adapted from reference 92. Copyright © 2016, Springer Nature Limited.)

Reaction conditions: 0.5 mmol reactant, 20mg Ru-based catalyst, 2 ml isopropanol, 20 bar H<sub>2</sub>, 60 °C, 24h.

### 1.3.4 Reactions of phenols

Phenol is the initial product from the hydrogenolysis and hydrolysis of diphenyl ether, so the conversion of phenol is important for the analysis of the reactions of diphenyl ether. On the other hand, phenol, the simplest phenolic monomer, has been widely chosen to be tested as a model compound for the

upgrading procedures of bio-derived compounds.<sup>93-96</sup> The investigations for the hydrogenation and deoxygenation of phenolic molecules are instructive for the reactions of diphenyl ether.

The hydrogenation of phenol over metal catalysts has been extensively reported, this reaction proceeds mainly in a sequential manner as shown in Figure 1-22A. The aromatic ring of phenol is first partially hydrogenated to an enol which is unstable and isomerizes rapidly to form cyclohexanone. Then the cyclohexanone can be further hydrogenated to form cyclohexanol.<sup>97-99</sup> In order to stop the secondary reaction, different catalysts and reaction conditions have been investigated to change the competition between step 1 and step 2 in Figure 1-22A. An impressive achievement was made by palladium catalyst with co-added Lewis acid under H<sub>2</sub>.<sup>99</sup> Lewis acid played an important role in both step 1 and step 2 for the selective hydrogenation of phenol (Figure 1-22B). In step 1, the Lewis acid coordination makes the aromatic ring more active, so cyclohexanone is formed quickly. In step 2, the further hydrogenation of cyclohexanone was inhibited by Lewis acid–base interaction.<sup>99</sup>

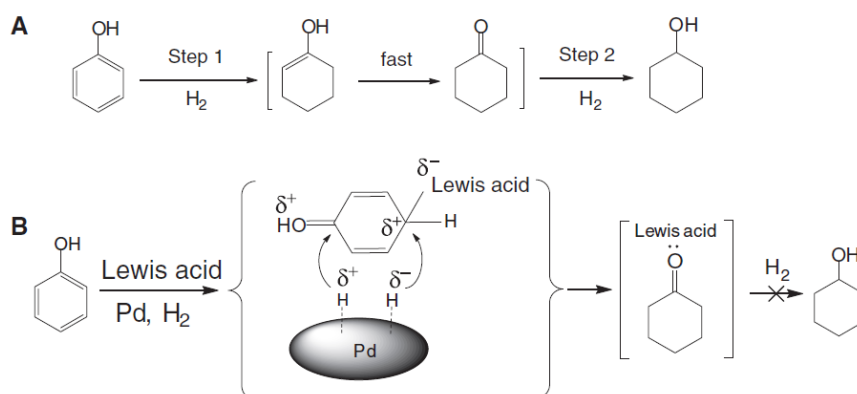


**Figure 1-22. (A) General reaction pathway for hydrogenation of phenol. (B) Possible mechanism of dual activation in phenol hydrogenation and stabilization of cyclohexanone by Lewis acid<sup>99</sup> (Adapted with permission from reference 99. Copyright © 2009, American Association for the Advancement of Science.)**

The previous synergistic catalytic system shows the possibility of direct synthesis of ketones from biomass-derived feedstock. Another pathway, the hydrodeoxygenation, has been broadly investigated via tandem catalytic reactions by metal and acid catalysts under H<sub>2</sub>.<sup>93, 100</sup> The phenol hydrodeoxygenation which generates cyclohexane proceeds in the aqueous phase through four steps as shown in Figure 1-23. Phenol hydrogenation, generating cyclohexanone and cyclohexanol, is the first step, and sequential cyclohexanone hydrogenation to cyclohexanol is the second. These two steps are catalyzed by a metal catalyst. The third step is the cyclohexanol dehydration to cyclohexene on acid sites. Then cyclohexene is reabsorbed on the metal surface and finally hydrogenated to cyclohexane. Different solvents also have been studied, and the reaction pathways are identical for phenol hydrodeoxygenation with Pd/C and HZSM-5 in polar (hexadecane) and apolar (water) phases.<sup>100</sup>

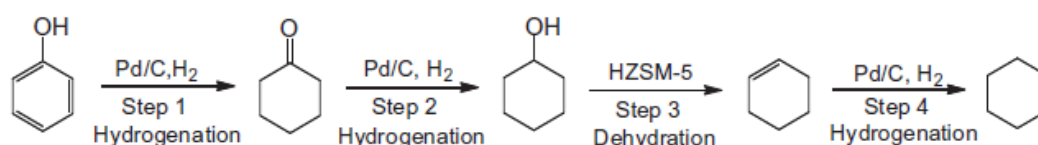


**Figure 1-23. Reaction pathway of hydrodeoxygenation of phenol on dual-functional catalysts of Pd/C and H-ZSM5.<sup>100</sup> (Adapted with permission from reference 100. Copyright © 2014, Elsevier Inc.)**

Reaction conditions: 10 g phenol, 80 ml water, 0.20 g Pd/C (1 wt.%), 0.02 g HZSM-5 (Si/Al = 45), 200 °C, 4 MPa H<sub>2</sub> and stirring at 700 rpm.

The hydrodeoxygenation of substituted phenols has also been widely studied, such as guaiacol and cresols.<sup>82, 95, 101</sup> The reactions are more complex for the substituted phenols as shown in Figure 1-24. Three types of C–O bonds, C<sub>(sp<sup>3</sup>)</sub>–OAr, C<sub>(sp<sup>2</sup>)</sub>–OMe, and C<sub>(sp<sup>2</sup>)</sub>–OH, are presented in guaiacol. The bond dissociation energies are 262–276, 409–421, and 466 kJ/mol, respectively.<sup>95</sup> The barrier of C–OH bond scission should be the highest, and it corresponds well with the experimental result in which the yield of methoxybenzene was lower than 0.1%.<sup>95</sup> The hydrogenolysis of C–OMe occurred in parallel with the hydrogenation of the aromatic ring. Comparing to phenol, the TOF of guaiacol hydrogenation is a magnitude slower under the same reaction conditions.<sup>95</sup> The low hydrogenation activity was caused by the steric influence of the ortho-substituted methoxy group which was concluded to make the coplanar adsorption of the aromatic ring more difficult compared to phenol and catechol.<sup>102</sup> The secondary reactions (C–O cleavage and hydrogen addition) of the initial products from guaiacol, such as phenol, anisole and 2-methoxycyclohexanol, are important and worth investigating especially when an acid catalyst is added into the system.

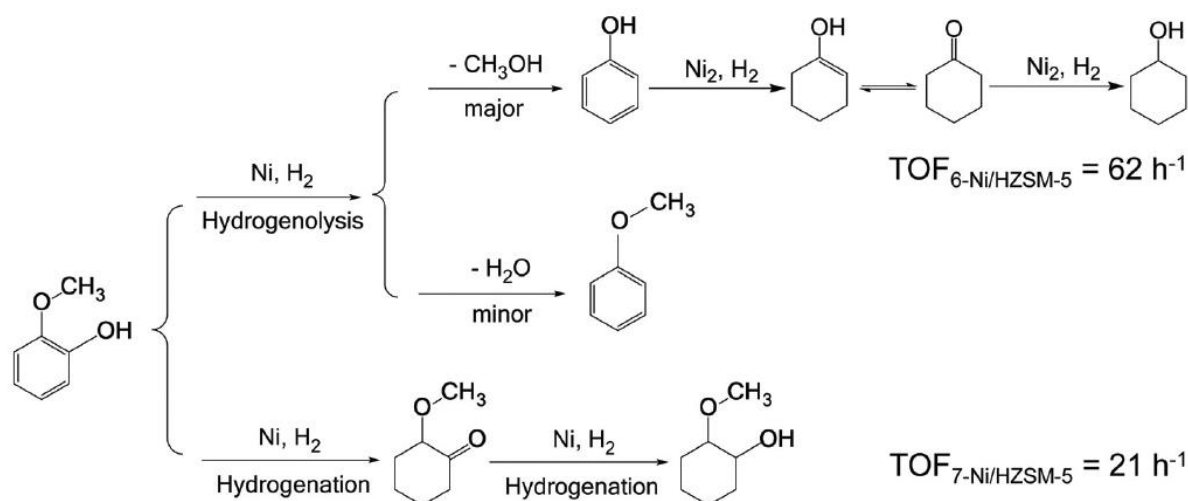


**Figure 1-24. Proposed reaction pathway of guaiacol hydrodeoxygenation over Ni/HZSM-5.<sup>95</sup> (Adapted with permission from reference 95. Copyright © 2015, Royal Society of Chemistry.)**

Reaction conditions: 1 g guaiacol, 0.05 g Ni/HZSM-5, 200 °C, 3 MPa H<sub>2</sub> (ambient temperature), stirring at 700 rpm.

Since hydrodeoxygenation of substituted phenols has been carefully investigated, different mechanisms have been proposed for the cleavage of the C-O bond in phenol (Figure 1-25). The first mechanism, transhydrogenation and deoxygenation, has been primarily proposed for bifunctional catalyst systems which contain metal and acid sites. The metal site catalyzes the hydrogenation of the aromatic ring and acid site cleaves the C-O bond and dehydrogenates the compound to form the deoxygenated products.<sup>103-104</sup> This mechanism starts with the hydrogenation of the phenolic compound to an equivalent cyclic and oxygenated alkane followed by deoxygenation. The C-O bond is weakened by the hydrogenation of the aromatic ring in the phenolic compound, it leads to a reasonably low activation energy barrier for the deoxygenation reaction.<sup>70, 105</sup> The second mechanism, direct deoxygenation, has been proposed for metal and oxide catalysts.<sup>70, 105-107</sup> It initiates with the direct scission of the C-O bond, followed by the hydrogenation of the aromatic compound to form the products. Due to the strong bond dissociation energy of the aromatic carbon oxygen bond, high operating temperatures are required for the C-O cleavage reaction step.<sup>105-107</sup> An alternative mechanism to the hydrogenation and direct deoxygenation mechanisms is the initial tautomerization mechanism.<sup>108-110</sup> Due to the vertical adsorption, the phenolic compounds are proposed to undergo a tautomerization to the equivalent ketone, followed by hydrogenation of the carbon oxygen double bond, and then dehydrated to form the equivalent deoxygenated aromatic product.<sup>109-110</sup> The tautomerization mechanism is theoretically proved for NiFe bimetallic catalyst. Because of the vertical adsorption of phenolic compounds, the ring hydrogenation and C-C bond cleavage reactions are limited by reducing the interaction between aromatic ring and metal surface.<sup>109</sup> These mechanistic studies of phenolic compounds give us some hints to investigate the cleavage of aryl ethers.

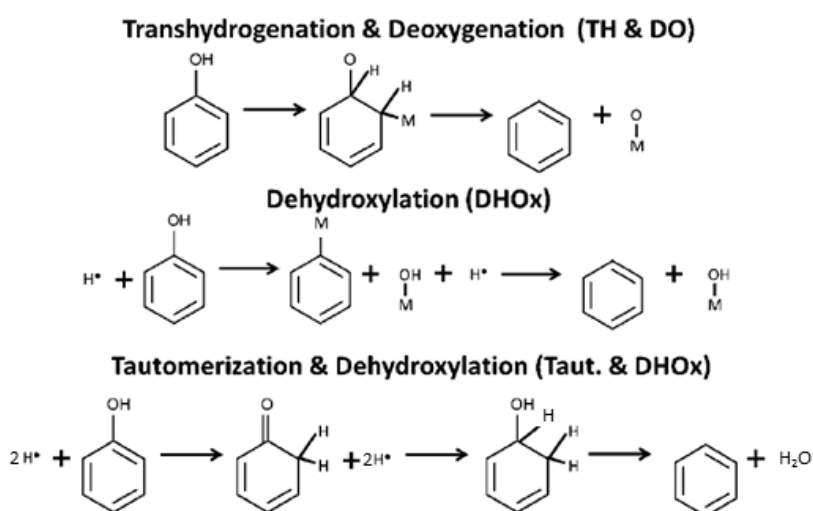


**Figure 1-25.** Possible deoxygenation reaction mechanisms for phenol on a metal catalyst surface (denoted by M).<sup>111</sup> (Reprinted and adapted with permission from reference 111. Copyright © 2015, American Chemical Society.)

## 1.4 Mechanistic studies

The reaction pathway, network and product distributions of diphenyl ether over different catalysts have been widely reported. However, relatively little information relevant to the mechanism of the conversion of diphenyl ether in liquid phase has been published in detail, especially for heterogeneous catalysts. Two examples of mechanistic studies of hydrogenolysis of aryl ethers over homogeneous catalysts are introduced below to show the recent discoveries and the methods applied in the investigations.

A comprehensive mechanistic analysis of the hydrogenolysis of diaryl ethers catalyzed by the combination of  $\text{Ni}(\text{COD})_2$  (COD = 1,5-cyclooctadiene) and an N-heterocyclic carbene (NHC) was reported by Hartwig's group.<sup>60</sup> Based on their previous studies about nickel based catalysts,<sup>51, 71, 76</sup> the authors carefully investigated the rate-determining step and the role of the co-added base (NaOt-Bu) shown in Figure 1-26. The kinetic measurements showed that the dependences of the initial rate on the concentration of ether and the concentration of Ni complex were first order, and the dependences on the concentration of NaOt-Bu and the pressure of  $\text{H}_2$  were zero order. The kinetic isotope effect from the reactions in  $\text{H}_2$  and  $\text{D}_2$  was found to be  $1.0 \pm 0.1$ . These data for the hydrogenolysis pathway indicated that the cleavage of the C–O bond in the diaryl ether by a Ni complex is rate determining, and the products of this step react with hydrogen and base does not. The control experiments for phenol and base showed that phenol reacts with the base to form phenoxide which does not react with the Ni species. The catalyst will decompose in the presence of phenol.<sup>60</sup>

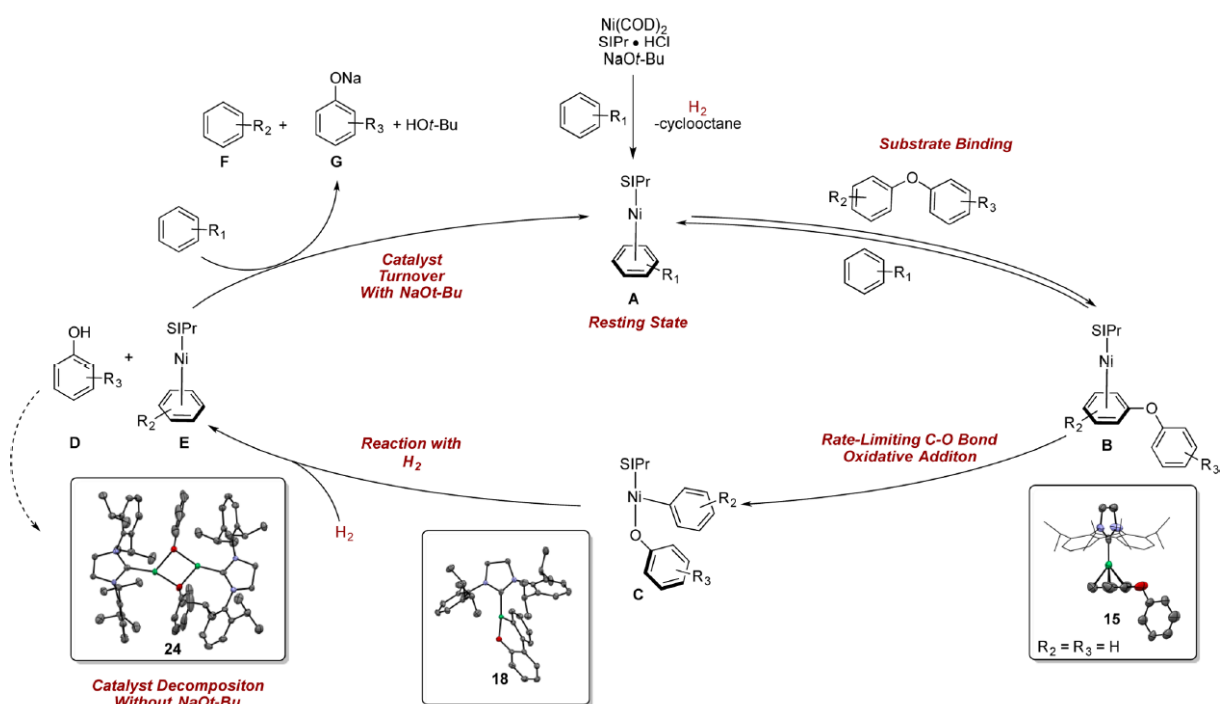


Figure 1-26. Mechanism for the Ni-catalyzed hydrogenolysis of diaryl ethers with NHC as ligand.<sup>60</sup> (Reprinted with permission from reference 60. Copyright © 2017, American Chemical Society.)



Small modifications in a catalytic system can cause large changes in mechanism. Martin's group showed that the cleavage of aryl ethers might occur along different pathways depending on the catalyst.<sup>62</sup> By experiments and theoretical calculations, they demonstrated that the oxidative addition into the C–OMe bond by  $\text{Ni}(\text{COD})_2/\text{PCy}_3$  does not take place under their reaction conditions, the reaction was proposed to undergo migratory insertion into the naphthyl C=C bond and elimination of  $\text{MeOSiR}_3$  to produce a  $\text{Ni}^{\text{I}}$  aryl complex.<sup>62</sup>

Apart from the experimental and theoretical studies for active site and the rate-determining step of the reactions, the isotopic tracing experiments also shed light on the mechanism by which the catalytic hydrogenolysis of aromatic C–O bonds operates.<sup>61</sup> Figure 1-27 shows the mechanisms of hydrogenolysis of deuterium-labeled  $\text{NaphOCD}_3$  (Naph = 2-naphthyl) catalyzed by  $\text{Ni}(\text{COD})_2$  and SIPr under  $\text{H}_2$ .<sup>61</sup> About 90% deuterium incorporated in the newly formed arene implies that reduction occurs by  $\beta$ -deuteride elimination from a methoxide ligand. The hydrogen source for the hydrogenolysis was not the  $\text{H}_2$ , this indicated that the  $\beta$ -H elimination from a nickel alkoxide (left part of Figure 1-27) was the mechanism rather than cleavage of the Ni–O bond by  $\text{H}_2$  (right part of Figure 1-27).

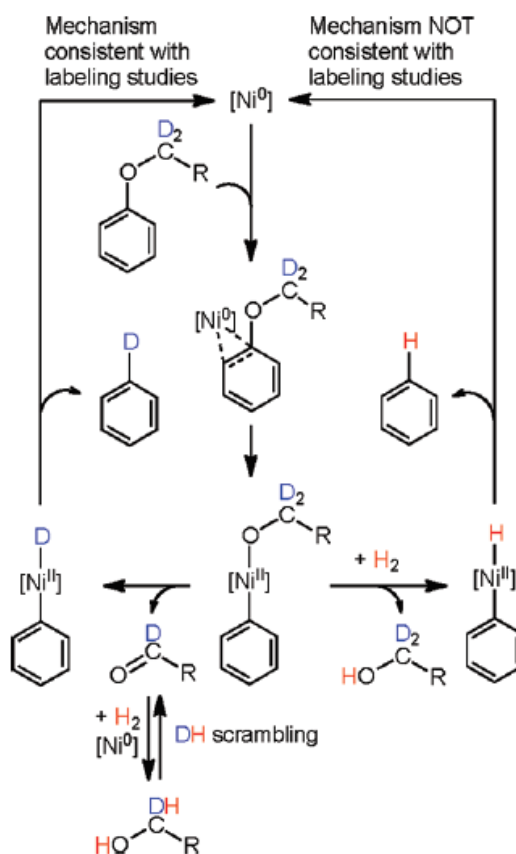


Figure 1-27. Mechanisms for the conversion of aryl alkyl ethers to arenes by  $[\text{Ni}]_0$  complex.<sup>61</sup> (Reprinted with permission from reference 61. Copyright © 2012, American Chemical Society.)

## 1.5 Scope of this thesis

The object of this research is to develop basic insight into catalyzed reactions of oxygen-containing bio-derived molecules at the liquid-solid interface of metal catalysts and to use this insight to enhance the rates along specific reaction pathways to enable conversions at low severity. The model compound, diphenyl ether, will be used as a practical example to derive the fundamental principles of catalysis at the solid-liquid interface using detailed kinetic investigations to understand the reaction mechanism. The ability to describe the practical surface chemistry and active sites on a molecular and atomic level will enable us to understand the principal mechanisms of catalysis at the solid-liquid interface. The main task of the present thesis is to provide fundamental understanding of the selective cleavage, hydrogenolysis and hydrolysis, of aromatic C-O bond in diaryl ether under reductive conditions over metal catalysts.

Table 1-1 shows the comparison of the selectivities of hydrogenolysis, hydrolysis and hydrogenation at full conversion of diphenyl ether over five supported metal catalysts under the same reaction conditions. The selectivity to hydrogenolysis of the metals scale as Ni > Pt > Ru > Rh > Pd, and the selectivity to hydrolysis scales as Pd > Rh = Ru > Ni > Pt. Palladium shows the highest selectivity (84 %) towards hydrolysis, and nickel is the best catalyst for hydrogenolysis (64 %). The following will start with the investigation of hydrolytic cleavage on palladium catalyst, then switch to the mechanistic study of hydrogenolysis over nickel catalyst, a comprehensive comparison of these metal catalysts will be presented afterward.

**Table 1-1. Selectivities of different reaction routes of diphenyl ether over different metal catalysts.**

Catalyst	Time / min	Conversion	Selectivity		
			Hydrogenolysis	Hydrolysis	Hydrogenation
64 wt. % Ni/SiO <sub>2</sub>	600	100%	64%	27%	8%
5 wt. % Ru/C	60	99%	23%	42%	36%
5 wt. % Pt/C	60	99%	31%	18%	50%
5 wt. % Rh/C	60	100%	8%	42%	50%
5 wt. % Pd/C	360	100%	1%	84%	15%

Reaction conditions: 10 mmol ether, 10 mg catalyst, 80 ml water, 40 bar of hydrogen, stirring at 700 ppm, 150 °C.

In Chapter 2, a new catalytic chemistry is reported for the selective reductive hydrolysis of diaryl and aryl alkyl ethers over supported metal catalysts in aqueous phase at relatively mild conditions. An uniquely selective vector is shown, with up to 80 % hydrolysis at complete conversion, e.g., with Pd. Isotopic labeling and kinetic analysis showed that reductive hydrolysis occurs via a hitherto

unconsidered mechanism involving partial hydrogenation of the aryl ring and addition of water to form hemiacetals which rapidly eliminate phenol (R = phenyl) or alcohol (R = alkyl or aralkyl).

In Chapter 3, the metal-catalyzed alcoholysis of aryl ethers in alcoholic solvent is demonstrated by replacing the water with methanol. This route is initiated by partial hydrogenation of the arene ring to an enol ether. Thus the strong aryl C-O bond is transformed to a vinylic C-O bond that is easily cleaved by methanol addition and R-OH elimination. The generality of the chemistry is explored using higher alcohols and other ethers.

In Chapter 4, mechanistic studies of nickel nanoparticles-catalyzed hydrogenolysis of aryl ether has been carried out in polar and apolar phases under reductive conditions. Hydrogenolysis was observed as the major route of the conversions of diphenyl ether in both solvents, which initially generates benzene and phenol. Hydrogen dependence and isotopic experiments of the hydrogenolysis showed that hydrogen addition is involved in the rate determining step. The reaction mechanism was concluded to be initiated by one hydrogen addition to the aromatic ring, then the weakened C-O bond cleaves on the metal surface.

In Chapter 5, the comparison of the reactivities and the selectivities of the reactions over four noble metal catalysts, Ru/C, Pt/C, Rh/C and Pd/C, in polar (water) and apolar (decalin) solvents is presented. The aromatic C-O bond is cleaved hydrogenolytically and/or hydrolytically, while in parallel the aromatic rings are hydrogenated without changing the molecular backbone. In decalin, only hydrogenolysis was observed for C-O cleavage and the selectivity varied from 2 % to 21 %. For each metal catalyst, the selectivity to hydrogenolysis did not change dramatically in water compared to decalin. The preference to hydrogenolysis of the C-O bond over hydrogenation of the aromatic ring increases in the order Pd/C < Rh/C < Pt/C  $\approx$  Ru/C, this is due to the differences of oxophilicity of different metal catalysts. For hydrolysis in water, a reverse trend was observed. Because the reductive hydrolysis occurs via partial hydrogenation (two hydrogen addition) and the mechanism occurs in parallel with hydrogenation, more reductive hydrolysis is obtained when the selectivity of hydrogenation is higher. We concluded that the reaction mechanisms of reductive hydrolysis and hydrogenolysis remained the same, as we established in Chapter 2 and Chapter 4, over different metal catalysts (Ni/SiO<sub>2</sub>, Ru/C, Pt/C, Rh/C and Pd/C) in different solvents (water and decalin).

The summary, conclusion and a brief outlook are given in Chapter 6.

## 1.6 References

1. Monthly Energy Review. **2018**, U.S. Energy Information Administration. <https://www.eia.gov/totalenergy/data/monthly/>.
2. World Energy Outlook 2017. **2017**, International Renewable Energy Agency. <https://www.iea.org/weo2017/>.
3. Energy Roadmap for 2050. **2011**, European Commission. <https://www.dccae.gov.ie/en-ie/energy/topics/Renewable-Energy/decarbonisation/Pages/2050-Landing-Page.aspx>.
4. Annual Energy Outlook 2018. **2018**, U.S. Energy Information Administration. <https://www.eia.gov/outlooks/aeo/>.
5. Ellabban, O.; Abu-Rub, H.; Blaabjerg, F., *Renewable and Sustainable Energy Reviews* **2014**, *39*, 748-764.
6. Re-thinking 2050. **2010**, European Renewable Energy Council. <http://www.rethinking2050.eu/>.
7. Renewable Energy Prospects for the European Union. **2018**, International Renewable Energy Agency. <http://www.irena.org/publications/2018/Feb/Renewable-energy-prospects-for-the-EU>.
8. Huber, G. W.; Iborra, S.; Corma, A., *Chemical Reviews* **2006**, *106* (9), 4044-4098.
9. Tuck, C. O.; Pérez, E.; Horváth, I. T.; Sheldon, R. A.; Poliakoff, M., *Science* **2012**, *337* (6095), 695-699.
10. Alonso, D. M.; Wettstein, S. G.; Dumesic, J. A., *Chemical Society Reviews* **2012**, *41* (24), 8075-98.
11. Dhepe, P. L.; Fukuoka, A., *ChemSusChem* **2008**, *1* (12), 969-975.
12. O'Sullivan, A. C., *Cellulose* **1997**, *4* (3), 173-207.
13. Huber, G. W.; Dumesic, J. A., *Catalysis Today* **2006**, *111* (1), 119-132.
14. Gallezot, P., *Chemical Society Reviews* **2012**, *41* (4), 1538-1558.
15. Wyman, C. E.; Dale, B. E.; Elander, R. T.; Holtzapple, M.; Ladisch, M. R.; Lee, Y. Y., *Bioresource Technology* **2005**, *96* (18), 1959-1966.
16. Dutta, S.; De, S.; Saha, B.; Alam, M. I., *Catalysis Science & Technology* **2012**, *2* (10), 2025-2036.
17. Ruppert, A. M.; Weinberg, K.; Palkovits, R., *Angewandte Chemie International Edition* **2012**, *51* (11), 2564-2601.
18. Hu, L. H.; Pan, H.; Zhou, Y. H.; Zhang, M., *Bioresources* **2011**, *6* (3), 3515-3525.
19. Doherty, W. O. S.; Mousavioun, P.; Fellows, C. M., *Industrial Crops and Products* **2011**, *33* (2), 259-276.
20. Stewart, D., *Industrial Crops and Products* **2008**, *27* (2), 202-207.
21. Calvo - Flores, F. G.; Dobado, J., A., *ChemSusChem* **2010**, *3* (11), 1227-1235.
22. Li, C.; Zhao, X.; Wang, A.; Huber, G. W.; Zhang, T., *Chemical Reviews* **2015**, *115* (21), 11559-624.
23. Gasser, C. A.; Hommes, G.; Schäffer, A.; Corvini, P. F.-X., *Applied Microbiology and Biotechnology* **2012**, *95* (5), 1115-1134.
24. Evtuguin, D. V.; Neto, C. P.; Silva, A. M. S.; Domingues, P. M.; Amado, F. M. L.; Robert, D.; Faix, O., *Journal of Agricultural and Food Chemistry* **2001**, *49* (9), 4252-4261.

25. Pinto, P. C. R.; Silva, E. A. B. d.; Rodrigues, A. E., *Industrial & Engineering Chemistry Research* **2011**, *50* (2), 741-748.
26. Zakzeski, J.; Bruijninx, P. C. A.; Jongerius, A. L.; Weckhuysen, B. M., *Chemical Reviews* **2010**, *110* (6), 3552-3599.
27. Vanholme, R.; Demedts, B.; Morreel, K.; Ralph, J.; Boerjan, W., *Plant Physiology* **2010**, *153* (3), 895-905.
28. Huber, G. W.; Corma, A., *Angewandte Chemie International Edition* **2007**, *46* (38), 7184-7201.
29. Zhao, C.; Lercher, J. A., *Angewandte Chemie International Edition* **2012**, *51* (24), 5935-5940.
30. Pandey, M. P.; Kim, C. S., *Chemical Engineering & Technology* **2010**, *34* (1), 29-41.
31. Dorrestijn, E.; Laarhoven, L. J. J.; Arends, I. W. C. E.; Mulder, P., *Journal of Analytical and Applied Pyrolysis* **2000**, *54* (1), 153-192.
32. Pepper, J. M.; Hibbert, H., *Journal of the American Chemical Society* **1948**, *70* (1), 67-71.
33. Brewer, C. P.; Cooke, L. M.; Hibbert, H., *Journal of the American Chemical Society* **1948**, *70* (1), 57-59.
34. Harris, E. E.; D'Ianni, J.; Adkins, H., *Journal of the American Chemical Society* **1938**, *60* (6), 1467-1470.
35. Corma, A.; Iborra, S.; Velty, A., *Chemical Reviews* **2007**, *107* (6), 2411-2502.
36. Mäki - Arvela, P.; Holmbom, B.; Salmi, T.; Murzin, D. Y., *Catalysis Reviews* **2007**, *49* (3), 197-340.
37. Pepper, J. M.; Supathna, P., *Canadian Journal of Chemistry* **1978**, *56* (7), 899-902.
38. Mu, W.; Ben, H.; Ragauskas, A.; Deng, Y., *BioEnergy Research* **2013**, *6* (4), 1183-1204.
39. Zhao, C.; Lercher, J. A., Catalytic Depolymerization and Deoxygenation of Lignin. 2013; pp 289-320.
40. Chakar, F. S.; Ragauskas, A. J., *Industrial Crops and Products* **2004**, *20* (2), 131-141.
41. Luo, Y.-R., BDEs of O-X bonds. In *Comprehensive Handbook of Chemical Bond Energies*, Luo, Y.-R., Ed. CRC Press: 2007; pp 255-368.
42. Zaheer, M.; Kempe, R., *ACS Catalysis* **2015**, *5* (3), 1675-1684.
43. Lu, J.; Wang, M.; Zhang, X.; Heyden, A.; Wang, F., *ACS Catalysis* **2016**, *6* (8), 5589-5598.
44. He, J.; Zhao, C.; Lercher, J. A., *Journal of the American Chemical Society* **2012**, *134* (51), 20768-20775.
45. Zhu, R.; Wang, B.; Cui, M.; Deng, J.; Li, X.; Ma, Y.; Fu, Y., *Green Chemistry* **2016**, *18* (7), 2029-2036.
46. Rahimi, A.; Ulbrich, A.; Coon, J. J.; Stahl, S. S., *Nature* **2014**, *515* (7526), 249-52.
47. Rahimi, A.; Azarpira, A.; Kim, H.; Ralph, J.; Stahl, S. S., *Journal of the American Chemical Society* **2013**, *135* (17), 6415-6418.
48. Lancefield, C. S.; Ojo, O. S.; Tran, F.; Westwood, N. J., *Angewandte Chemie International Edition* **2014**, *54* (1), 258-262.
49. Hanson, S. K.; Wu, R.; Silks, L. A. P., *Angewandte Chemie International Edition* **2012**, *51* (14), 3410-3413.
50. Wang, Y.; Wang, Q.; He, J.; Zhang, Y., *Green Chemistry* **2017**, *19* (13), 3135-3141.
51. Sergeev, A. G.; Hartwig, J. F., *Science* **2011**, *332* (6028), 439-443.
52. Huuska, M.; Rintala, J., *Journal of Catalysis* **1985**, *94* (1), 230-238.

53. Wenkert, E.; Michelotti, E. L.; Swindell, C. S., *Journal of the American Chemical Society* **1979**, *101* (8), 2246-2247.
54. Cornella, J.; Zarate, C.; Martin, R., *Chemical Society Reviews* **2014**, *43* (23), 8081-8097.
55. Rosen, B. M.; Quasdorf, K. W.; Wilson, D. A.; Zhang, N.; Resmerita, A.-M.; Garg, N. K.; Percec, V., *Chemical Reviews* **2011**, *111* (3), 1346-1416.
56. Grobelny, Z., *European Journal of Organic Chemistry* **2004**, *2004* (14), 2973-2982.
57. Yu, D.-G.; Li, B.-J.; Shi, Z.-J., *Accounts of Chemical Research* **2010**, *43* (12), 1486-1495.
58. Pedley, J. B.; Naylor, R. D.; Kirby, S. P.; Pedley, J. B., *Thermochemical data of organic compounds*. Chapman and Hall: London; New York, 1986.
59. Mesganaw, T.; Garg, N. K., *Organic Process Research & Development* **2013**, *17* (1), 29-39.
60. Saper, N. I.; Hartwig, J. F., *Journal of the American Chemical Society* **2017**, *139* (48), 17667-17676.
61. Kelley, P.; Lin, S.; Edouard, G.; Day, M. W.; Agapie, T., *Journal of the American Chemical Society* **2012**, *134* (12), 5480-3.
62. Cornella, J.; Gómez-Bengoa, E.; Martin, R., *Journal of the American Chemical Society* **2013**, *135* (5), 1997-2009.
63. Chen, Z.; Zeng, H.; Girard Simon, A.; Wang, F.; Chen, N.; Li, C. J., *Angewandte Chemie International Edition* **2015**, *54* (48), 14487-14491.
64. Zeng, H.; Qiu, Z.; Domínguez-Huerta, A.; Hearne, Z.; Chen, Z.; Li, C.-J., *ACS Catalysis* **2017**, *7* (1), 510-519.
65. Zeng, H.; Cao, D.; Qiu, Z.; Li, C. J., *Angewandte Chemie International Edition* **2018**, *57* (14), 3752-3757.
66. Chatterjee, M.; Chatterjee, A.; Ishizaka, T.; Kawanami, H., *Catalysis Science & Technology* **2015**, *5* (3), 1532-1539.
67. He, J.; Zhao, C.; Mei, D.; Lercher, J. A., *Journal of Catalysis* **2014**, *309*, 280-290.
68. Shimizu, K.; Miki, K.; Saitou, I., *Fuel* **1997**, *76* (1), 23-27.
69. Penninger, J. M. L.; Kersten, R. J. A.; Baur, H. C. L., *The Journal of Supercritical Fluids* **1999**, *16* (2), 119-132.
70. Furimsky, E., *Applied Catalysis A: General* **2000**, *199* (2), 147-190.
71. Gao, F.; Webb, J. D.; Hartwig, J. F., *Angewandte Chemie International Edition* **2016**, *55* (4), 1474-8.
72. Wang, X.; Rinaldi, R., *Energy & Environmental Science* **2012**, *5* (8), 8244-8260.
73. Wang, X.; Rinaldi, R., *Angewandte Chemie International Edition* **2013**, *52* (44), 11499-503.
74. Fedorov, A.; Toutov, A. A.; Swisher, N. A.; Grubbs, R. H., *Chemical Science* **2013**, *4* (4), 1640-1645.
75. Nichols, J. M.; Bishop, L. M.; Bergman, R. G.; Ellman, J. A., *Journal of the American Chemical Society* **2010**, *132* (36), 12554-12555.
76. Sergeev, A. G.; Webb, J. D.; Hartwig, J. F., *Journal of the American Chemical Society* **2012**, *134* (50), 20226-20229.
77. Zhang, J.; Teo, J.; Chen, X.; Asakura, H.; Tanaka, T.; Teramura, K.; Yan, N., *ACS Catalysis* **2014**, *4* (5), 1574-1583.
78. Song, Q.; Wang, F.; Cai, J.; Wang, Y.; Zhang, J.; Yu, W.; Xu, J., *Energy & Environmental Science* **2013**, *6* (3), 994.

79. Molinari, V.; Giordano, C.; Antonietti, M.; Esposito, D., *Journal of the American Chemical Society* **2014**, *136* (5), 1758-1761.
80. Matson, T. D.; Barta, K.; Iretskii, A. V.; Ford, P. C., *Journal of the American Chemical Society* **2011**, *133* (35), 14090-14097.
81. Barta, K.; Ford, P. C., *Accounts of Chemical Research* **2014**, *47* (5), 1503-1512.
82. Shao, Y.; Xia, Q.; Dong, L.; Liu, X.; Han, X.; Parker, S. F.; Cheng, Y.; Daemen, L. L.; Ramirez-Cuesta, A. J.; Yang, S.; Wang, Y., *Nature Communications* **2017**, *8*, 16104.
83. Wu, H.; Song, J.; Xie, C.; Wu, C.; Chen, C.; Han, B., *ACS Sustainable Chemistry & Engineering* **2018**, *6* (3), 2872-2877.
84. Konnerth, H.; Zhang, J.; Ma, D.; Prechtel, M. H. G.; Yan, N., *Chemical Engineering Science* **2015**, *123*, 155-163.
85. Siskin, M.; Katritzky, A. R.; Balasubramanian, M., *Energy & Fuels* **1991**, *5* (5), 770-771.
86. Katritzky, A. R.; Barcock, R. A.; Balasubramanian, M.; Greenhill, J. V.; Siskin, M.; Olmstead, W. N., *Energy & Fuels* **1994**, *8* (2), 487-497.
87. Penninger, J. M. L.; Kersten, R. J. A.; Baur, H. C. L., *The Journal of Supercritical Fluids* **2000**, *17* (3), 215-226.
88. Varga, T. R.; Fazekas, Z.; Ikeda, Y.; Tomiyasu, H., *The Journal of Supercritical Fluids* **2002**, *23* (2), 163-167.
89. Roberts, V. M.; Knapp, R. T.; Li, X.; Lercher, J. A., *ChemCatChem* **2010**, *2* (11), 1407-1410.
90. Luo, Z.; Wang, Y.; He, M.; Zhao, C., *Green Chemistry* **2016**, *18* (2), 433-441.
91. Maegawa, T.; Akashi, A.; Yaguchi, K.; Iwasaki, Y.; Shigetsura, M.; Monguchi, Y.; Sajiki, H., *Chemistry – A European Journal* **2009**, *15* (28), 6953-6963.
92. Cui, X.; Surkus, A. E.; Junge, K.; Topf, C.; Radnik, J.; Kreyenschulte, C.; Beller, M., *Nature Communications* **2016**, *7*, 11326.
93. Zhao, C.; Kasakov, S.; He, J.; Lercher, J. A., *Journal of Catalysis* **2012**, *296*, 12-23.
94. Kasakov, S.; Zhao, C.; Baráth, E.; Chase, Z. A.; Fulton, J. L.; Camaioni, D. M.; Vjunov, A.; Shi, H.; Lercher, J. A., *Chemistry – A European Journal* **2015**, *21* (4), 1567-1577.
95. Song, W.; Liu, Y.; Barath, E.; Zhao, C.; Lercher, J. A., *Green Chemistry* **2015**, *17* (2), 1204-1218.
96. Teles, C. A.; Rabelo-Neto, R. C.; de Lima, J. R.; Mattos, L. V.; Resasco, D. E.; Noronha, F. B., *Catalysis Letters* **2016**, *146* (10), 1848-1857.
97. Zhuang, L.; Li, H.; Dai, W.; Qiao, M., *Chemistry Letters* **2003**, *32* (11), 1072-1073.
98. Yoon, Y.; Rousseau, R.; Weber, R. S.; Mei, D.; Lercher, J. A., *Journal of the American Chemical Society* **2014**, *136* (29), 10287-98.
99. Liu, H.; Jiang, T.; Han, B.; Liang, S.; Zhou, Y., *Science* **2009**, *326* (5957), 1250-1252.
100. He, J.; Zhao, C.; Lercher, J. A., *Journal of Catalysis* **2014**, *309*, 362-375.
101. Liu, X.; An, W.; Turner, C. H.; Resasco, D. E., *Journal of Catalysis* **2018**, *359*, 272-286.
102. Zhao, C.; He, J.; Lemonidou, A. A.; Li, X.; Lercher, J. A., *Journal of Catalysis* **2011**, *280* (1), 8-16.
103. Foster, A. J.; Do, P. T. M.; Lobo, R. F., *Topics in Catalysis* **2012**, *55* (3), 118-128.
104. Zhao, C.; Camaioni, D. M.; Lercher, J. A., *Journal of Catalysis* **2012**, *288*, 92-103.

105. Badawi, M.; Paul, J.-F.; Payen, E.; Romero, Y.; Richard, F.; Brunet, S.; Popov, A.; Kondratieva, E.; Gilson, J.-P.; Mariey, L.; Travert, A.; Maugé, F., *Oil & Gas Science and Technology - Revue d'IFP Energies nouvelles* **2013**, 68 (5), 829-840.
106. Odebunmi, E. O.; Ollis, D. F., *Journal of Catalysis* **1983**, 80 (1), 56-64.
107. Filley, J.; Roth, C., *Journal of Molecular Catalysis A: Chemical* **1999**, 139 (2), 245-252.
108. Kim, D. I.; Allen, D. T., *Industrial & Engineering Chemistry Research* **1994**, 33 (12), 2942-2945.
109. Nie, L.; de Souza, P. M.; Noronha, F. B.; An, W.; Sooknoi, T.; Resasco, D. E., *Journal of Molecular Catalysis A: Chemical* **2014**, 388-389, 47-55.
110. Nie, L.; Resasco, D. E., *Journal of Catalysis* **2014**, 317, 22-29.
111. Hensley, A. J. R.; Wang, Y.; McEwen, J.-S., *ACS Catalysis* **2015**, 5 (2), 523-536.



## Chapter 2 Palladium Catalyzed Hydrolytic Cleavage of Aromatic C-O Bonds

*Palladium catalyzes reductive hydrolytic cleavage of aromatic ether C–O bonds with high selectivities via a hitherto unconsidered mechanism involving partial hydrogenation of the phenyl group to a vinylic ether that rapidly adds water to form a hemiacetal which then undergoes elimination to cyclohexanone and phenol/alkanol products.*

---

This chapter is based on the article: Wang, M. et al. Palladium-Catalyzed Hydrolytic Cleavage of Aromatic C–O Bonds, *Angewandte Chemie International Edition* 2017, 56 (8), 2110-2114. Copyright (2017), with permission from John Wiley and Sons and Copyright Clearance Center. (license number: 4395600214446) M. W. designed and performed the experiments, did the data analysis and wrote the manuscript. H. S., D. M. C. and J.A.L. contributed with discussion of results and with correction of the manuscript.

## 2.1 Introduction

Catalytic cleavage of C-O bonds in aromatic ethers is an important step for the conversion of oxygen-rich lignocellulosic plant biomass to deoxygenated fuels and commercial chemicals<sup>1-5</sup> and is challenging because of the strength and stability of these linkages.<sup>6-11</sup> Cleavage of C-O bonds can occur via oxidation,<sup>12-13</sup> transfer hydrogenation,<sup>14-15</sup> hydrogenolysis,<sup>16-19</sup> hydrolysis/solvolytic<sup>20-21</sup> and radical-mediated<sup>22</sup> pathways, among others.<sup>3, 23</sup> Hydrogenolytic cleavage of strong aryl C-O bonds over heterogeneous metal catalysts requires high temperatures and H<sub>2</sub> pressures and occurs along with arene reduction.<sup>1, 11</sup> In a recent breakthrough, Hartwig and co-workers used homogeneous nickel complexes<sup>17</sup> in the presence of NaO<sup>t</sup>Bu base to catalyze selective cleavage of aryl C-O bonds at relatively mild condition in *m*-xylene solvent, without hydrogenating the arene rings and cleaving aliphatic C-O bonds. The reaction could also be accomplished using Ni nanoparticles.<sup>18-19</sup> Supported Ni or NiM (M = Ru, Rh, Au and Pd) bimetallic catalysts can catalyze this cleavage at significantly higher rates in water, but always lead also to some extent of ring saturation.<sup>16, 24-25</sup>

Hydrolysis of the aromatic C-O bond is known to be challenging, requiring harsh conditions such as using water near or above its supercritical point or strong acids/bases at high temperatures.<sup>26-27</sup> Supported Ni catalysts have been observed to promote hydrolysis in the presence of H<sub>2</sub>, although to a lesser extent than to hydrogenolysis.<sup>24</sup> He et al. hypothesized that hydrolysis occurs along the same reaction path as hydrogenolysis, with cleavage of ether bonds by Ni and subsequent addition of H· and OH· (from water dissociation).<sup>24</sup>

Here, we report that supported Pd catalysts are active and highly selective toward ether hydrolysis (> 80 % at complete conversion) at relatively mild temperatures (~200 °C) in aqueous phase with pressurized H<sub>2</sub> (typically 40 bar) present. As opposed to the conventional acid-catalyzed hydrolysis (ArOR + H<sub>2</sub>O → ArOH + ROH), we show that hydrolytic aryl ether cleavage on Pd occurs by a hitherto unconsidered mechanism requiring H<sub>2</sub> addition followed by the water attack. Hereafter, we define this pathway as “reductive hydrolysis” (C<sub>6</sub>H<sub>5</sub>OR + nH<sub>2</sub> + H<sub>2</sub>O → C<sub>6</sub>H<sub>(6+2n)</sub>O + ROH). Prior work with Pd catalysts has not identified this reaction, due to the use of non-aqueous<sup>28-29</sup> or water-alcohol<sup>30</sup> solvents (the alcohol serving as hydrogen donor instead of H<sub>2</sub>) which disfavor reductive hydrolysis making the hydrogenation and/or hydrolysis steps uncompetitive with hydrogenolysis.

## 2.2 Experimental

### 2.2.1 Chemicals and commercial catalysts

The chemicals were purchased from commercial suppliers and used as provided: diphenyl ether (Sigma-Aldrich, >99% GC assay), cyclohexyl phenyl ether (Sigma-Aldrich, >95% GC assay), 2-phenylethyl phenyl ether (Frinton Laboratories, >99% GC assay), n-butyl phenyl ether (Sigma-Aldrich, >99% GC assay), cyclohex-1-enyl phenyl ether (eNovation Chemicals, 95%), benzene (Sigma-Aldrich, >99.5% GC assay), phenol (Sigma-Aldrich, >99% GC assay), cyclohexanone (Sigma-Aldrich, >99% GC assay), cyclohexanol (Sigma-Aldrich, >99% GC assay), dichloromethane (Sigma-Aldrich, >99.5% GC assay), 5 wt. % Pd/C (Sigma-Aldrich), 5 wt. % Pt/C (Sigma-Aldrich), 64 wt. % Ni/SiO<sub>2</sub> (Strem Chemicals, Inc.), H<sub>2</sub> (>99.999%), N<sub>2</sub> (> 99.999%), H<sub>2</sub><sup>18</sup>O (Cambridge Isotope Laboratories, Inc., 99.9%) and normal H<sub>2</sub>O (Milli-Q, ultrapure water dispenser system).

The dispersion of the 5 wt. % Pd/C is 31 % as measured by H<sub>2</sub> chemisorption.<sup>31</sup> The 0.2-wt. % Pd/C catalyst was prepared by mixing 0.1 g of the 5 wt. % Pd/C with 2.4 g activated carbon (Sigma-Aldrich, Darco®, 20-40 mesh), manually stirring and shaking the mixture for 3 hours to promote homogeneity.

### 2.2.2 Catalyst testing

The detailed reaction conditions are described in the figure captions and table footnotes. Typically, the reactions were carried out in a Parr autoclave reactor (Series 4848, 300 mL) in the presence of H<sub>2</sub> or N<sub>2</sub>. First, the ether, catalyst and solvent (water or decalin, 80 mL) were added into the Parr reactor at room temperature. After the reactor was flushed with H<sub>2</sub> or N<sub>2</sub> three times, the autoclave was pressurized with H<sub>2</sub> or N<sub>2</sub>, and the reaction was conducted at a certain temperature with a stirring speed of 700 rpm. Although the reduced metal catalysts had been exposed to air during storage, the facile reduction of oxidized Pd overlayers under reaction conditions<sup>31</sup> during heat-up ensured that reactions should be exclusively catalyzed by metallic Pd. After the reaction, the reactor (300 mL Parr reactor or 2 mL cell) was quenched to ambient temperature by an ice/water mixture, and the contents in the reactor were extracted using dichloromethane and analyzed by GC-MS, i.e., an Agilent 7890A GC equipped with a HP-5MS 25 m × 0.25 μm (i.d.) column and coupled with Agilent 5975C MS. 1,3-Dimethoxybenzene was used as an internal standard for quantification purposes. The carbon balances for all the reported experiments were 90 ± 5%. The turnover frequency (TOF) was calculated from conversion < 20 % and based on the number of surface Pd atoms measured by H<sub>2</sub> chemisorption.

For experiments using isotopically labeled substrates, a 2 mL small reactor cell<sup>31</sup> made of 316-type stainless steel was used, where the ether (50 mg), catalyst (1.0 mg) and water (1 mL) were loaded. Then

the cell was purged and filled by H<sub>2</sub> for five cycles at room temperature. The closed cell was pressurized with 40 bar of hydrogen, heated to 190 °C, and the solution was stirred by a Teflon-coated magnetic stir bar. After the reaction, the reactor (300 mL Parr reactor or 2 mL cell) was quenched to ambient temperature by an ice/water mixture, and the contents in the reactor were extracted using dichloromethane and analyzed by GC-MS.

Because benzene and cyclohexane are generated only by hydrogenolysis (no cleavage of aromatic and aliphatic C-OH), the C-based selectivity of hydrogenolysis is twice the summed selectivity of benzene and cyclohexane. The selectivity to hydrolysis is calculated by subtracting the selectivities to hydrogenolysis and hydrogenation from 100%.

## 2.3 Result and discussion

### 2.3.1 Kinetic studies of supported palladium catalysts

Diphenyl ether was first tested as the simplest diaryl ether model that contains one of the strongest structural links in lignin, the 4-O-5 type linkage (bond dissociation energy: 314 kJ·mol<sup>-1</sup>).<sup>1, 32</sup> The pathways for C-O bond cleavage of diphenyl ethers are broadly classified into hydrogenation, hydrogenolysis and hydrolysis (reductive or non-reductive). Note that not all hydrogenation events are counted towards the “hydrogenation” category. Here, “hydrogenation” is limited to reactions that saturate the aromatic rings without changing the molecular backbone (i.e., cyclohexyl phenyl ether and dicyclohexyl ether). The kinetic primary products from hydrogenolysis are benzene and phenol (1:1), while two phenol molecules can be generated from non-reductive hydrolysis of one ether molecule, via conventional hydrolysis<sup>26-27</sup> or via the path proposed for Ni.<sup>24</sup>

As we mentioned in Chapter 1, we firstly evaluated three different supported metal catalysts (Pd/C, Pt/C, Ni/SiO<sub>2</sub>) in water at 40 bar H<sub>2</sub> (entry 1, 6 and 7, Table 2-1). The dominant pathway was reductive hydrolysis for Pd (80 - 88 %), hydrogenolysis for Pt (40 %) and Ni (60 %) at quantitative conversions of diphenyl ether (selectivities given as % carbon unless noted otherwise). The strong preference for reductive hydrolysis and small extents of hydrogenolysis were confirmed as intrinsic characteristics of Pd by using other supported metallic Pd catalysts (e.g., Pd/Al<sub>2</sub>O<sub>3</sub> and 10 wt. % Pd/C, entry 2 and 3, Table 2-1).

The distribution of products was independent of the amount of Pd/C over a wide range of diphenyl ether: Pd ratios (100-44000). Besides hydrolysis of diphenyl ether also can be catalyzed by acid in harsh conditions (1 g of ether, 1 g of 15% phosphoric acid, 315 C and 72 h),<sup>26</sup> we proved the reductive

hydrolysis over Pd was not acid assisted by control experiments. Adding phosphoric acid together with Pd/C only changed the reactivity and selectivity of the reaction marginally (Figure 2-1), indicating that acid-catalyzed pathways do not contribute to the observed reductive hydrolysis of diphenyl ether on metals at 200 °C.

**Table 2-1. Reactions of diphenyl ether.<sup>[a]</sup>**

Entry	Catalyst	Solvent and atmosphere	Carbon selectivity <sup>[b]</sup> , %		
			Hydrogenolysis	Hydrolysis	Hydrogenation
1	5 wt. % Pd/C	H <sub>2</sub> O, H <sub>2</sub>	2	88	10
2	5 wt. % Pd/Al <sub>2</sub> O <sub>3</sub>	H <sub>2</sub> O, H <sub>2</sub>	4	80	16
3	10 wt. % Pd/C	H <sub>2</sub> O, H <sub>2</sub>	2	88	10
4	5 wt. % Pd/C	Decalin, H <sub>2</sub>	3	-	97
5	5 wt. % Pd/C	H <sub>2</sub> O, N <sub>2</sub>			
6	Pt/C	H <sub>2</sub> O, H <sub>2</sub>	40	30	30
7	Ni/SiO <sub>2</sub>	H <sub>2</sub> O, H <sub>2</sub>	60	38	2

<sup>[a]</sup> Reaction conditions: from entry 1 to 7, reactant was diphenyl ether (1.70 g), catalyst was 10.0 mg 5 wt. % Pd/C, 10.0 mg 5 wt. % Pd/Al<sub>2</sub>O<sub>3</sub>, 10.0 mg 10 wt. % Pd/C, 10.0 mg 5 wt. % Pt/C or 300 mg 64 wt.% Ni/SiO<sub>2</sub>, solvent (80 ml), atmosphere (40 bar gauge pressure of hydrogen at room temperature or 4 bar of nitrogen), temperature was 200 °C, stirring at 700 rpm, reaction time was 2, 12, 1, 2, 12, 0.5, 12 hours respectively. <sup>[b]</sup> Calculated at >95% conversion: hydrogenolysis = 2×(cyclohexane+benzene); hydrolysis = (phenol+cyclohexanone+cyclohexanol)-hydrogenolysis; hydrogenation = (phenyl cyclohexyl ether + dicyclohexyl ether).

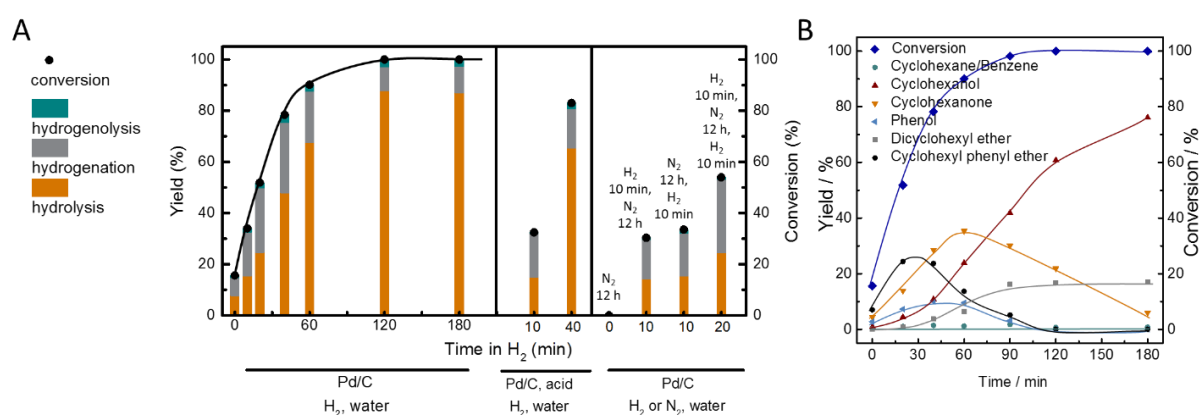


**Figure 2-1. (A) Different path yields and conversion of diphenyl ether at different reaction times in a number of control experiments. (B) Product distribution curves from the reaction of diphenyl ether corresponding to the left side of A.**

Reaction conditions: ether (1.70 g), 5 wt. % Pd/C (10.0 mg), water (80 ml), 30 mg 85%  $\text{H}_3\text{PO}_4$  (when used),  $\text{H}_2$  (40 bar gauge pressure at room temperature) or  $\text{N}_2$  (4 bar gauge pressure at room temperature), temperature (200 °C), stirring at 700 rpm. The time of reaction being 0 min means the reactor was cooled immediately when the temperature reached 200 °C, with the time spent on heat-up being 13-15 min.

The temporal evolution of products during the conversion of diphenyl ether on Pd/C in water was investigated at 190 °C (Figure 2-2A, Figure 2-3A). Cyclohexyl phenyl ether, phenol and cyclohexanone were the only primary kinetic products. Importantly, phenol and cyclohexanone were initially formed in a 1:1 yield ratio (Figure 2-4A), instead of two phenol molecules expected from conventional, non-reductive hydrolysis.<sup>27</sup> As phenol was hardly hydrogenated to cyclohexanone in the presence of diphenyl ether (Figure 2-2A, Table 2-2), we dismiss the possibility that hydrolysis of diphenyl ether first forms phenol, of which half is, hydrogenated on the Pd surface to cyclohexanone. The yields of these products increased linearly for conversions up to 20 %, with constant selectivities of 50 % cyclohexyl phenyl ether, 25 % phenol and 25 % cyclohexanone. Thus, the initial selectivities toward reductive hydrolysis and hydrogenation were nearly 50 % and 50 %, respectively (Figure 2-4). As the reaction proceeded, the yield of cyclohexyl phenyl ether increased to a maximum of 17 % and then decreased to zero at 100 % conversion (Figure 2-2A). The selectivities to cyclohexanone, cyclohexanol and dicyclohexyl ether increased, at the expense of phenol and cyclohexyl phenyl ether. At 900 min, the selectivities to the hydrogenation and reductive hydrolysis products became: 47 % cyclohexanone, 25 % cyclohexanol, 17 % phenol, and 8 % dicyclohexyl ether. Hydrogenolysis (cyclohexane and benzene) remained low (2-3%) during the entire course of reaction.

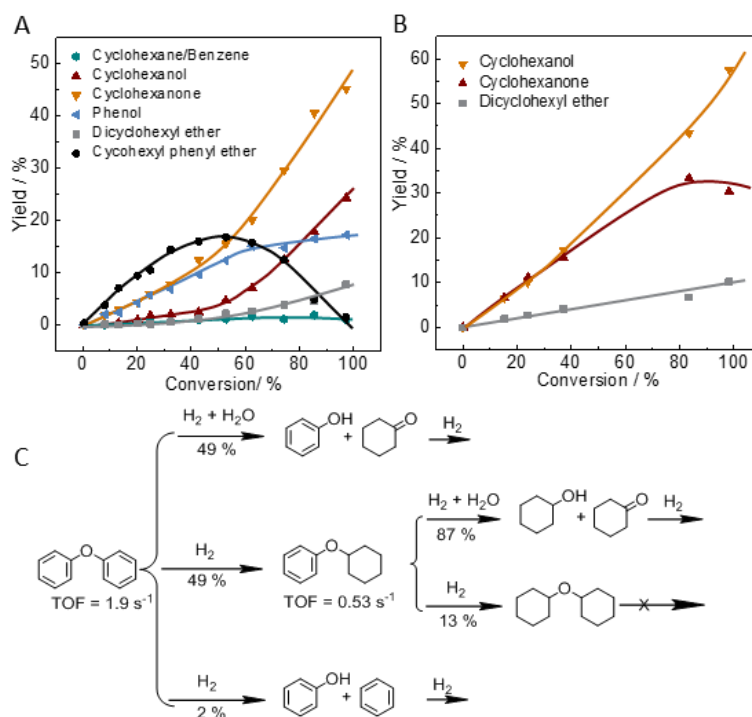


**Figure 2-2. Product distribution from the reaction of diphenyl ether (A) and cyclohexyl phenyl ether (B) over Pd/C as a function of conversion. (C) Reaction pathways and selectivities of diphenyl ether.**

Reaction conditions for (A): diphenyl ether (1.70 g, 0.010 mol), 0.2 wt % Pd/C (40.0 mg,  $2.3 \times 10^{-7}$  mol of  $\text{Pd}_{\text{surf}}$ , prepared by diluting the 5 wt. % Pd/C with activated carbon),  $\text{H}_2\text{O}$  (80 mL), hydrogen 40 bar, 190 °C, stirring at 700 rpm, time (0 ~ 900 min) and for (B): cyclohexyl phenyl ether (0.18 g, 0.001 mol), 0.2 wt % Pd/C (30.0 mg,  $1.7 \times 10^{-7}$  mol of  $\text{Pd}_{\text{surf}}$ ),  $\text{H}_2\text{O}$  (80 mL), hydrogen 40 bar, 190 °C, stirring at 700 rpm, time (0 ~ 540 min). The corresponding yield-time plots are shown in Figure 2-3. The TOF of cyclohexyl phenyl ether was calculated from separate experiments with cyclohexyl phenyl ether.

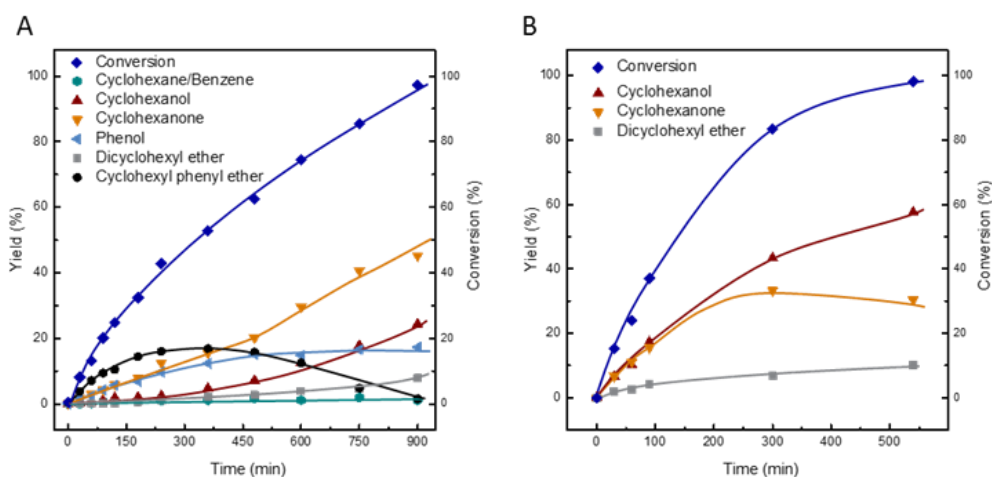


**Figure 2-3. The corresponding yield-time plots of Figure 2-2. (A) Diphenyl ether. (B) Cyclohexyl phenyl ether.**

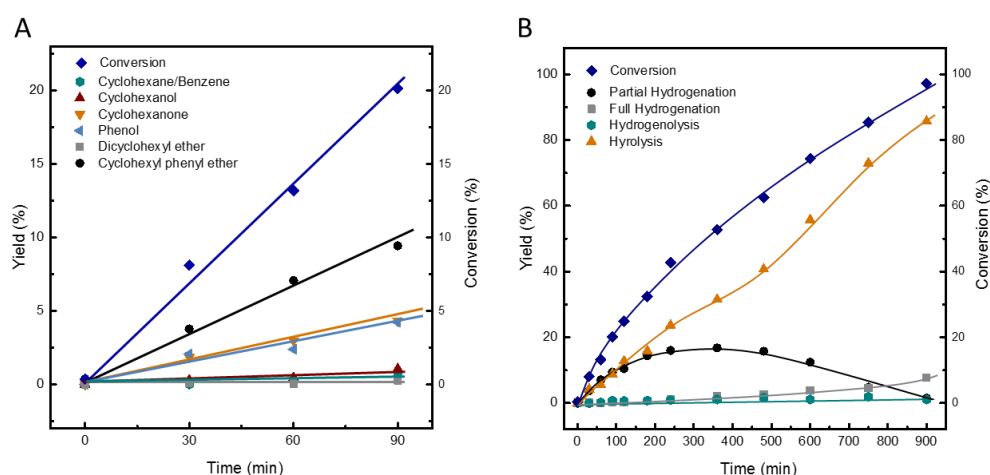


**Figure 2-4. (A) Initial part of the product distribution curve of diphenyl ether in Figure 2-2. (B) Different path yields calculated from the product yields of diphenyl ether shown in Figure 2-2, with partial hydrogenation referring to cyclohexyl phenyl ether and full hydrogenation referring to dicyclohexyl ether.**

**Table 2-2. Control reaction of phenol and diphenyl ether on Pd/C<sup>[a]</sup>.**

Entry	Reactant	Conversion (%)	TOF <sup>[b]</sup> (s <sup>-1</sup> )
1	0.010 mol diphenyl ether	8.1	1.9
2	0.020 mol phenol	8.4	4.0
3	0.010 mol diphenyl ether + 0.010 mol phenol	8.0 <sup>[c]</sup> ND <sup>[d]</sup>	1.9 <sup>[c]</sup> ND <sup>[d]</sup>

<sup>[a]</sup> Reaction condition: reactant, H<sub>2</sub>O (80 mL), 0.2 wt.% Pd/C (40.0 mg,  $2.3 \times 10^{-7}$  mol of Pd<sub>surf.</sub>), 190 °C, 40 bar H<sub>2</sub>, time (30 min), stirring at 700 rpm. <sup>[b]</sup> The turnover frequency (TOF) was calculated based on the number of surface Pd atoms measured by H<sub>2</sub> chemisorption. <sup>[c]</sup> For diphenyl ether. <sup>[d]</sup> For phenol, ND means none detected.

The conversion pathways of cyclohexyl phenyl ether were explored independently (Figure 2-2B). The major products were cyclohexanol, cyclohexanone and dicyclohexyl ether during the entire 540-min reaction, with negligible yields of phenol, benzene and cyclohexane. The initial conversion rate of cyclohexyl phenyl ether (TOF = 0.53 s<sup>-1</sup>) was lower than that of diphenyl ether (TOF = 1.9 s<sup>-1</sup>). The selectivities toward reductive hydrolysis and hydrogenation pathways were relatively constant at 87 % and 13 %, respectively. Under the same conditions, however, no reactivity of dicyclohexyl ether was observed. Thus, the pathways for C-O bond cleavage of diphenyl ethers are summarized in Figure 2-2C, accounting for the remarkable increase in reductive hydrolysis with reaction time (Figure 2-4B). As was for diphenyl ether, the primary products from Pd-mediated reductive hydrolysis of cyclohexyl phenyl ether were cyclohexanone and cyclohexanol (1:1), in contrast to cyclohexanol and phenol from conventional hydrolysis.



To better understand the high selectivity to ether hydrolysis on Pd/C, we also performed the reactions in decalin (H<sub>2</sub> atmosphere) and in water (N<sub>2</sub> atmosphere). When decalin was used as the solvent, hydrogenation of the aromatic rings accounted for 97 % selectivity. C<sub>6</sub>-oxygenates were produced in exactly the same quantity as the sum of benzene and cyclohexane, apparently as a result of the lack of water to initiate hydrolysis pathways.

Reactions did not occur in water under 4 bar N<sub>2</sub> even after 12 h (entry 5, Table 2-1). In a control experiment (Figure 2-1), where the reaction mixture (ether, Pd/C, water) was first heated at 200 °C for 12 h under N<sub>2</sub> and then reacted for another 10 min under H<sub>2</sub>, the conversion and product distribution were identical to those obtained without the first 12 h under N<sub>2</sub>. In another control experiment with a reversed order of operation, where the mixture was first reacted at 200 °C for 10 min under H<sub>2</sub> and then heated for another 12 h under N<sub>2</sub>, hardly any reactions took place while under N<sub>2</sub> (Figure 2-1). Neither hydrogenation nor hydrogenolysis occurred in absence of H<sub>2</sub>. The fact that even hydrolysis did not proceed in the absence of H<sub>2</sub> suggests that water does not directly attack the aryl C–O bond of diphenyl ether to initiate hydrolysis. The results of these control experiments further indicate that no reactive intermediate forms and accumulates in the absence of H<sub>2</sub> and that the reactive intermediate for hydrolysis is also not any of the detectable products. Most likely, hydrolysis of the ether bond has to follow partial hydrogenation of diphenyl ether to undetected reactive species, existing in amounts below detection limit.

### 2.3.2 Control experiments of 1-phenoxy-cyclohexene

One of such partially hydrogenated, highly reactive intermediates could be cyclohex-1-enyl phenyl ether, which was tested as the starting substrate under a variety of conditions (Table 2-3). In contrast to diphenyl ether, this vinylic aryl ether did not undergo hydrogenation, but was hydrolyzed rapidly, forming equimolar cyclohexanone and phenol (Eq. 2-1) with a total selectivity of 99.9 % at all conditions tested (with or without Pd/C, H<sub>2</sub> or N<sub>2</sub>). The reaction occurred already considerably in water at 100 °C without any external catalyst, but was significantly promoted by the presence of Pd/C (Table 2-3). At 190 °C, hydrolysis of cyclohex-1-enyl phenyl ether was also much faster, requiring no catalyst or H<sub>2</sub>, than the conversion of diphenyl ether.

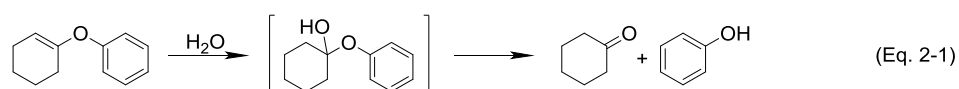


**Table 2-3. Reaction of cyclohex-1-enyl phenyl ether.<sup>[a]</sup>**

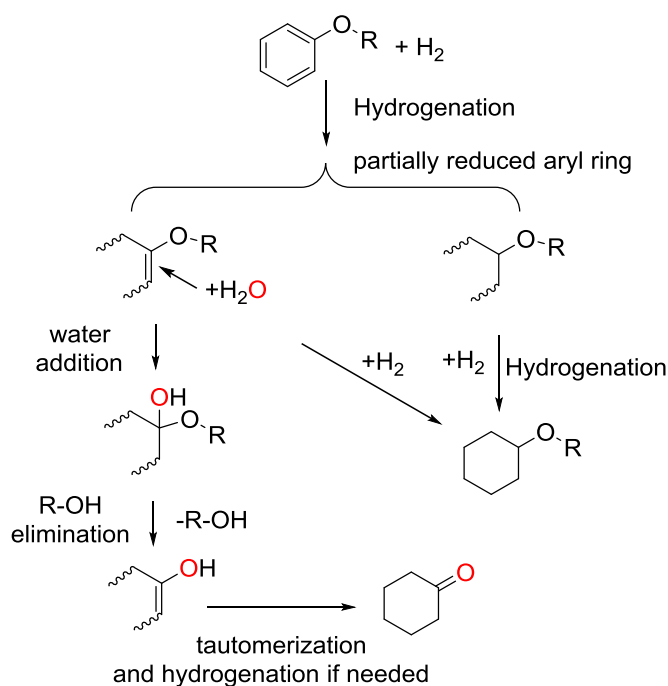
Reaction	100 °C			190 °C		
Catalyst (mg)	0	15	15	0	4	4
	H <sub>2</sub>	N <sub>2</sub>	H <sub>2</sub>	H <sub>2</sub>	N <sub>2</sub> <sup>b</sup>	H <sub>2</sub>
Time (min)	60			10		
Conversion (%)	13	85	94	72	98	74
Selectivity (%)	Hydrolysis	99.9	99.9	99.9	99.9	99.9
	Dehydrogenation	~ 0.1	~ 0.1	< 0.1	~ 0.1	~ 0.1

<sup>[a]</sup> Reaction condition: ether (0.2 g), H<sub>2</sub>O (80 mL), 0.2 wt.% Pd/C, 100 or 190 °C, 40 bar H<sub>2</sub> or 4 bar N<sub>2</sub>, stirring at 700 rpm. <sup>[b]</sup> It takes 25 min to heat up from room temperature to 190 °C in the presence of N<sub>2</sub>, while taking 15 min in the presence of H<sub>2</sub>.

### 2.3.3 Hypothesis of the reaction mechanism of reductive hydrolysis

Taken together, the above results lead us to propose a novel pathway for the reductive hydrolysis of diphenyl ether on Pd in the aqueous phase (R = Ph, Figure 2-5). Stepwise hydrogen addition events first occur at one of the aromatic rings forming two types of ether intermediates. In one, the ether oxygen is connected to a vinylic carbon (e.g., cyclohex-1-enyl phenyl ether), while in the other, the ether oxygen is connected to an alkyl carbon (e.g., cyclohex-3-enyl phenyl ether). In principle, these intermediates can be further hydrogenated to stable ether products (cyclohexyl phenyl ether and dicyclohexyl ether). However as shown above, vinylic ether intermediates undergo almost exclusively hydrolysis.

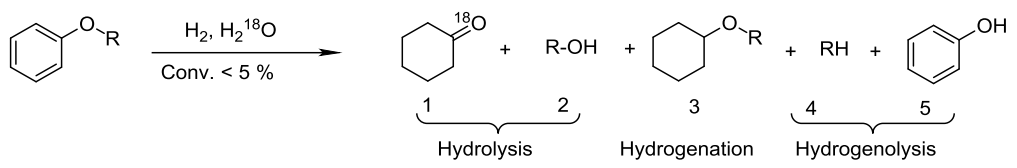
The hydrolysis of vinyl ethers in aqueous phase is known to occur even at ambient temperature, via rate-limiting protonation and fast water addition to form a hemiacetal; in the next fast step, the hemiacetal eliminates R-OH (one of the stable primary products) and forms an enol which quickly tautomerizes to a ketone.<sup>33</sup> In the case of diphenyl ether, such a mechanistic framework predicts equimolar formation of phenol (R-OH) and cyclohexanone along the initial reductive hydrolysis pathway, while for cyclohexyl phenyl ether, cyclohexanol (R-OH) and cyclohexanone will be the stable primary products from reductive hydrolysis, fully consistent with the experimental observations discussed above (Figure 2-2). Without partial hydrogenation of the aromatic ring, acid-catalyzed hydrolysis at the aryl C–O bonds cannot occur at these temperatures (e.g., 200 °C). On metals such as Pd, olefinic moieties are highly reactive under hydrogenating conditions, preventing direct chromatographic and spectroscopic observations of the partially hydrogenated intermediates (excepting cyclohexanone). Therefore, additional experiments were performed to provide evidence for the postulated reductive hydrolysis pathways.



**Figure 2-5.** Postulated mechanistic pathways for reductive hydrolysis of aryl ether on Pd surfaces. R = phenyl, cyclohexyl, phenylethyl, n-butyl in this work.

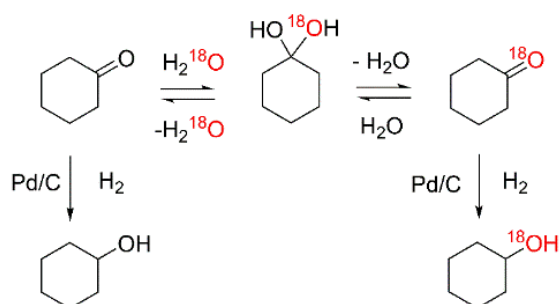
### 2.3.4 Isotope labelling experiments by $\text{H}_2^{18}\text{O}$

As diagrammed in Figure 2-5, the mechanism predicts that the initially formed cyclohexanone should contain oxygen exclusively from water while phenol should contain oxygen solely from the ether. This was confirmed by isotope labelling experiments using  $\text{H}_2^{18}\text{O}$  and unlabeled diphenyl ether. After one-half hour at 190 °C (<5% conversion; entry 1, Table 2-4) no  $^{18}\text{O}$  was incorporated into the phenol whereas the cyclohexanone had incorporated >90 %  $^{18}\text{O}$ . However, the observation of  $^{18}\text{O}$ -labeled cyclohexanone is not a sufficient proof for the hypothesis, since cyclohexanone was observed to also incorporate  $^{18}\text{O}$  under the same conditions presumably via rapid equilibration with the geminal diol (Figure 2-6).<sup>34</sup> On the other hand, the phenol being completely unlabeled is entirely consistent with the proposed mechanism. If, as an alternative mechanism, ether cleavage preceded  $\text{H}_2^{18}\text{O}$  addition or  $^{18}\text{OH}$ -addition (via dissociative water adsorption) to the phenyl and phenoxy fragments, half of the initially formed phenol would contain  $^{18}\text{O}$ , in contradiction with the observation.

**Table 2-4. Selectivities (mol. %) of initial products of aryl ethers catalyzed by Pd/C in  $^{18}\text{O}$  labeled water.<sup>[a]</sup>**


entry	R	1	2	3	4	5
1	Phenyl	31	26	41	1	1 <sup>[b]</sup>
2	Cyclohexyl	46	46	8	-	-
3 <sup>[c]</sup>	Phenylethyl	32	32	5	3	3
4	n-butyl	45	48	7	-	-

<sup>[a]</sup> Reaction conditions: ether (50.0 mg), 0.2 wt. % Pd/C (1.0 mg, prepared by diluting the 5 wt. % Pd/C with activated carbon), water ( $\text{H}_2^{18}\text{O}$ , 1.0 ml),  $\text{H}_2$  (40 bar at room temperature), 190 °C, 0.5 h. <sup>[b]</sup> Since **2** and **5** were identical in this case, the selectivity to phenol from hydrogenolysis was inferred from that of **4**. <sup>[c]</sup> The selectivity toward hydrogenation of the R-group (phenylethyl) was 25%.

**Figure 2-6. Control experiment of cyclohexanone in 50 wt%  $^{18}\text{O}$  labeled water.**

Reaction condition: cyclohexanone (50.0 mg), 0.2 wt. % Pd/C (1.0 mg), water (1.0 ml), hydrogen (40 bar gauge pressure at room temperature), temperature (190 °C), 0.5 h. Conversion of cyclohexanone to cyclohexanol was 5 %; the  $^{18}\text{O}/^{16}\text{O} \sim 1$  in both the recovered cyclohexanone and the cyclohexanol product, showing that oxygen exchange in cyclohexanone was fast compared to hydrogenation.

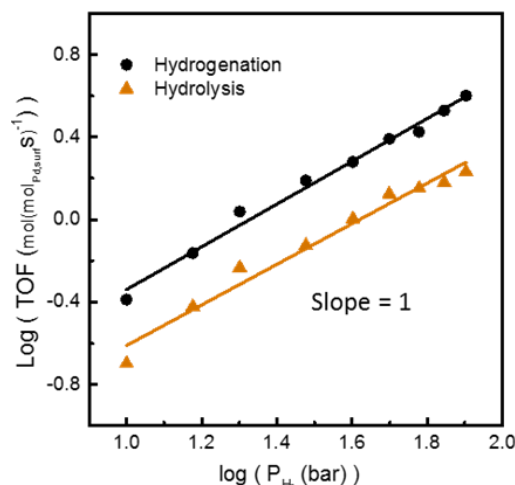


**Figure 2-7. Dependencies of the conversion rates of diphenyl ether on hydrogen partial pressure.**

Here, the hydrogenation was counted by summing the yields of cyclohexyl phenyl ether, phenol and cyclohexanone. The product distributions were obtained at conversions lower than 20 %. Reaction conditions: ether (1.70 g), 0.2 wt. % Pd/C (40.0 mg), water (8.0 ml), hydrogen (10 – 80 bar gauge pressure at room temperature), temperature (190 °C), 0.5 – 24 h, stirring at 700 rpm.

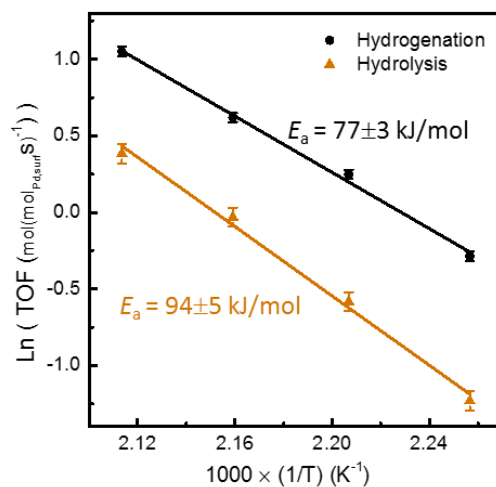


**Figure 2-8. Arrhenius plots [ $\ln(\text{TOF})$  vs  $1/T$ ] for the conversion of diphenyl ether.**

Reaction conditions: ether (1.70 g),  $\text{H}_2\text{O}$  (80 mL), 0.2 wt.% Pd/C (40.0 mg), 443–473 K, 4 MPa  $\text{H}_2$ , stirring at 700 rpm.

Additionally, we investigated the  $\text{H}_2$  pressure dependencies for hydrogenation and reductive hydrolysis pathways of diphenyl ether. Product selectivities did not change with  $\text{H}_2$  pressure. The rates of hydrogenation and reductive hydrolysis were both shown to be first order with respect to the  $\text{H}_2$  pressure (Figure 2-7). An identical  $\text{H}_2$  pressure dependency for hydrogenation and reductive hydrolysis is possible, as the conversion is proposed to be initiated by a series of common H-addition steps prior to

the branching of pathways (Figure 2-5). The disparate activation energies measured for the two pathways (Figure 2-8) clearly reject the possibility of a common rate-determining step (RDS). Additional insight comes from the constant reaction order in H<sub>2</sub> despite 8-fold variation in H<sub>2</sub> pressure (10-80 bar). Considering the stronger adsorption of ether and phenol than H-atoms on Pd surface,<sup>28, 35</sup> we conclude that the (sub)surface coverage of H is relatively low on Pd under the reaction conditions. At low H-coverages, the kinetic observations, i.e., reductive hydrolysis and hydrogenation pathways showing the same first order in H<sub>2</sub> but different activation energies, are consistent with a mechanistic scenario in which the second H-addition is the RDS for the hydrogenation pathway, while the RDS for reductive hydrolysis occurs after the addition of at least two hydrogen atoms (see Appendix for detailed derivations of rate expressions). DFT calculations are being undertaken to validate this hypothesis.

To explore the generality of the novel mechanistic framework, we performed reactions of aryl ethers (Ar-O-R) containing R-groups other than phenyl, i.e., cyclohexyl, 2-phenylethyl and *n*-butyl, all in H<sub>2</sub><sup>18</sup>O at conversions <5 % to minimize the impact of secondary reactions (entry 2-4, Table 2-4). All of these ethers produced cyclohexanone-<sup>18</sup>O and R-<sup>16</sup>OH as the initial products with a molar ratio of nearly 1:1, confirming that the mechanism depicted in Figure 2-5 also applies to these aryl ethers. Remarkably, reductive hydrolysis of ethers with C<sub>aromatic</sub>-O-C<sub>aliphatic</sub> linkages always occurred at the stronger aryl C-O bond, rather than the weaker aliphatic C-O bond, in contrast to the cleavage pattern observed for aryl alkyl ether on Ni/SiO<sub>2</sub> in the aqueous phase.<sup>24</sup> This should not be seen as a violation of the bond dissociation energy; instead, it is due to partial hydrogenation of the aromatic ring, leading to vinyl moieties that are much more reactive toward water attack.

## 2.4 Conclusions

In conclusion, we have demonstrated that Pd catalysts are active and highly selective (up to 90% at quantitative conversions) toward the reductive hydrolysis of diaryl and aryl alkyl ethers in aqueous phase at relatively mild conditions and exhibit very limited hydrogenolysis. We have identified a novel pathway for the Pd-catalyzed reductive hydrolysis of aryl ethers, which is initiated by partial hydrogenation of the arene ring to vinyl ether-type intermediates highly susceptible to water attack. This pathway contrasts the often postulated acid-catalyzed ether cleavage pathway which does not require H<sub>2</sub>. It is also distinct from the metal-mediated direct ether cleavage (without direct H<sub>2</sub> participation) followed by recombination of the fragments with surface H· and ·OH radicals from water dissociation at the metal surface.<sup>24</sup> We currently think the reason that Pd is better at hydrolysis than Ni or Pt is related to the activity of the metals to catalyze hydrogen addition to C=C bonds. Ni is the slowest in converting diphenyl ether, giving little hydrogenation product, whereas Pt is fastest at converting

diphenyl ether and gives the most dicyclohexyl ether. Future work will be directed toward exploring the effects of ring substituent and understanding the origin of the preference for reductive hydrolysis pathways on Pd.

## 2.5 Acknowledgements

This work was supported by the U.S. Department of Energy, Office of Science, Office of Basic Energy Sciences, Division of Chemical Sciences, Geosciences, and Biosciences. Portions of the work were performed at the William R. Wiley Environmental Molecular Science Laboratory, a national scientific user facility sponsored by the DOE's Office of Biological and Environmental Research located at Pacific Northwest National Laboratory, a multi-program national laboratory operated for DOE by Battelle Memorial Institute.

## 2.6 Appendix

### 2.6.1 Derivation of rate equations

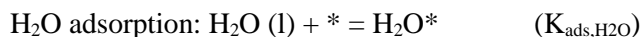
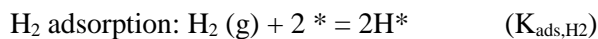
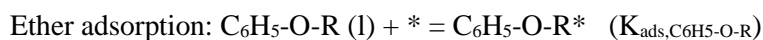
We derive a set of kinetic expressions that are consistent with the observed rate dependencies on H<sub>2</sub> pressure (1<sup>st</sup> order, Figure 2-7) and ether concentration (0<sup>th</sup> order, Table 2-5). We provided arguments in the main text that the coverage of H-adatoms is very low.

**Table 2-5. Reactant dependency of the conversion rates of diphenyl ether.** <sup>[a]</sup>

Mass (g)	TOF <sup>[b]</sup> (s <sup>-1</sup> )	
	Hydrogenation <sup>[c]</sup>	Reductive hydrolysis
0.2	1.76	0.92
0.46	1.58	0.75
0.85	1.65	0.87
1.7	1.86	0.97
3.42	1.61	0.83
5.1	1.78	0.81

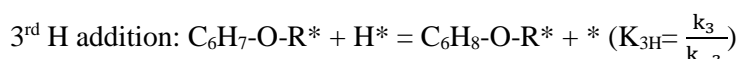
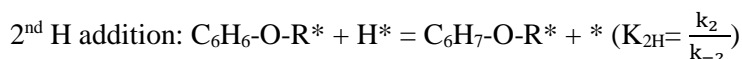
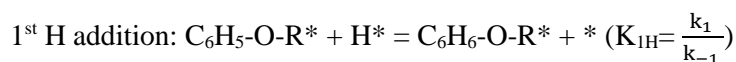
<sup>[a]</sup> Reaction condition: diphenyl ether, H<sub>2</sub>O (80 mL), 0.2 wt.% Pd/C (40.0 mg,  $2.3 \times 10^{-7}$  mol of Pd<sub>surf.</sub>), 190 °C, 40 bar H<sub>2</sub>, time (30 min), stirring at 700 rpm. <sup>[b]</sup> Turnover frequency (TOF) was calculated from conversion under 20 % and based on the number of surface Pd atoms measured by H<sub>2</sub> chemisorption. <sup>[c]</sup> The hydrogenation was counted by summing the yields of cyclohexyl phenyl ether, phenol and cyclohexanone.

1) Within the mechanistic framework proposed in Scheme 1 (main text), we first assume adsorption for reactants (ether and H<sub>2</sub>) and solvent (H<sub>2</sub>O) are quasi-equilibrated:



Assuming any of the above steps to be rate-determining does not lead to rate expressions consistent with the observed reaction orders.

2) Hydrogen-addition steps then follow to produce the highly reactive partially hydrogenated vinyl-type ether intermediates:

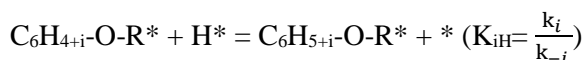


.....

....

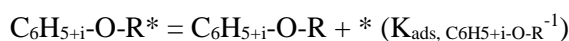
...

The general equation for i-th H addition can be written as:

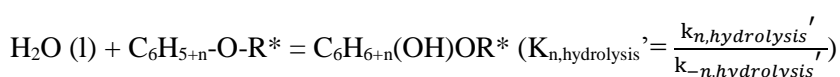


where  $k_i$  and  $k_{-i}$  are the forward and reverse rate constants for the i-th H addition step. Some of the steps are quasi-equilibrated or kinetically irrelevant, while some could be rate-determining.

3) Potentially, some of the ether intermediates (those with even numbers of H added) can desorb into the liquid phase, also assumed to be rapid and quasi-equilibrated:



4) Water (adsorbed or liquid phase) attack can potentially occur on any of the surface vinyl-type ether intermediates (i.e., water addition of the vinylic ethers to hemiacetal):





5) Hydrolyzed products (hemiacetal) then eliminate ROH, tautomerize and desorb from the surface. These steps are assumed to be rapid and kinetically irrelevant.

6) Applying site balance to all surface species, we have:

$$[*]_0 = [*] + [H^*] + [H_2O^*] + \Sigma[\text{Ether}^*]$$

where  $[*]_0$  is the total number of sites available at the surface, approximated as the number of exposed surface atoms determined by  $H_2$  chemisorption

At low conversions, the most abundant ether is the reactant, so it can be reasonably assumed that the following equation holds:

$$[*]_0 = [*] (1 + (K_{ads,H_2}[H_2])^{0.5} + K_{ads,H_2O}[H_2O] + K_{ads,C_6H_5-O-R}[C_6H_5-O-R])$$

The rate of the reaction equals to the rate of the rate-determining step (RDS):  $r = r_{rds}$

(i) If the RDS is one of the H-addition steps, the rate equation (for the (i+1)-th H-addition to be RDS) would be:

$$r = k_{i+1}[C_6H_{5+i}-O-R^*][H^*]$$

$$TOF = \frac{r}{[*]_0} = \frac{k_{i+1}K_{ads,C_6H_5-O-R}[C_6H_5-O-R](K_{1H}K_{2H}...K_{iH})(K_{ads,H_2}[H_2])^{0.5(i+1)}}{1 + (K_{ads,H_2}[H_2])^{0.5} + K_{ads,H_2O}[H_2O] + K_{ads,C_6H_5-O-R}[C_6H_5-O-R]}$$

(Eq. 2-2)

(ii) If the RDS is one of the water attack steps, the rate equation (for hydrolysis of the n-H-added vinylic ether intermediate) would be:

$$r = k_{n,hydrolysis}[C_6H_{5+n}-O-R^*][H_2O^*] \text{ (surface water attack)}$$

$$r = k_{n,hydrolysis}'[C_6H_{5+n}-O-R^*][H_2O] \text{ (liquid water attack)}$$

$$TOF = \frac{k_{n,hydrolysis}K_{ads,C_6H_5-O-R}[C_6H_5-O-R]K_{ads,H_2O}[H_2O](K_{1H}K_{2H}...K_{nH})(K_{ads,H_2}[H_2])^{0.5n}}{1 + (K_{ads,H_2}[H_2])^{0.5} + K_{ads,H_2O}[H_2O] + K_{ads,C_6H_5-O-R}[C_6H_5-O-R]}$$

(surface water attack, Eq. 2-3)

$$TOF = \frac{k_{n,hydrolysis}'K_{ads,C_6H_5-O-R}[C_6H_5-O-R][H_2O](K_{1H}K_{2H}...K_{nH})(K_{ads,H_2}[H_2])^{0.5n}}{1 + (K_{ads,H_2}[H_2])^{0.5} + K_{ads,H_2O}[H_2O] + K_{ads,C_6H_5-O-R}[C_6H_5-O-R]}$$

(liquid water attack, Eq. 2-4)

7) No appreciable change in the overall reaction order was observed when the pressure of  $H_2$  ( $[H_2]$ ) varied by a factor of 8, indicating that  $[H^*]$  is low and can be neglected from the denominator term, such that:

H-addition RDS:

$$\text{TOF} = \frac{r}{[*]_0} = \frac{k_{i+1}K_{\text{ads,C6H5-O-R}}[C_6H_5\text{-O-R}](K_{1H}K_{2H}\dots K_{iH})(K_{\text{ads,H}_2}[\text{H}_2])^{0.5(i+1)}}{1 + K_{\text{ads,H}_2\text{O}}[\text{H}_2\text{O}] + K_{\text{ads,C6H5-O-R}}[C_6H_5\text{-O-R}]}$$

(Eq. 2-5)

$$\text{TOF} = \frac{k_{\text{n,hydrolysis}}K_{\text{ads,C6H5-O-R}}[C_6H_5\text{-O-R}]K_{\text{ads,H}_2\text{O}}[\text{H}_2\text{O}](K_{1H}K_{2H}\dots K_{nH})(K_{\text{ads,H}_2}[\text{H}_2])^{0.5n}}{1 + K_{\text{ads,H}_2\text{O}}[\text{H}_2\text{O}] + K_{\text{ads,C6H5-O-R}}[C_6H_5\text{-O-R}]}$$

(surface water attack, Eq. 2-6)

$$\text{TOF} = \frac{k_{\text{n,hydrolysis}}'K_{\text{ads,C6H5-O-R}}[C_6H_5\text{-O-R}][\text{H}_2\text{O}](K_{1H}K_{2H}\dots K_{nH})(K_{\text{ads,H}_2}[\text{H}_2])^{0.5n}}{1 + K_{\text{ads,H}_2\text{O}}[\text{H}_2\text{O}] + K_{\text{ads,C6H5-O-R}}[C_6H_5\text{-O-R}]}$$

(liquid water attack, Eq. 2-7)

8) The measured reaction orders in H<sub>2</sub> were close to 1 for both hydrogenation and hydrolysis, but the activation energies were significantly different, indicating that the two pathways do not share the same RDS. For hydrogenation pathways, we consider that the second H-addition is the RDS (i = 1 in Equation 2-2). For hydrolysis, the RDS is hypothesized to be the water addition to the double bond in the vinylic ether. The dependence of rates on the mass of ether reactant (concentration is not presently known) suggests that empty site and surface adsorbed water are also much smaller in concentrations than ether-derived species.

## 2.7 References

1. Zakzeski, J.; Bruijninx, P. C. A.; Jongerius, A. L.; Weckhuysen, B. M., *Chemical Reviews* **2010**, *110* (6), 3552-3599.
2. Xu, C.; Arancon, R. A. D.; Labidi, J.; Luque, R., *Chemical Society Reviews* **2014**, *43* (22), 7485-7500.
3. Li, C.; Zhao, X.; Wang, A.; Huber, G. W.; Zhang, T., *Chemical Reviews* **2015**, *115* (21), 11559-11624.
4. Himmel, M. E.; Ding, S.-Y.; Johnson, D. K.; Adney, W. S.; Nimlos, M. R.; Brady, J. W.; Foust, T. D., *Science* **2007**, *315* (5813), 804-807.
5. Ragauskas, A. J.; Beckham, G. T.; Biddy, M. J.; Chandra, R.; Chen, F.; Davis, M. F.; Davison, B. H.; Dixon, R. A.; Gilna, P.; Keller, M.; Langan, P.; Naskar, A. K.; Saddler, J. N.; Tschaplinski, T. J.; Tuskan, G. A.; Wyman, C. E., *Science* **2014**, *344* (6185), 1246843.
6. Grobelny, Z., *European Journal of Organic Chemistry* **2004**, *2004* (14), 2973-2982.
7. Song, Q.; Wang, F.; Cai, J.; Wang, Y.; Zhang, J.; Yu, W.; Xu, J., *Energy & Environmental Science* **2013**, *6* (3), 994.
8. Besson, M.; Gallezot, P.; Pinel, C., *Chemical Reviews* **2014**, *114* (3), 1827-1870.
9. Cornella, J.; Zarate, C.; Martin, R., *Chemical Society Reviews* **2014**, *43* (23), 8081-8097.
10. Zaheer, M.; Kempe, R., *ACS Catalysis* **2015**, *5* (3), 1675-1684.
11. Furimsky, E., *Applied Catalysis A: General* **2000**, *199* (2), 147-190.
12. Bruijninx, P. C. A.; Weckhuysen, B. M., *Nature Chemistry* **2014**, *6* (12), 1035-1036.
13. Hanson, S. K.; Wu, R.; Silks, L. A. P., *Angewandte Chemie International Edition* **2012**, *51* (14), 3410-3413.
14. Nichols, J. M.; Bishop, L. M.; Bergman, R. G.; Ellman, J. A., *Journal of the American Chemical Society* **2010**, *132* (36), 12554-12555.
15. Ferrini, P.; Rinaldi, R., *Angewandte Chemie International Edition* **2014**, *53* (33), 8634-8639.
16. Zhang, J.; Teo, J.; Chen, X.; Asakura, H.; Tanaka, T.; Teramura, K.; Yan, N., *ACS Catalysis* **2014**, *4* (5), 1574-1583.
17. Sergeev, A. G.; Hartwig, J. F., *Science* **2011**, *332* (6028), 439-443.
18. Sergeev, A. G.; Webb, J. D.; Hartwig, J. F., *Journal of the American Chemical Society* **2012**, *134* (50), 20226-9.
19. Gao, F.; Webb, J. D.; Hartwig, J. F., *Angewandte Chemie International Edition* **2016**, *55* (4), 1474-8.
20. Huber, G. W.; Iborra, S.; Corma, A., *Chemical Reviews* **2006**, *106* (9), 4044-4098.
21. Chatterjee, M.; Chatterjee, A.; Ishizaka, T.; Kawanami, H., *Catalysis Science & Technology* **2015**, *5* (3), 1532-1539.
22. Son, S.; Toste, F. D., *Angewandte Chemie International Edition* **2010**, *49* (22), 3791-3794.
23. Fedorov, A.; Toutov, A. A.; Swisher, N. A.; Grubbs, R. H., *Chemical Science* **2013**, *4* (4), 1640-1645.
24. He, J.; Zhao, C.; Lercher, J. A., *Journal of the American Chemical Society* **2012**, *134* (51), 20768-20775.

25. Konnerth, H.; Zhang, J.; Ma, D.; Precht, M. H. G.; Yan, N., *Chemical Engineering Science* **2015**, *123*, 155-163.
26. Siskin, M.; Katritzky, A. R.; Balasubramanian, M., *Energy & Fuels* **1991**, *5* (5), 770-771.
27. Roberts, V. M.; Knapp, R. T.; Li, X.; Lercher, J. A., *ChemCatChem* **2010**, *2* (11), 1407-1410.
28. Lu, J.; Wang, M.; Zhang, X.; Heyden, A.; Wang, F., *ACS Catalysis* **2016**, *6* (8), 5589-5598.
29. Paone, E.; Espro, C.; Pietropaolo, R.; Mauriello, F., *Catalysis Science & Technology* **2016**, *6* (22), 7937-7941.
30. Galkin, M. V.; Sawadjoon, S.; Rohde, V.; Dawange, M.; Samec, J. S. M., *ChemCatChem* **2014**, *6* (1), 179-184.
31. Chase, Z. A.; Fulton, J. L.; Camaioni, D. M.; Mei, D.; Balasubramanian, M.; Pham, V.-T.; Zhao, C.; Weber, R. S.; Wang, Y.; Lercher, J. A., *The Journal of Physical Chemistry C* **2013**, *117* (34), 17603-17612.
32. Luo, Y.-R., BDEs of O–X bonds. In *Comprehensive Handbook of Chemical Bond Energies*, Luo, Y.-R., Ed. CRC Press: 2007; pp 255-368.
33. Kresge, A. J.; Sagatys, D. S.; Chen, H. L., *Journal of the American Chemical Society* **1977**, *99* (22), 7228-7233.
34. Taylor, P., Nucleophilic attack at the carbonyl group. In *Mechanism and synthesis*, Taylor, P., Ed. Cambridge, UK : Royal Society of Chemistry: 2006; pp 21-25.
35. Li, G.; Han, J.; Wang, H.; Zhu, X.; Ge, Q., *ACS Catalysis* **2015**, *5* (3), 2009-2016.

## Chapter 3 Palladium Catalyzed Reductive Insertion of Alcohols in Aryl Ether Bonds

*Reductive alcoholysis of aryl ethers catalyzed by palladium in alcoholic solvent is initiated by partial hydrogenation of the arene ring to an enol ether. Thus cleavage of the strong aryl C-O bond is achieved via methanol addition to the enol ether and R-OH elimination.*

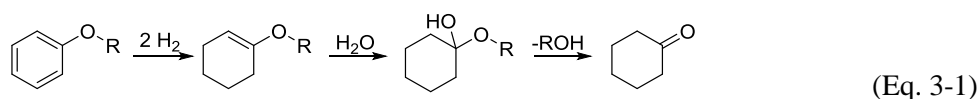
---

This chapter is based on the article: Wang, M. et al. Palladium-Catalyzed Reductive Insertion of Alcohols into Aryl Ether Bonds. *Angewandte Chemie International Edition* 2018, 57 (14), 3747-3751. Copyright (2018), with permission from John Wiley and Sons and Copyright Clearance Center. (license number: 4395620796670) M. W. designed and performed the experiments, did the data analysis and wrote the manuscript. O. Y. G., D. M. C. and J.A.L. contributed with discussion of results and with correction of the manuscript.

### 3.1 Introduction

Lignin, which contains 40 % of the energy content in lignocellulose, has been widely studied as feedstock for energy and chemicals production.<sup>1-5</sup> These studies show that profoundly new approaches are needed for the potential value in lignin to be realized. New catalysts, reactions, and mechanistic insights are required for efficient lignin depolymerization and selective deoxygenation of the resulting fragments.<sup>6-11</sup> Because of the strength and stability of the linkages, catalytic cleavage of C-O bonds in aromatic ethers is an important step in this chemistry.<sup>11-16</sup> Several ways of cleaving ether bonds have been reported in the last decade in addition to the classic acid-catalyzed hydrolytic cleavage. These include metal-catalyzed hydrogenolysis, hydrolysis or oxidative cleavage.<sup>17-21</sup> Reductive cleavage of ether bonds is conceptually an elegant pathway to convert (polymeric) ethers to alkanes, alcohols and other ethers.<sup>6, 17, 21-23</sup> Of particular interest is the catalysis of solvolytic routes that may conceptually allow to catalyze more complex reaction products.

In Chapter 2, we reported a detailed study of the mechanism of the selective hydrolytic cleavage of the arene-oxygen bond in aromatic ethers.<sup>24</sup> Initiated by partial hydrogenation of the arene ring to an enol ether, the aromatic C-O bond is cleaved in this mechanism by insertion of water. Water rapidly adds to the enol ether to form a hemi-ketal, which undergoes elimination to cyclohexanone and phenol/alkanol (Eq. 3-1).<sup>24-25</sup>



Even though water is the cheapest and commonly used solvent for hydrothermal liquefaction of biomass, it shows lower productivity of the water-insoluble oil product and yields very viscous bio-oil. Oil-soluble solvent may be a better choice for the depolymerization reaction if the water assisted cleavage mechanism can be generally expanded to solvent assisted cleavage mechanism.<sup>26-27</sup>

Methanol was used as an oil-soluble solvent under supercritical conditions for base catalyzed lignin depolymerization.<sup>28</sup> Recently, Ford and co-authors used copper-doped porous metal oxide catalysts in supercritical methanol to transform renewable feedstocks, such as cellulose, organosoluble lignin, and even lignocellulose composites, into organic liquids.<sup>6, 22</sup> For model compound reactions, alkanol (e.g., methanol, ethanol and isopropanol) is also widely used with different metal catalysts in hydrogen as mentioned before,<sup>22, 29-30</sup> and apart from full hydrogenation, hydrogenolysis was the other major reaction pathway.

The question arises now, whether alcohols can also cleave such ether bonds and can be used for transesterification.<sup>31</sup> Indeed, mixtures of ethers and hydrocarbons were obtained from biogenic polymers in supercritical methanol, indicating that such insertion of alcohols into ether bonds could

take place, if the carbon atom is sufficiently reactive.<sup>6, 22</sup> It should be noted in passing that C<sub>1</sub>-C<sub>4</sub> alkanols are also proposed as environmentally benign solvents for bio-oil upgrading under mild conditions.<sup>29-30, 32</sup>

In principle, the enol ether intermediate (Eq. 3-1) may react in alcoholic solvents to give reductive alcoholysis products. However, while several examples of the conversion of aryl ethers on supported metals in alcoholic solvents have been reported,<sup>6, 22, 29-30, 32</sup> reductive metal-catalyzed alcoholysis has not been demonstrated. In contrast, reaction with supported Ni catalysts led predominantly to hydrogenolysis,<sup>17, 21</sup> as also reported for other supported metals.<sup>32-33</sup>

In order to develop quantitative methanolysis, we report here a mechanistic study of the reductive methanolysis of diphenyl ether and phenyl cyclohexyl ether as examples of di-aryl ethers as well as aryl-alkyl ethers. Extending our previous work<sup>24</sup> on reductive hydrolysis of aryl ethers (e.g., PhOPh and PhOR) suggests that reduction in methanol should occur as in Figure 3-1 to produce methoxycyclohexane) and ROH, or when R = Ph, phenol which ultimately is converted to methoxycyclohexane and cyclohexanol.

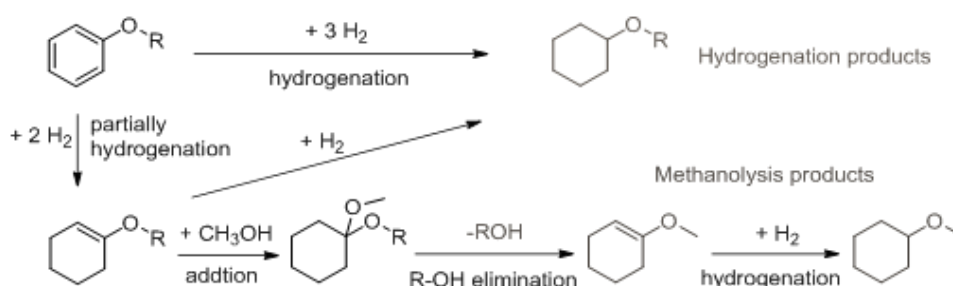


**Figure 3-1. Reductive methanolysis of aryl ether on palladium.**

## 3.2 Experimental

### 3.2.1 Chemicals and commercial catalysts

The chemicals were purchased from commercial suppliers and used as provided: diphenyl ether (Sigma-Aldrich, >99% GC assay), cyclohexyl phenyl ether (Sigma-Aldrich, >95% GC assay), cyclohex-1-enyl phenyl ether (eNovation Chemicals, 95%), phenol (Sigma-Aldrich, >99% GC assay), cyclohexanone (Sigma-Aldrich, >99% GC assay), cyclohexanol (Sigma-Aldrich, >99% GC assay), 5 wt. % Pd/C (Sigma-Aldrich), methanol (Sigma-Aldrich, anhydrous, 99.8%), H<sub>2</sub> (>99.999%), N<sub>2</sub> (> 99.999%).

The dispersion of the Pd/C was 31 % as measured by H<sub>2</sub> chemisorption. Pd on the surface was named as Pd<sub>surf</sub>.

### 3.2.2 Catalyst testing

The detailed reaction conditions are described in the figure captions and table footnotes. Typically, the reactions were carried out in a Parr autoclave reactor (Series 4848, 300 mL) in the presence of H<sub>2</sub> or N<sub>2</sub>. First, the substrate, catalyst and methanol (80 mL) were added into the Parr reactor at room temperature. After the reactor was flushed with H<sub>2</sub> or N<sub>2</sub> three times, the autoclave was pressurized with H<sub>2</sub> or N<sub>2</sub>, and the reaction was conducted at a certain temperature with a stirring speed of 700 rpm. Although the reduced metal catalysts had been exposed to air during storage, the facile reduction of oxidized Pd overlayers under reaction conditions<sup>34</sup> during heat-up ensured that reactions should be exclusively catalyzed by metallic Pd.

After the reaction, the reactor was quenched to ambient temperature by an ice/water mixture, and 0.5 ml of the contents in the reactor was filtered by a syringe filter (0.2  $\mu$ m PTFE) and analyzed by GC-MS, i.e., an Agilent 7890A GC equipped with a HP-5MS 25 m  $\times$  0.25  $\mu$ m (i.d.) column and coupled with Agilent 5975C MS. 1,3-Dimethoxybenzene was used as an internal standard for quantification purposes. 1-Methoxycyclohexene and dimethoxycyclohexane were detected and analyzed by MS from the GC separation.<sup>35</sup> The relative response factor of methoxycyclohexane was used for 1-methoxycyclohexene and dimethoxycyclohexane in GC analysis. Carbon balances in all experiments were better than 95 %. Turnover frequencies (TOF) were calculated from conversions of < 20 % and based on the number of surface Pd atoms measured by H<sub>2</sub> chemisorption. The selectivity is defined as the number of C atoms in specific products divided by the number of C atoms in the total products, multiplied by 100%. Because benzene and cyclohexane are generated only by hydrogenolysis (no cleavage of aromatic and aliphatic C-OH), the C-based selectivity of hydrogenolysis is twice the summed selectivity of benzene and cyclohexane. The selectivity to reductive methanolysis is calculated by subtracting the selectivities to hydrogenolysis and hydrogenation from 100%.

## 3.3 Result and discussion

### 3.3.1 Reactions of diphenyl ether and related compounds on Pd/C in methanol

In agreement with the above formulated hypothesis, diphenyl ether was almost fully converted on 5 wt. % Pd/C (conversion = 92 %) after 48 h in H<sub>2</sub> (Entry 1, Table 3-1) at 200 °C, while no reaction was observed in N<sub>2</sub> atmosphere (Entry 2, Table 3-1). Reductive methanolysis is the dominant mechanism as indicated by the high selectivity to 1-methoxycyclohexane (39 %). Hydrogenolysis occurred to a minor extent, with only trace amounts of benzene and cyclohexane having been detected (1 % selectivity). Although the non-reductive methanolysis, i.e., transesterification (generating phenol and



anisole), may occur in the presence of an acid or base catalyst,<sup>36</sup> this pathway was not observed on Pd/C. The reaction order of 0.4 for diphenyl ether (Figure 3-2) points to high coverage of the ether. The reaction order of 1.7 for H<sub>2</sub> indicates, assuming stepwise H addition, that the conversion of enol ether (2H-addition product) is the rate-determining step.

**Table 3-1 Reactions of related compounds on Pd/C in methanol.<sup>[a]</sup>**

Entry	Reactant	Time/h	Conv./%	Carbon Selectivity/%									TOF /s <sup>-1</sup>
				b	c	d	e	f	g	h	i	j+k	
1	a	48	92	16	10	-	-	34	39	-	-	1	-
2 <sup>[b]</sup>	a	48	-	-	-	-	-	-	-	-	-	-	-
3	a	0.25	16	80	<1	9	<1	<1	8	<1	<1	1	0.06
4	b	0.25	10	-	25	-	2	36	31	1	4	1	0.04
5	c	10	-	-	-	-	-	-	-	-	-	-	-
6	d	1	20	-	-	-	10	4	60	7	19	-	0.19
7 <sup>[c]</sup>	e	0.1	100	-	-	-	-	-	100	-	-	-	>4
8	f	10	-	-	-	-	-	-	-	-	-	-	-

<sup>[a]</sup>Reaction conditions: 20 mg 5 wt. % Pd/C ( $2.9 \times 10^{-6}$  mol of Pd<sub>surf.</sub>), methanol (80 ml), reactant (1 mmol for entries 1-5 and 10 mmol for entries 6-8), hydrogen (40 bar gauge pressure at RT), temperature (200 °C) and stirring (700 rpm). <sup>[b]</sup>N<sub>2</sub> (4 bar at RT) was used instead of H<sub>2</sub>. <sup>[c]</sup>Low conversions were not obtained because of the high reactivity of e. The product distribution did not change when the reaction time was varied from 0.1 to 10 h.

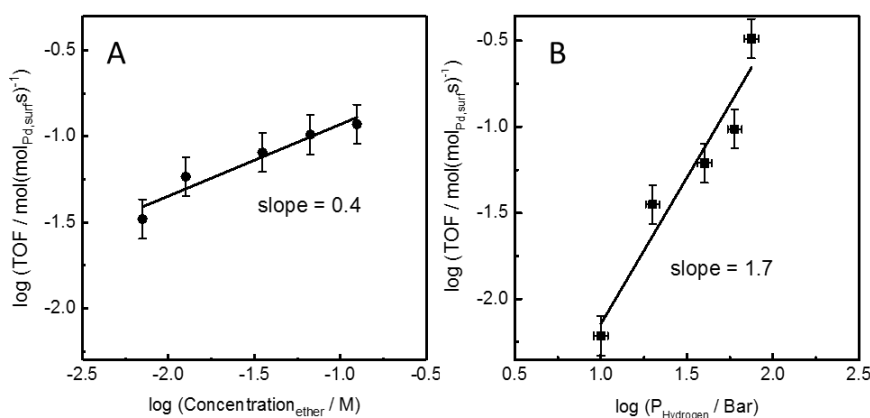


**Figure 3-2. Dependencies of the conversion rates of diphenyl ether on concentration of the ether (A) and hydrogen partial pressure (B).**

The reactions were obtained at conversions lower than 20 %. Reaction conditions: ether (0.0005 – 0.010 mol), 5 wt. % Pd/C (20.0 mg), methanol (80 ml), hydrogen (10 – 75 bar gauge pressure at room temperature), temperature (200 °C), reaction time (5 – 150 min), stirring at 700 rpm.

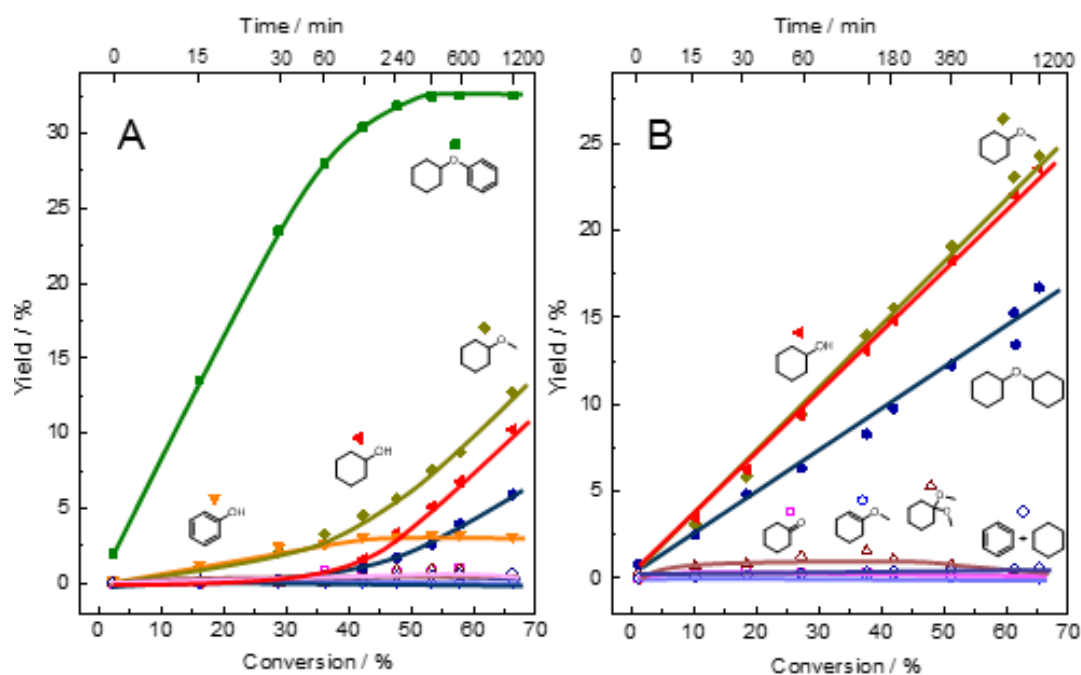


**Figure 3-3. Product distributions for the reactions of diphenyl ether (A) and cyclohexyl phenyl ether (B) over Pd/C as a function of conversion.**

Reaction conditions: ether (0.001 mol), 5 wt % Pd/C (20.0 mg, 2.9  $\mu\text{mol}$  of  $\text{Pd}_{\text{surf}}$ , ether: $\text{Pd}_{\text{surface}}$  = 350), methanol (80 ml),  $\text{H}_2$  (40 bar), 200  $^{\circ}\text{C}$ , stirring (700 rpm). As it takes 15 min to heat up the reactor from room temperature to 200  $^{\circ}\text{C}$ , the conversion at 0 min occurred during heat up. Time-Yield plots are presented in Figure 3-4.

As several intermediates were formed during the reaction of diphenyl ether, and many secondary reactions could occur, compounds b to f in Table 3-1 (entries 4-8) were also reacted in the presence of Pd/C and  $\text{H}_2$  under identical conditions. Compounds b to i were formed at low conversions of diphenyl ether (Table 3-1, entry 3), while only c, f and g were final products (Table 3-1, Entries 5, 8 and 7), because they did not react in methanol on the same time scale.

Cyclohexyl phenyl ether (80 %), phenol (9 %) and methoxycyclohexane (8 %) were the main products at 16 % conversion of diphenyl ether (Table 3-1, Entry 3), indicating that hydrogenation (80 %) dominates the initial phase of the reactions. In contrast, the selectivity to hydrogenation was much lower (25 %) and methanolysis, i.e., the sum of products f, g, h, and i in Table 3-1 was much higher (73 %) in the reaction of cyclohexyl phenyl ether (Table 3-1, Entry 4). Phenol hydrogenation in methanol occurred with a significantly faster rate ( $\text{TOF} = 0.19 \text{ s}^{-1}$ ) than ether cleavage, forming methoxycyclohexane as the major product (Table 3-1, Entry 6) and methoxycyclohexene and dimethoxycyclohexane as minor products. Cyclohexanone reacted with  $\text{H}_2$  and methanol forming methoxycyclohexane as the only product at 100% conversion (Table 3-1, Entry 7), with a rate ( $> 4 \text{ s}^{-1}$ ) even faster than phenol hydrogenation. Thus, in methanol, phenol and cyclohexanone are important

contributors to methoxycyclohexane. 1-Methoxycyclohexene, however, was not detected as a major product, due to its high reactivity. As we show later, cyclohexanone, methoxycyclohexene and dimethoxycyclohexane are hypothesized to be equilibrated.<sup>37</sup>

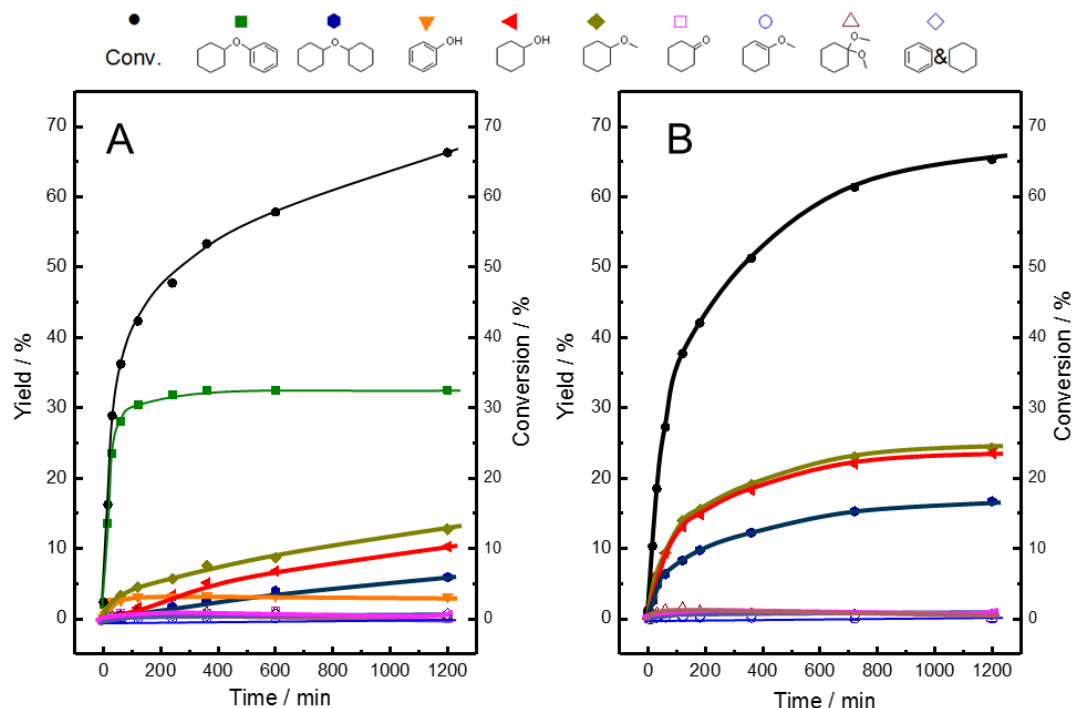


**Figure 3-4. Yield-time plots for the reactions of diphenyl ether (a) and cyclohexyl phenyl ether (b) over Pd/C as a function of conversion.**

Hydrogenation was the dominant reaction of diphenyl ether (Figure 3-3A) leading to cyclohexyl phenyl ether as the main product. Dicyclohexyl ether started to form at 35 % conversion. For the reaction of cyclohexyl phenyl ether (Figure 3-3B), the yields of three major products, cyclohexanol, methoxycyclohexane and dicyclohexyl ether, increased continuously during the reaction period, with almost constant C-selectivities, 36 %, 37 % and 25 %, respectively. For both reactants, diphenyl ether and cyclohexyl phenyl ether, the initial C-O cleavage products were R-OH (R = phenyl or cyclohexyl, respectively) and methoxycyclohexane at a 1:1 molar ratio.

The product distributions from diphenyl ether and phenyl cyclohexyl ether are consistent with the reaction pathways in Figure 3-1. 1-Phenoxycyclohexene is hypothesized to form via hydrogenation of diphenyl ether, just as 1-methoxycyclohexene has been observed in anisole hydrogenation.<sup>23-24, 35</sup>

The ethers converted more than 10 % at 15 min, but did not fully convert after 20 hours (Figure 3-4). This may be due to the reaction order of ether and competitive adsorptions between reactants and products. For diphenyl ether, the reaction order is not zero which means that the rate will decrease when the concentration of diphenyl ether drops (Figure 3-2). The competition between intermediates and reactant

also slows down the reaction, when the reaction starts with mixtures, diphenyl ether and cyclohexyl phenyl ether, or diphenyl ether and phenol, all the chemicals react at the beginning and the TOFs are smaller than the TOFs from individual reactions (Table 3-2).

**Table 3-2. Control reaction of diphenyl ether, cyclohexyl phenyl ether and phenol on Pd/C.<sup>[a]</sup>**

Entry	Reactants	Time / h	Conversion / %	TOF / s <sup>-1</sup>
1	1 mmol diphenyl ether	0.25	16	0.06
2	5 mmol diphenyl ether	1	20	0.10
3	1 mmol cyclohexyl phenyl ether	0.25	10	0.04
4	5 mmol phenol	1	28	0.14
5	1 mmol diphenyl ether and 1 mmol cyclohexyl phenyl ether	0.5	13 <sup>[b]</sup>	0.02
			16 <sup>[c]</sup>	0.03
6	5 mmol diphenyl ether and 5 mmol phenol	2	19 <sup>[b]</sup>	0.05
			13 <sup>[d]</sup>	0.03

<sup>[a]</sup> Reaction condition: reactant, methanol (80 mL), 5 wt.% Pd/C (20.0 mg), 200 °C, 40 bar H<sub>2</sub>, stirring at 700 rpm. <sup>[b]</sup> The conversion of diphenyl ether was calculated by the consumption of diphenyl ether. <sup>[c]</sup> The conversion of cyclohexyl phenyl ether was calculated by summing the consumption and the estimated generation from diphenyl ether. <sup>[d]</sup> The conversion of phenol calculated by summing the consumption and the estimated generation from diphenyl ether.

### 3.3.2 Control experiments for 1-phenoxy-cyclohexene

As 1-phenoxy-cyclohexene was generated during hydrogenation of diphenyl ether, methanolysis to 1-methoxycyclohexene and phenol was hypothesized to occur. To test this hypothesis, 1-phenoxy-cyclohexene was reacted with methanol in the presence and absence of H<sub>2</sub> and of a catalyst. In addition, the equilibration among 1-methoxycyclohexene, cyclohexanone, hemiketal and ketal in methanol was explored under the reaction conditions (Eq. 3-2).

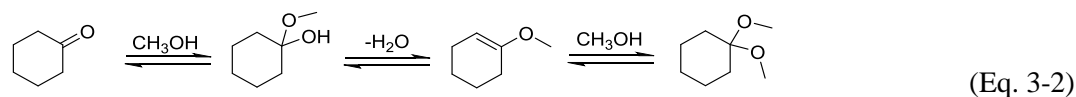
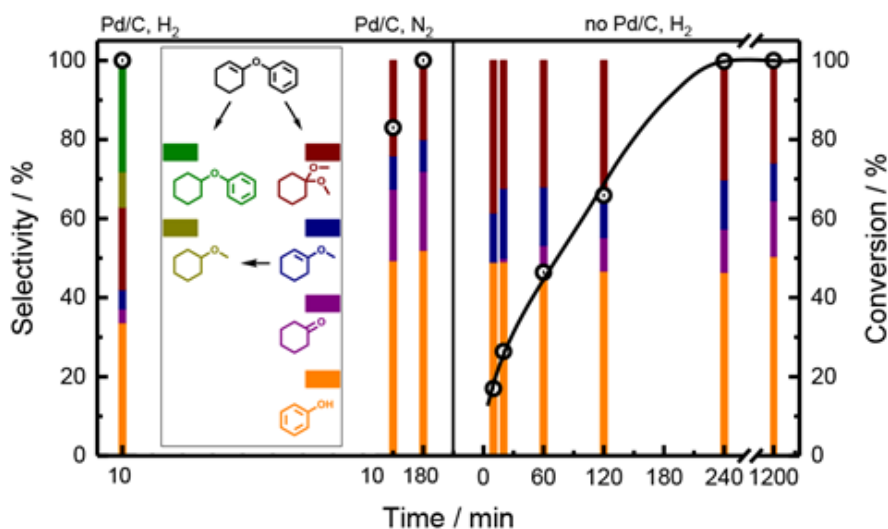


Figure 3-5 shows conversion/selectivity data for the reaction of 1-phenoxy-cyclohexene in methanol under a variety of conditions (with or without Pd/C, H<sub>2</sub> or N<sub>2</sub>). With Pd/C and H<sub>2</sub> at 200 °C, 1-phenoxy-cyclohexene was fully converted in 10 min, which is much faster than the conversion rate of diphenyl ether under the same conditions. The selectivity to hydrogenation (cyclohexyl phenyl ether) was 28 %; the other products (72 %) could all be attributed to methanolysis. Consistent with methanolysis (Eq. 3-3), the molar ratio between phenol and methoxycyclohexene or its derived

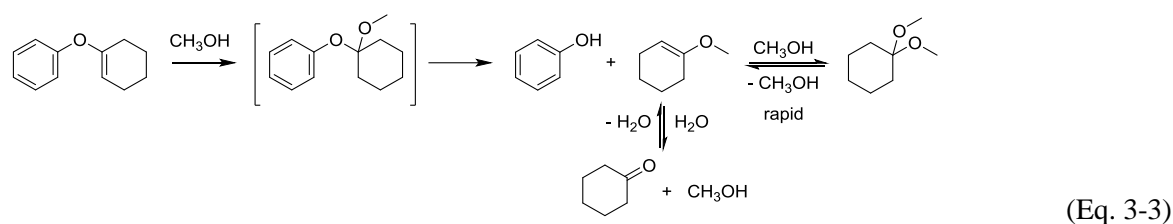
compounds (including cyclohexanone, methoxycyclohexene, dimethoxycyclohexane and methoxycyclohexane) was 1:1.



**Figure 3-5. Control experiments using 1-phenoxy-cyclohexene as reactant.**

Reaction conditions: ether (0.001 mol), 5 wt % Pd/C (0 or 10.0 mg), methanol (80 ml), N<sub>2</sub> (4 bar) or H<sub>2</sub> (40 bar), 200 °C, stirring (700 rpm). Data points are presented in Table 3-3.

Under N<sub>2</sub>, the Pd/C catalyzed conversion of 1-phenoxy-cyclohexene was slower than the rates in H<sub>2</sub>, and hydrogenation was not observed (Figure 3-5). The ratio between cyclohexanone, 1-methoxycyclohexene and the ketal was approximately 2:1:3 at both 10 min and 180 min reaction times, suggesting that these compounds are equilibrated in the absence of H<sub>2</sub>. Without the presence of a catalyst the reaction under H<sub>2</sub> was even slower than in the presence of catalyst, while equimolar amounts of phenol and 1-methoxycyclohexene-derived compounds were formed (Eq. 3-3). After 10 min of reaction under these conditions, only phenol, 1-methoxycyclohexene and 1,1-dimethoxycyclohexane were formed, while cyclohexanone was not detected. The absence of cyclohexanone at the initial stage excludes the possibility that 1-phenoxy-cyclohexene undergoes hydrolysis (e.g., with adventitious water in the solvent) which would produce cyclohexanone as the initial product. The interconversion between 1-methoxycyclohexene and the ketal appeared to be fast, in view of the constant ratio of 1:3 during the entire reaction. In contrast, cyclohexanone increased gradually with increasing reaction time, indicating that cyclohexanone was a secondary product and that the interconversion between cyclohexanone and 1-methoxycyclohexene was slow without Pd/C. Since methanolysis of 1-phenoxy-cyclohexene is competitive with hydrogenation and occurs even in the absence of catalyst (Figure 3-5), we conclude that the C-O bonds in diphenyl ether and cyclohexyl phenyl ether are cleaved via the enol ether intermediates, e.g., as shown in Eq. 3-3 for 1-phenoxy-cyclohexene.

Table 3-3. Control experiments using 1-phenoxycyclohexene as reactant.<sup>[a]</sup>

Catalyst	Atmosphere	Time/min	Conv./%	Selectivities / %					
Pd/C	H <sub>2</sub>	10	100	34	3	5	21	9	28
Pd/C	N <sub>2</sub>	10	83	49	18	8	24		
		180	100	52	18	9	21		
Pd/C	H <sub>2</sub>	10	17	49	0	12	39		
		20	26	49	1	18	32		
		60	46	48	5	15	32		
		120	66	47	8	12	32		
		240	99	46	11	12	30		
		1200	100	50	15	9	26		

<sup>[a]</sup>Reaction conditions: ether (0.001 mol), 5 wt % Pd/C (0 or 10.0 mg), methanol (80 ml), N<sub>2</sub> (4 bar) or H<sub>2</sub> (40 bar), 200 °C, stirring (700 rpm).

### 3.3.3 Control experiments for cyclohexanone

While the conversion of 1-phenoxycyclohexene does not require a catalyst to occur with appreciable rates, the presence of Pd/C increases the rates tenfold. As a consequence, the equilibrium between cyclohexanone–methoxycyclohexene is reached about hundred times faster in the presence of catalyst than in the uncatalyzed reaction. When cyclohexanone was the starting reactant (2<sup>nd</sup> and 3<sup>rd</sup> experiments in Figure 3-6), the equilibrium between cyclohexanone, methoxycyclohexene and dimethoxycyclohexane (the ratio being 2:1:3, see details in Appendix) was reached in ≤10 min in the presence of Pd/C compared to 24 h in the absence of Pd/C at 200 °C.

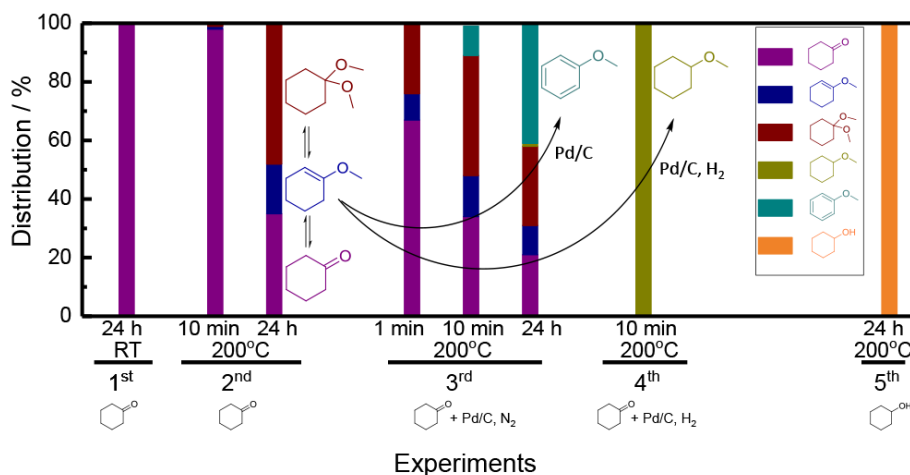


**Figure 3-6. Control experiments with cyclohexanone in methanol.**

Reaction conditions: substrate (0.001 mol), 5 wt % Pd/C (0 or 10.0 mg), methanol (80 ml), N<sub>2</sub> (4 bar) or H<sub>2</sub> (40 bar), RT or 200 °C, stirring (700 rpm).

Without H<sub>2</sub>, dehydrogenation of methoxycyclohexene occurred on Pd forming anisole (3<sup>rd</sup> experiment in Figure 3-6). With H<sub>2</sub> (4<sup>th</sup> experiment in Figure 3-6), hydrogenation rapidly reached completion within 10 min, producing only methoxycyclohexane but not cyclohexanol. This indicates that the hydrogenation rate of cyclohexanone is significantly slower than that of methoxycyclohexene. To test whether methoxycyclohexane was generated only from hydrogenation of methoxycyclohexene and not by etherification of cyclohexanol with methanol, cyclohexanol was used as the reactant in a control experiment; products were not detected after 24 h under the same reaction conditions (Table 3-1, entry 8; 5<sup>th</sup> experiment in Figure 3-6).

The various pathways for the reaction of diphenyl ether are summarized in Figure 3-7. The C-O bond cleavage of diphenyl ether in methanol is initiated by partial reduction and methanolysis of the intermediate enol ether. The initial selectivity to reductive methanolysis is 18 % for diphenyl ether and 73 % for cyclohexyl phenyl ether, lower than the selectivities for reductive hydrolysis in aqueous phase (49 % and 87 % for diphenyl ether and cyclohexyl phenyl ether, respectively).<sup>24</sup> For diphenyl ether, the difference in selectivities of the two solvents, water and methanol, is attributed to the different rates of solvolysis of 1-phenoxy-cyclohexene; e.g., in the absence of catalyst, 72 % of 1-phenoxy-cyclohexene is converted in 10 min in water,<sup>24</sup> compared to 66 % in 120 min in methanol (Figure 3-5). Thus, when 1-phenoxy-cyclohexene is formed from partial hydrogenation of diphenyl ether and desorbed from the metal surface, it reacts rapidly with water, whereas in methanol it re-adsorbs on the metal and is hydrogenated. Hydrogenation of diphenyl ether accounts for 80% C-selectivity in methanol, as compared to 49% in the aqueous phase.<sup>24</sup> For the conversion of the primary product aryl ether, the initial

products from Pd-mediated reductive methanolysis are methoxycyclohexene and cyclohexanol (1:1), the former being rapidly hydrogenated to methoxycyclohexane.

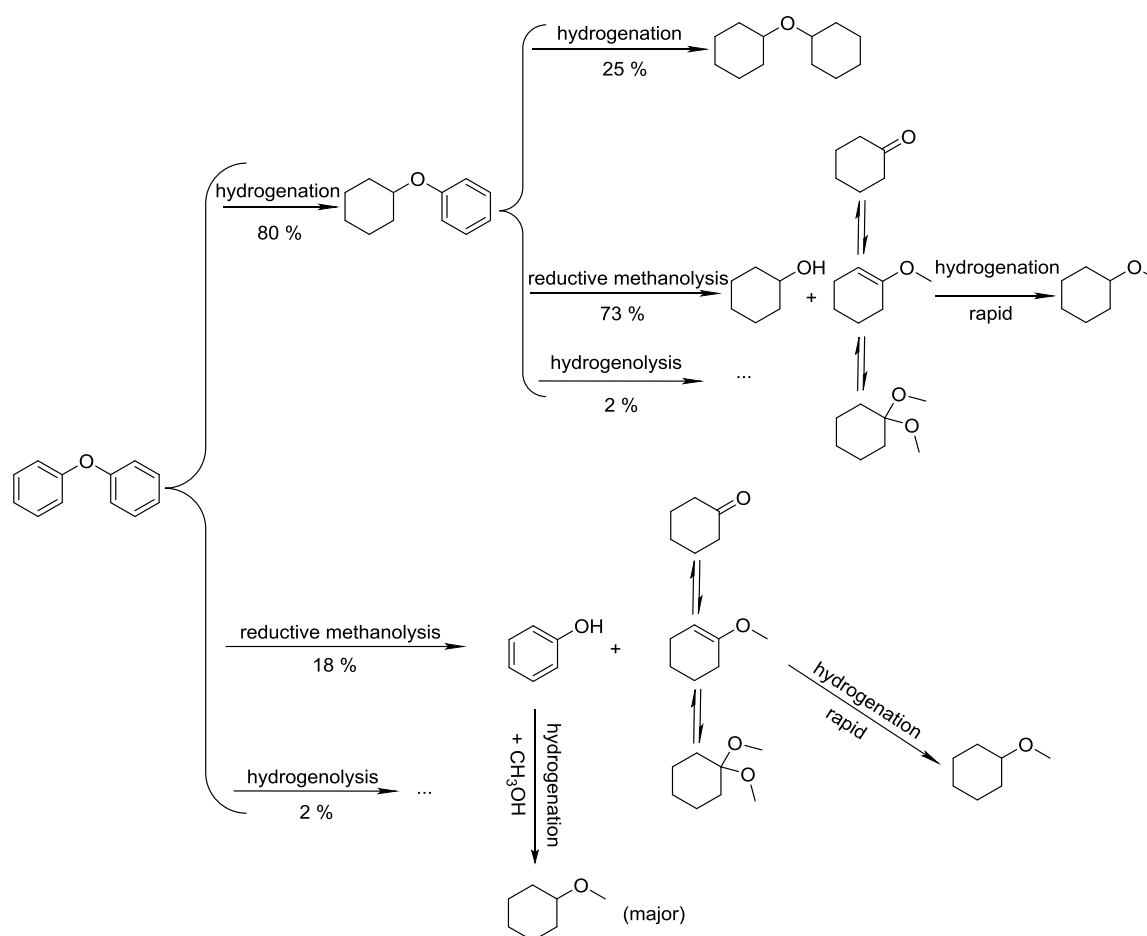


**Figure 3-7.** Reaction pathways and selectivities of diphenyl ether in methanol under hydrogen over Pd/C catalyst.

### 3.3.4 Reaction of higher alcohols and other ethers

The generality of reductive transesterification was explored using higher alcohols and other ethers. The results are shown in Table 3-4, Table 3-5 and Table 3-6. The selectivity for conversion of diphenyl ether to products of reductive solvolysis (predominately, cyclohexanol and  $\text{C}_6\text{H}_{11}\text{-O-R}$ ) followed the trend (Table 3-4): methanol (72%) > ethanol (47%) > 1-propanol (44%) > 2-propanol (32%). As the selectivities are determined by the competition between solvolysis and hydrogenation of the intermediate enol ether, we suggest that addition of R-OH to the double bond in cyclohexenyl phenyl ether becomes slower than hydrogenation, because of steric hindrance induced in the transition state and ketal product by the increasing size of the R group (from  $\text{CH}_3$  to isopropyl).

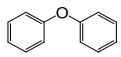
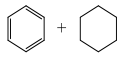
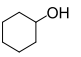
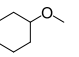
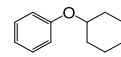
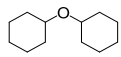
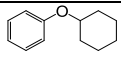
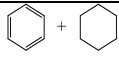
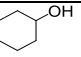
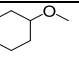
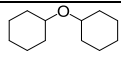
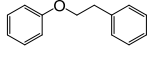
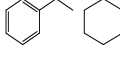
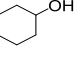
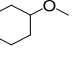
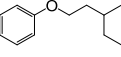
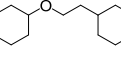
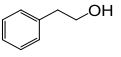
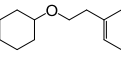
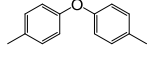
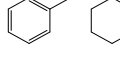
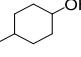
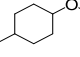
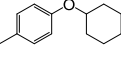
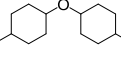


**Table 3-4. Turnover frequencies and reaction pathway selectivities at high conversion of the Pd/C-catalyzed transformation of diphenyl ether in various alcohols or in decalin as solvent.<sup>[a]</sup>**

Solvent/R-OH	TOF / s <sup>-1</sup>	Carbon selectivity / % <sup>[b]</sup>		
		Hydrogenolysis	Solvolysis	Hydrogenation
Water/H	2.9	2 ± 1	88 ± 2	10 ± 2
Methanol/CH <sub>3</sub>	0.06	2 ± 1	72 ± 2	26 ± 2
Ethanol/CH <sub>3</sub> CH <sub>2</sub>	0.21	4 ± 2	47 ± 5	49 ± 5
1-Propanol/CH <sub>3</sub> CH <sub>2</sub> CH <sub>2</sub>	0.35	4 ± 2	44 ± 5	52 ± 5
2-Propanol/(CH <sub>3</sub> ) <sub>2</sub> CH <sub>2</sub>	1.6	6 ± 2	32 ± 5	62 ± 5
Decalin	10	3 ± 1	-	97 ± 1

<sup>[a]</sup>Reaction conditions: 20 mg 5 wt. % Pd/C ( $2.9 \times 10^{-6}$  mol of Pd<sub>surf.</sub>) or 20 mg 0.2 wt. % Pd/C ( $1.2 \times 10^{-7}$  mol of Pd<sub>surf.</sub>), solvent (80 ml), diphenyl ether (1 mmol), hydrogen (40 bar gauge pressure at RT), temperature (200 °C) and stirring (700 rpm). TOFs were calculated from conversions of < 20 %. <sup>[b]</sup> Calculated at > 90 % conversion: hydrogenolysis = 2×(cyclohexane+benzene); solvolysis = (cyclohexyl-OR+cyclohexanol+phenol+cyclohexanone+cyclohexenyl-OR+acetal) - hydrogenolysis; hydrogenation = (cyclohexyl phenyl ether+dicyclohexyl ether).

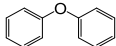
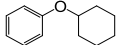
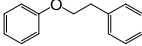
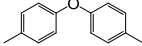
**Table 3-5. Product selectivities at high conversion of the Pd/C-catalyzed transformation of various aryl ethers in methanol.<sup>[a]</sup>**

Reactant	Carbon selectivity at high conversion / % <sup>[b]</sup>				
	Hydrocarbons	Oxygen-containing cleavage products		Hydrogenation products	
					
	1	34	39	16	10
					
	1	36	38		25
					
	1 0.5	2	17	20	26
					
				2.5	21
					
	6 1	18	23	20	32

<sup>[a]</sup>Reaction conditions: 20 mg 5 wt. % Pd/C ( $2.9 \times 10^{-6}$  mol of Pd<sub>surf.</sub>), methanol (80 ml), reactant (1 mmol), hydrogen (40 bar gauge pressure at RT), temperature (200 °C) and stirring (700 rpm). <sup>[b]</sup> Calculated at > 90 % conversion.

When 2-phenylethyl phenyl ether and p-tolyl ether were reacted in methanol, the selectivity to methanolysis was 40 % and 34 % respectively (Table 3-6). These selectivities are comparable to the selectivities reported above for diphenyl ether (72 %) and cyclohexyl phenyl ether (73 %). These observations show that solvolysis on Pd is generally available to aryl ethers, although alcohols that have bulky alkyl groups are expected to produce low yields.

**Table 3-6. Turnover frequencies and reaction pathway selectivities at high conversion of the Pd/C-catalyzed transformation of various aryl ethers in methanol.<sup>[a]</sup>**

Reactant	TOF / s <sup>-1</sup>	Carbon selectivity at high conversion / % <sup>[b]</sup>		
		Hydrogenolysis	Methanolysis	Hydrogenation
Diphenyl ether 	0.06	2 ± 1	72 ± 2	26 ± 2
Cyclohexyl phenyl ether 	0.04	2 ± 1	73 ± 2	25 ± 2
2-Phenylethyl phenyl ether 	0.04	3 ± 1	40 ± 5	57 ± 5
p-Tolyl ether 	0.03	14 ± 2	34 ± 5	52 ± 5

<sup>[a]</sup>Reaction conditions: 20 mg 5 wt. % Pd/C ( $2.9 \times 10^{-6}$  mol of Pd<sub>surf.</sub>), methanol (80 ml), reactant (1 mmol), hydrogen (40 bar gauge pressure at RT), temperature (200 °C) and stirring (700 rpm). TOFs were calculated from conversions of < 20 %. <sup>[b]</sup> Calculated from Table 3-5: hydrogenolysis = 2×(hydrocarbons cleavage products); solvolysis = (oxygen-containing cleavage products) - hydrogenolysis; hydrogenation = (products from aromatic ring hydrogenation without cleavage).

### 3.4 Conclusions

In conclusion, the solvolytic cleavage of C-O bonds in diaryl and aryl alkyl ethers on Pd occurs in alcohols under relatively mild conditions following partial reduction of the aryl ring. Thus, for aryl alkyl ethers, the aryl C-O bond, rather than the alkyl C-O bond, is cleaved because it becomes a vinylic C-O bond in the intermediate enol ether. Reductive alcoholysis is initiated by selective partial hydrogenation of the aryl ring to an enol ether intermediate that is susceptible to attack by alcohols. The attack however, is slower than attack by water, thus, the selectivity to alcoholysis is lower than for hydrolysis under comparable conditions.<sup>24</sup> We infer that this solvolysis mechanism applies also to a variety metal catalysts in the presence of H<sub>2</sub> or reducing equivalents. A determining factor is the selectivity of the metal to catalyze hydrogenation of the enol ether, a feature that needs to be explored in greater detail.

### 3.5 Acknowledgements

This work was supported by the U.S. Department of Energy, Office of Science, Office of Basic Energy Sciences, Division of Chemical Sciences, Geosciences, and Biosciences. Portions of the work were performed at the William R. Wiley Environmental Molecular Science Laboratory, a national scientific user facility sponsored by the DOE's Office of Biological and Environmental Research located at Pacific Northwest National Laboratory, a multi-program national laboratory operated for DOE by Battelle Memorial Institute.

### 3.6 Appendix

#### 3.6.1 Equilibrium between cyclohexanone, methoxycyclohexene and dimethoxycyclohexane

When reaction was started from cyclohexanone in methanol at 200 °C without catalyst, the equilibrium between cyclohexanone, methoxycyclohexene and dimethoxycyclohexane was achieved at 24 h (2<sup>nd</sup> experiments in Figure 3-6), and the ratio being 35:17:48 or 2:1:3. We collected the data at 48 h, the ratio did not change (34:17:49). In the presence of Pd/C (3<sup>rd</sup> experiments in Figure 3-6), this ratio was almost reached in 10 min (34: 15:41) and maintained in 24 h (22:9:27). When we measured the reaction of 1-phenoxy cyclohexene (Figure 3-5), methoxycyclohexene was generated initially from transesterification, then cyclohexanone and dimethoxycyclohexane were formed. The equilibrium ratio (2:1:3) was reached instantly with Pd/C compare to 4 h in the absence of Pd/C.

### 3.7 References

1. Regalbuto, J. R., *Science* **2009**, *325* (5942), 822-824.
2. Ragauskas, A. J.; Williams, C. K.; Davison, B. H.; Britovsek, G.; Cairney, J.; Eckert, C. A.; Frederick, W. J.; Hallett, J. P.; Leak, D. J.; Liotta, C. L.; Mielenz, J. R.; Murphy, R.; Templer, R.; Tschaplinski, T., *Science* **2006**, *311* (5760), 484-489.
3. Willems, P. A., *Science* **2009**, *325* (5941), 707-708.
4. Rinaldi, R.; Jastrzebski, R.; Clough, M. T.; Ralph, J.; Kennema, M.; Bruijninx, P. C. A.; Weckhuysen, B. M., *Angewandte Chemie International Edition* **2016**, *55* (29), 8164-8215.
5. Ferrini, P.; Rinaldi, R., *Angewandte Chemie International Edition* **2014**, *53* (33), 8634-8639.
6. Barta, K.; Ford, P. C., *Accounts of Chemical Research* **2014**, *47* (5), 1503-1512.
7. Huber, G. W.; Iborra, S.; Corma, A., *Chemical Reviews* **2006**, *106* (9), 4044-4098.
8. Li, C.; Zhao, X.; Wang, A.; Huber, G. W.; Zhang, T., *Chemical Reviews* **2015**, *115* (21), 11559-11624.
9. Gallezot, P., *ChemSusChem* **2008**, *1* (8-9), 734-737.
10. Rinaldi, R.; Schuth, F., *Energy & Environmental Science* **2009**, *2* (6), 610-626.
11. Zakzeski, J.; Bruijninx, P. C. A.; Jongerius, A. L.; Weckhuysen, B. M., *Chemical Reviews* **2010**, *110* (6), 3552-3599.
12. Grobelny, Z., *European Journal of Organic Chemistry* **2004**, *2004* (14), 2973-2982.
13. Song, Q.; Wang, F.; Cai, J.; Wang, Y.; Zhang, J.; Yu, W.; Xu, J., *Energy & Environmental Science* **2013**, *6* (3), 994.
14. Besson, M.; Gallezot, P.; Pinel, C., *Chemical Reviews* **2014**, *114* (3), 1827-1870.
15. Cornella, J.; Zarate, C.; Martin, R., *Chemical Society Reviews* **2014**, *43* (23), 8081-8097.
16. Zaheer, M.; Kempe, R., *ACS Catalysis* **2015**, *5* (3), 1675-1684.
17. Sergeev, A. G.; Hartwig, J. F., *Science* **2011**, *332* (6028), 439-443.
18. Bruijninx, P. C. A.; Weckhuysen, B. M., *Nature Chemistry* **2014**, *6* (12), 1035-1036.
19. Chatterjee, M.; Chatterjee, A.; Ishizaka, T.; Kawanami, H., *Catalysis Science & Technology* **2015**, *5* (3), 1532-1539.
20. Hanson, S. K.; Wu, R.; Silks, L. A. P., *Angewandte Chemie International Edition* **2012**, *51* (14), 3410-3413.
21. Gao, F.; Webb, J. D.; Hartwig, J. F., *Angewandte Chemie International Edition* **2016**, *55* (4), 1474-8.
22. Matson, T. D.; Barta, K.; Iretskii, A. V.; Ford, P. C., *Journal of the American Chemical Society* **2011**, *133* (35), 14090-14097.
23. Barrett, J. A.; Gao, Y.; Bernt, C. M.; Chui, M.; Tran, A. T.; Foston, M. B.; Ford, P. C., *ACS Sustainable Chemistry & Engineering* **2016**, *4* (12), 6877-6886.
24. Wang, M.; Shi, H.; Camaioni, D. M.; Lercher, J. A., *Angewandte Chemie International Edition* **2017**, *56* (8), 2110-2114.
25. Meng, Q.; Hou, M.; Liu, H.; Song, J.; Han, B., *Nature Communications* **2017**, *8*, 14190.

26. Azadi, P.; Inderwildi, O. R.; Farnood, R.; King, D. A., *Renewable and Sustainable Energy Reviews* **2013**, *21*, 506-523.
27. Xiu, S.; Shahbazi, A., *Renewable and Sustainable Energy Reviews* **2012**, *16* (7), 4406-4414.
28. Miller, J. E.; Evans, L.; Littlewolf, A.; Trudell, D. E., *Fuel* **1999**, *78* (11), 1363-1366.
29. Cui, X.; Surkus, A. E.; Junge, K.; Topf, C.; Radnik, J.; Kreyenschulte, C.; Beller, M., *Nature Communications* **2016**, *7*, 11326.
30. Molinari, V.; Giordano, C.; Antonietti, M.; Esposito, D., *Journal of the American Chemical Society* **2014**, *136* (5), 1758-1761.
31. Watanabe, W. H.; Conlon, L. E., *Journal of the American Chemical Society* **1957**, *79* (11), 2828-2833.
32. Song, Q.; Cai, J.; Zhang, J.; Yu, W.; Wang, F.; Xu, J., *Chinese Journal of Catalysis* **2013**, *34* (4), 651-658.
33. Zhang, J.; Teo, J.; Chen, X.; Asakura, H.; Tanaka, T.; Teramura, K.; Yan, N., *ACS Catalysis* **2014**, *4* (5), 1574-1583.
34. Chase, Z. A.; Fulton, J. L.; Camaioni, D. M.; Mei, D.; Balasubramanian, M.; Pham, V.-T.; Zhao, C.; Weber, R. S.; Wang, Y.; Lercher, J. A., *The Journal of Physical Chemistry C* **2013**, *117* (34), 17603-17612.
35. Widegren, J. A.; Finke, R. G., *Inorganic Chemistry* **2002**, *41* (6), 1558-1572.
36. Ogata, Y.; Okano, M., *Journal of the American Chemical Society* **1949**, *71* (9), 3212-3213.
37. Kubler, D.; Sweeney, L., *The Journal of Organic Chemistry* **1960**, *25* (8), 1437-1440.

## Chapter 4 Mechanistic Studies of Hydrogenolysis of Aryl Ethers Catalyzed by Nickel Nanoparticles

*Hydrogenolysis was observed as the major route of the conversion of diphenyl ether in water and decalin under H<sub>2</sub> over nickel catalyst, which initially generates benzene and phenol. H<sub>2</sub> dependence and isotopic experiments showed that hydrogen addition is involved in the rate determining step. The reaction mechanism was concluded to be initiated by one hydrogen addition to the aromatic ring by kinetic measurements and theoretical calculations. The weakened C-O bond cleaves on the metal surface afterward.*

---

DFT (density functional theory) calculations in this chapter were provided by Dr. Donghai Mei (PNNL, USA)

## 4.1 Introduction

Activation of the aryl C–O bond in aromatic ethers is a needed strategy for lignin depolymerization<sup>1-4</sup> and a versatile synthetic step for cross-coupling<sup>5-6</sup>. However it is typically difficult to cleave the strong aryl C–O bond.<sup>7-9</sup> The identification and understanding of catalysts that selectively cleave aromatic C–O bonds would be a significant advance.<sup>10-17</sup> Recently, transition-metal catalysts, both heterogeneous and homogeneous, have been identified for both oxidative and reductive cleavage of C–O bonds under mild reaction conditions.<sup>6, 18-27</sup> Nickel-based catalysts are widely investigated because of the unique selectivity of hydrogenolysis of aryl ethers in the liquid phase.<sup>9, 15, 28-32</sup>

Since Hartwig's group reported homogeneous nickel complexes-catalyzed hydrogenolysis of diaryl ethers in the presence of NaOtBu<sup>10</sup> some information relevant to the mechanism of nickel complexes catalyzed hydrogenolysis of aromatic C–O bonds have been published.<sup>12, 15, 32-34</sup> The intermediates, status of the catalyst, source of the hydrogen and the rate-determining step have been carefully investigated via experimental measurements<sup>12, 15, 29</sup> and theoretical calculations<sup>32-33</sup>. These mechanistic studies illustrated large changes in mechanism across the catalytic systems even with small modifications.<sup>15</sup> Although plenty of nickel based heterogeneous catalysts have shown higher selectivity and even better reactivity than molecular catalysts for this reaction in polar or apolar phases<sup>31, 35-38</sup>, detailed information for the reaction mechanism over Ni nanoparticles is rare.

Here, we systematically compared the reaction routes of diphenyl ether over supported nickel catalyst (Ni/SiO<sub>2</sub>) in polar (water) and apolar (decalin) solvents under H<sub>2</sub>. Catalytic reactions and kinetic studies indicate that benzene and phenol are the initial products of hydrogenolysis and hydrogen addition is involved in the rate-determining step of the catalytic cycle. Isotopic studies show a strong kinetic isotopic effect ( $KIE_{H/D}=5.7$ ) and identify the position of D in the products by tracing the deuterium. With density functional theory (DFT) calculations, we show that hydrogenolysis occurs by an unconsidered mechanism initiated by first hydrogen addition to the aromatic ring. The C–O bond easily cleaves afterward because of the weakened strength of the bond.

## 4.2 Experimental

### 4.2.1 Chemicals and commercial catalysts

The chemicals were purchased from commercial suppliers and used as provided: diphenyl ether (Sigma-Aldrich, >99% GC assay), cyclohexyl phenyl ether (Sigma-Aldrich, >95% GC assay), benzyl phenyl ether (Sigma-Aldrich, >98% GC assay), benzene (Sigma-Aldrich, >99.5% GC assay), phenol (Sigma-

Aldrich, >99% GC assay), cyclohexanone (Sigma-Aldrich, >99% GC assay), cyclohexanol (Sigma-Aldrich, >99% GC assay), dichloromethane (Sigma-Aldrich, >99.5% GC assay), 64 wt. % Ni/SiO<sub>2</sub> (Strem Chemicals, Inc.), H<sub>2</sub> (>99.999%), N<sub>2</sub> (> 99.999%), D<sub>2</sub> (Sigma-Aldrich, 99.9 atom % D) and normal H<sub>2</sub>O (Milli-Q, ultrapure water dispenser system). The dispersion of the Ni/SiO<sub>2</sub> is 7 % as measured by H<sub>2</sub> chemisorption.

#### 4.2.2 Catalyst tests

The detailed reaction conditions are described in the figure captions and table footnotes. Typically, the reactions were carried out in Parr autoclave reactors (Series 4848, 300 mL reactor for aqueous phase reactions and 100 mL reactor for decalin) in the presence of H<sub>2</sub>. First, the catalyst and solvent were loaded into the reactor at room temperature. After the reactor was flushed with H<sub>2</sub> three times, the autoclave was pressurized with H<sub>2</sub> to 40 bar, then the reactor was kept at 200 °C or 170 °C for 3 hours to reduce the catalyst. The reactant was added at room temperature after the reactor was quenched and the system was flushed with H<sub>2</sub> three times again. The reaction was conducted at a certain temperature with a stirring speed of 700 rpm.

After the reaction, the reactor was quenched to ambient temperature by an ice/water mixture, and the contents in the reactor from the aqueous phase were extracted using dichloromethane and analyzed by GC-MS, i.e., an Agilent 7890A GC equipped with a HP-5MS 25 m × 0.25 μm (i.d.) column and coupled with Agilent 5975C MS. Products from reactions in decalin were directly measured after the dilution by dichloromethane. 1,3-Dimethoxybenzene was used as an internal standard for quantification purposes. The carbon balances for all the reported experiments were 90 ± 5%. The turnover frequency (TOF) was calculated from conversion < 20 % and based on the number of surface Ni atoms measured by H<sub>2</sub> chemisorption.

Because benzene and cyclohexane are generated only by hydrogenolysis (no cleavage of aromatic and aliphatic C-OH), the C-based selectivity of hydrogenolysis is twice the summed selectivity of benzene and cyclohexane. The selectivity to hydrolysis is calculated by subtracting the selectivities to hydrogenolysis and hydrogenation from 100%.

#### 4.2.3 DFT calculations

Spin-polarized density functional theory (DFT) periodic slab calculations were performed using the Vienna ab initio simulation package (VASP).<sup>39-40</sup> The effective cores were described by the projector-augmented wave (PAW) method.<sup>41-42</sup> The valence electrons of all atoms were expanded in a plane wave basis set with a cutoff energy of 400 eV. The Perdew-Burke-Ernzerhof (PBE) functional<sup>43</sup> was used to



evaluate the exchange and correlation effects. The atomic structures were relaxed using either the conjugate gradient algorithm or the quasi-Newton method until the forces on all unconstrained atoms are less than 0.05 eV/Å. To involve van der Waals interaction, all calculations were performed using the optB88-vdW functional.

We used the Ni (111) surface to simulate the elementary steps in hydrogenolysis and hydrogenation of diphenyl ether. The Ni (111) surface was modeled by a four-layer slab, consisting of 128 Ni atoms, with a vacuum space of 12 Å. The atoms in the bottom two layers were fixed during relaxation and those in the top two layers together with the adsorbates were allowed to relax. For geometry optimization, a (1×1×1) k-point grid was used to generate the K-points. The adsorption energy was defined as

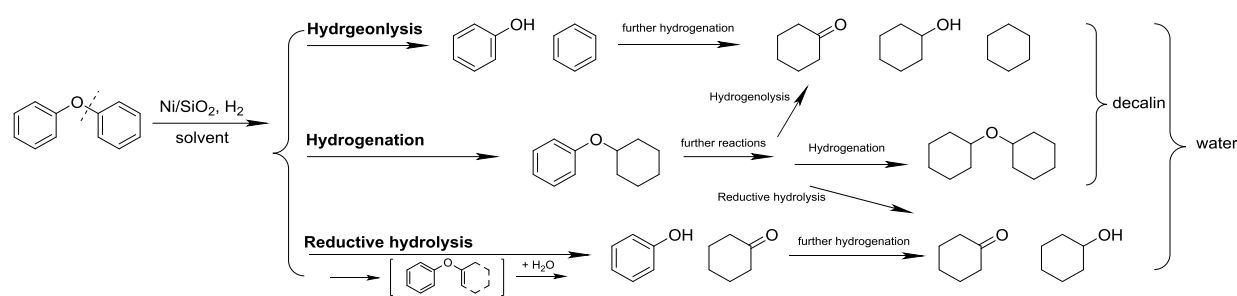
$$E_{ads} = E_{(adsorbate/slab)} - E_{adsorbate} - E_{(bare\ slab)}$$

where  $E_{(adsorbate/slab)}$ ,  $E_{adsorbate}$ ,  $E_{(bare\ slab)}$  represent the energies of surface slab with the adsorbate, the isolated adsorbate molecule and the slab, respectively. According to this definition, a negative value indicates an exothermic process and a positive value corresponds to an endothermic process. Normal mode analysis was applied to all stable and transition states.

## 4.3 Result and discussion

### 4.3.1 Reactions of diphenyl ether over Ni catalyst in water and decalin

The reactions are broadly classified into hydrogenation, hydrogenolysis and hydrolysis, and the hydrogenation is limited to reactions which saturate the aromatic rings without changing the molecular backbone (i.e., cyclohexyl phenyl ether and dicyclohexyl ether). The efforts to evaluate the reactions of diphenyl ether over a supported nickel catalyst under various conditions began with aqueous phase reactions. The conversions of diphenyl ether were kept below 20 % to minimize the influence of secondary reactions. At 200 °C (Table 4-1, entry 1), hydrogenolysis is the dominant mechanism (80 %) as indicated by the high selectivity to benzene (40 %). The slightly lower selectivity of phenol (36 %) indicates that benzene and phenol (1:1) are the kinetic primary products from hydrogenolysis, and phenol can be easily hydrogenated under the reaction condition. Since more C<sub>6</sub>-OH (phenol is 36 %, cyclohexanone is 8 % and cyclohexanol is 10 %) was generated than benzene, hydrolysis also occurs as a minor reaction route in aqueous phase.

**Table 4-1. Reactions and products selectivities of diphenyl ether.<sup>[a]</sup>**

Entry	Solvent	Temp. / °C	H <sub>2</sub> / bar	TOF <sup>b</sup> / h <sup>-1</sup>	Products carbon selectivity / %							Reaction selectivity <sup>c</sup> / %		
												Hydrogenolysis	Hydrogenation	Hydrolysis
1	Water	200	40	1600	40	-	36	8	10	6	-	80	6	14
2	Water	150	40	140	36	-	6	4	43	11	-	72	11	17
3	Decalin	150	40	830	5	10	1	-	13	61	10	29	71	-
4	Decalin	150	12	300	16	2	1	-	16	57	8	35	65	-
5	Decalin	150	5	160	15	6	1	-	20	56	2	42	58	-

<sup>a</sup> Reaction conditions: Diphenyl ether (1.70 g), 64 wt. % Ni/SiO<sub>2</sub> catalyst (10 mg), solvent (water 80 ml or decalin 40 ml), stirring at 700 rpm. <sup>b</sup> Calculated at < 20 % conversion <sup>c</sup> hydrogenolysis = 2 × (cyclohexane+benzene); hydrolysis = (phenol+cyclohexanone+cyclohexanol) - hydrogenolysis; hydrogenation=(phenyl cyclohexyl ether+dicyclohexyl ether).

Since rapid conversion (TOF = 1600 h<sup>-1</sup>) was observed at higher temperature, the following reactions were obtained at 150 °C (Table 4-1, entry 2). Hydrogenolysis still dominates the conversion of diphenyl ether with slightly lower selectivity (72 %) than at higher temperature. Figure 4-1A shows the product distributions for the conversion of diphenyl ether in water at 150 °C under 40 bar of hydrogen. The major products were cyclohexanol, benzene and cyclohexyl phenyl ether. Cyclohexanol was formed by fast hydrogenation of phenol. The yield of cyclohexyl phenyl ether increased at conversions lower than 90 %, then decreased, and the selectivity of hydrolysis slightly increased at conversions higher than 90 % (Figure 4-2), it suggests that cyclohexyl phenyl ether is the primary hydrogenation product and the increasing selectivity of hydrolysis comes from the hydrolysis of cyclohexyl phenyl ether.

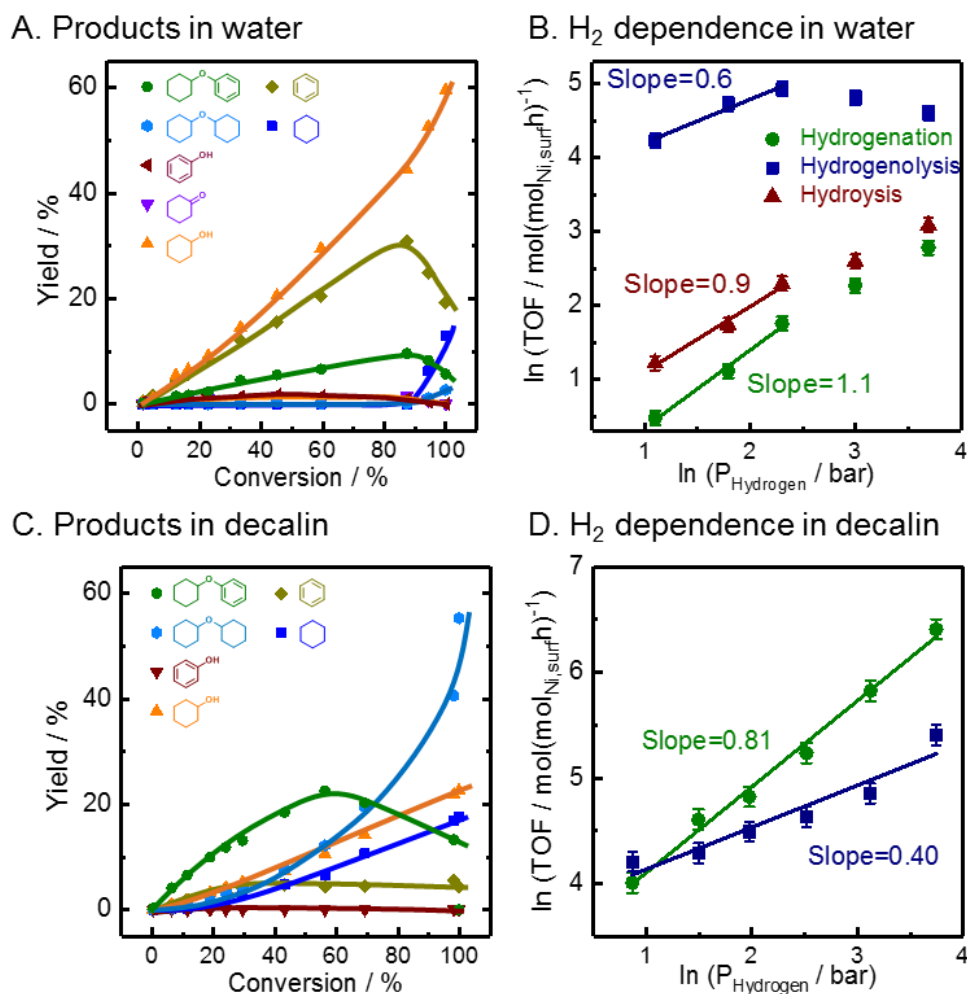


**Figure 4-1. Product distributions as a function of conversion and hydrogen dependencies for the reactions of diphenyl ether over Ni/SiO<sub>2</sub> in water (A) and decalin (C).**

The time-yield plots are shown in Figure 4-2 and Figure 4-3. Reaction conditions are listed in the footnote of Figure 4-2 and Figure 4-3, reaction temperatures are 150 °C and the H<sub>2</sub> pressure is 40 bar in water and 12 bar in decalin. For B and D, H<sub>2</sub> pressure varies from 2.4 to 42 bar.

The reaction orders in H<sub>2</sub> pressure for the reaction pathways were determined within 3 – 40 bar H<sub>2</sub> (Figure 4-1B). The H<sub>2</sub> dependences for hydrogenation and hydrolysis in the aqueous phase were measured to be first order (1.1 for hydrogenation and 0.9 for hydrolysis) in the range of 3 – 10 bar H<sub>2</sub>, and they showed similar trends at higher pressures. Since we have demonstrated that the mechanism of reductive hydrolysis of diphenyl ether over palladium catalysts is initiated by partial hydrogenation which generates the enol ether as the intermediate,<sup>16</sup> the observation of the same hydrogen dependencies between hydrolysis and hydrogenation over nickel catalyst indicates that the hydrolysis undergoes the mechanism as shown in Table 4-1.

The reaction order in H<sub>2</sub> pressure for hydrogenolysis is different from other two pathways, it is half order (0.6) in the range of 3 – 10 bar H<sub>2</sub> and shows negative order at higher pressures. This non-zero order indicates that the hydrogen addition is involved in the rate-determining step of hydrogenolysis.<sup>15</sup> Generally, the changes of the reaction orders in H<sub>2</sub> were caused by the change of surface coverages of hydrogen and ether on the Ni surface at H<sub>2</sub> pressure higher than 10 bar in aqueous phase.<sup>31</sup>

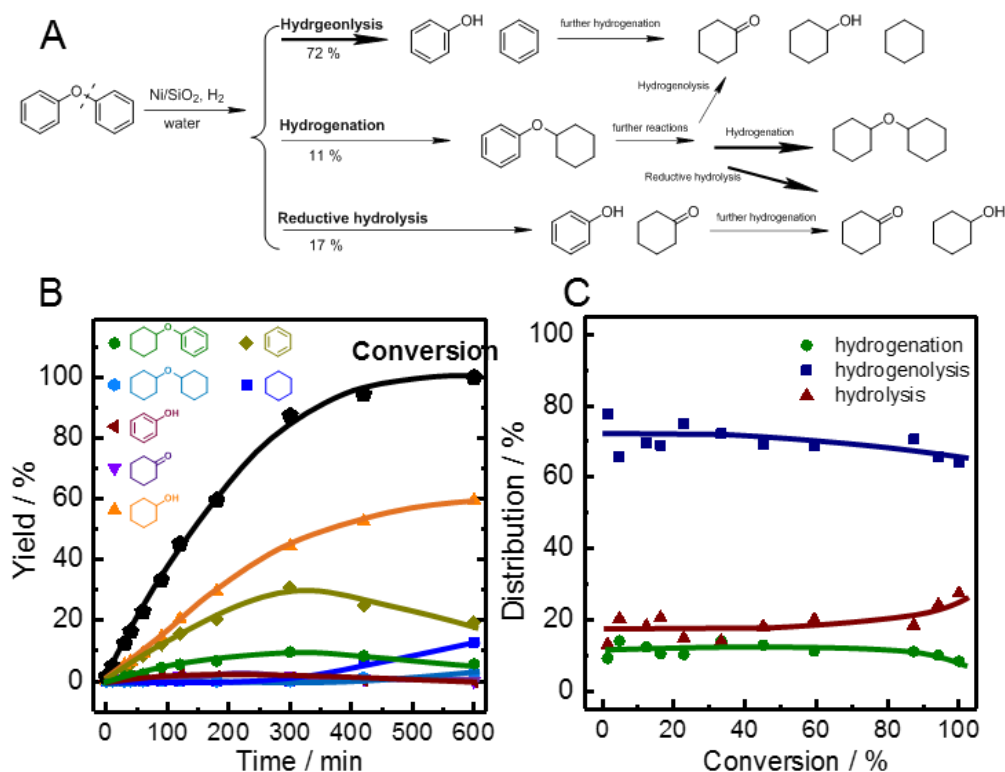


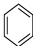
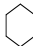
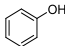
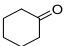
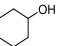
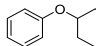
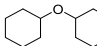
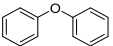
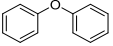
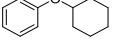
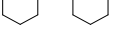
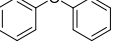
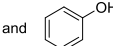
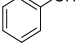
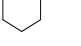
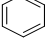
**Figure 4-2. (A) Reaction pathways and selectivities to diphenyl ether on Ni catalyst in water. Time-yield plots (B) and distributions of the reaction pathways (C) from the reaction.**

Reaction conditions: ether (1.70 g), 64 wt. % Ni/SiO<sub>2</sub> catalyst (20 mg), water 80 ml, 150 °C and 40 bar of hydrogen at room temperature, stirring at 700 rpm.

The reactions of diphenyl ether were carried out in an apolar solvent (decalin) under different H<sub>2</sub> pressures (Table 4-1, entries 3 - 5). The ether converts faster in decalin (TOF = 830 h<sup>-1</sup>) than in water (TOF = 140 h<sup>-1</sup>) under the same H<sub>2</sub> pressure and temperature. Four major products, i.e., benzene, cyclohexanol, cyclohexyl phenyl ether and dicyclohexyl ether, were obtained. Hydrogenation dominates the reaction across the different H<sub>2</sub> pressures. Because water was not presented during the reaction, hydrogenolysis is the only C-O bond cleavage reaction in decalin, forming benzene and phenol (1 : 1), which were further hydrogenated to cyclohexane and cyclohexanol. The ratios between the selectivity of C<sub>6</sub> molecules (benzene and cyclohexane) and C<sub>6</sub>-OH molecules (phenol and cyclohexanol) were close to 1 : 1. Comparing to diphenyl ether (TOF = 290 h<sup>-1</sup>), phenol was rapidly

hydrogenated to cyclohexanone and cyclohexanol in the presence (TOF = 1700 h<sup>-1</sup>) or absence (TOF = 2100 h<sup>-1</sup>) of diphenyl ether, and cyclohexyl phenyl ether (TOF = 110 h<sup>-1</sup>) and benzene (TOF = 120 h<sup>-1</sup>) were converted with comparable rates under 12 bar of H<sub>2</sub> (Table 4-2). The high reactivity of phenol explained the trace yield of phenol that we obtained in decalin even though phenol is the initial product from the hydrogenolysis of diphenyl ether. Detailed product distributions of diphenyl ether in decalin at 150 °C under 12 bar of hydrogen are shown in Figure 4-1C. Cyclohexyl phenyl ether was the major product at conversions lower than 60 %. Due to the secondary reactions of cyclohexyl phenyl ether, 31 % of hydrogenolysis and 69 % of hydrogenation (Table 4-2), the overall selectivity of hydrogenolysis was increased from 35 % at low conversion to 44 % at full conversion (Figure 4-3).

**Table 4-2. Control experiments for diphenyl ether in decalin<sup>[a]</sup>**

Entry	Reactant	molar / mmol	Time / min	Conversion / %	TOF / h <sup>-1</sup> <sup>[b]</sup>	Selectivity / %						
						hydrocarbons		oxygenates			ethers	
												
1		10	30	11	290	16	2	1		16	57	8
2		10	480	99.8	-	4	18			22		56
3		10	60	17	110	2	14			15		69
4		10	480	N.D.	N.D.							
5	 and 	10	15	1	52							
		20		16	1700							
6		20	15	20	2100				31	69		
7		20	480	N.D.	N.D.							
8		20	120	9	120		100					

<sup>[a]</sup> Reaction condition: reactant, decalin (40 mL), 64 wt.% Ni/SiO<sub>2</sub> (10.0 mg, 7.6 × 10<sup>-6</sup> mol of Ni<sub>surf.</sub>), 150 °C, 12 bar H<sub>2</sub>, stirring at 700 rpm. <sup>[b]</sup> The turnover frequency (TOF) was calculated based on the number of surface Ni atoms measured by H<sub>2</sub> chemisorption. ND means none detected.

In the apolar phase, reaction orders in  $H_2$  for hydrogenolysis and hydrogenation of diphenyl ether were determined to be 0.4 and 0.8 within 2.4 – 42 bar of  $H_2$ , respectively (Figure 4-1D). The constant reaction order in  $H_2$  despite 18-fold variation in  $H_2$  pressure indicates that the surface coverage of H is relatively low under the reaction conditions. At low H-coverages, in water and decalin, the kinetic observations, i.e., hydrogenolysis is half order and reductive hydrolysis and hydrogenation are first order in  $H_2$ , point to a mechanistic scenario in which the first H-addition is involved in the rate-determining step for the hydrogenolysis pathway (see Appendix for detailed derivations of rate expressions).

In summary, the C-O bond of diphenyl ether was cleaved in decalin via hydrogenolysis while the reductive hydrolysis route occurred as the other parallel reaction pathway for the C-O bond cleavage in water under  $H_2$ . The selectivity to hydrogenation was 11 % in the aqueous phase but 71 % in an apolar solvent (150 °C and 40 bar of  $H_2$ ).

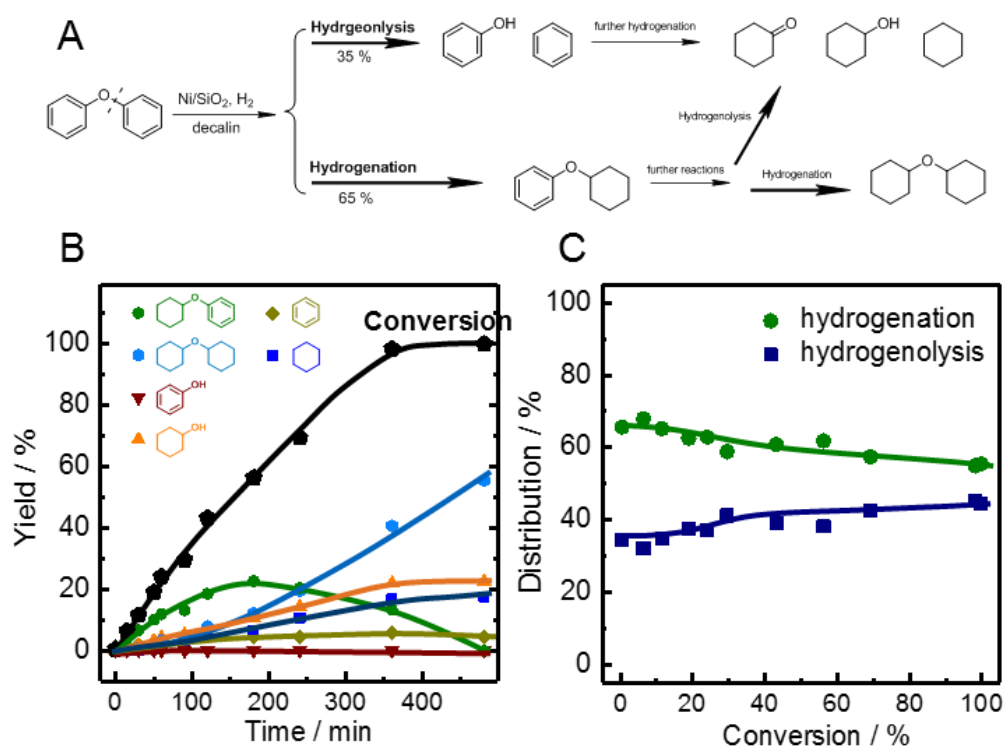


**Figure 4-3. (A) Reaction pathways and selectivities of diphenyl ether on Ni catalyst in decalin. Time-yield plots (B) and distributions of the reaction pathways (C) from the reaction.**

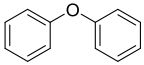
Reaction conditions: ether (1.70 g), 64 wt. %  $Ni/SiO_2$  catalyst (10 mg), decalin 40 ml, 150 °C and 12 bar of hydrogen at room temperature, stirring at 700 rpm.

### 4.3.2 Isotopic experiments of diphenyl ether

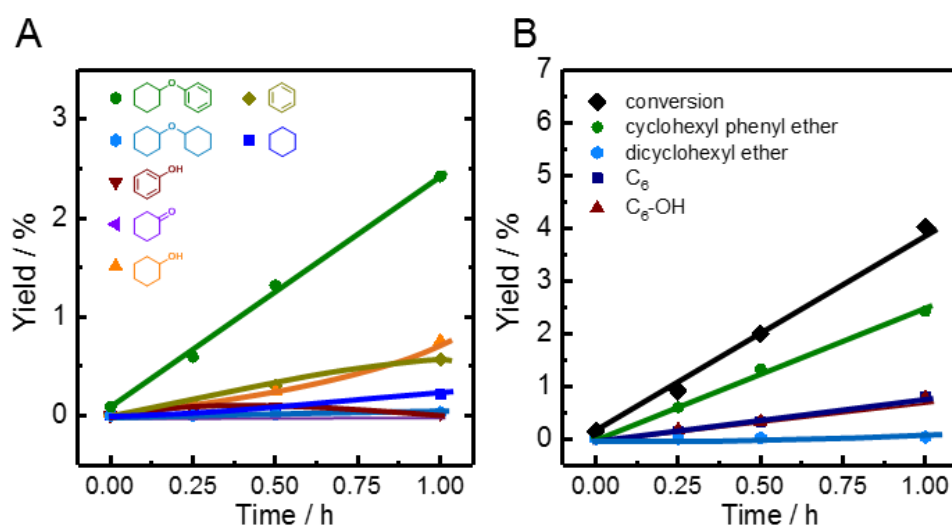
In order to validate the participation of hydrogen in the rate-determining step of hydrogenolysis and understand the mechanism, the conversion of diphenyl ether were obtained under H<sub>2</sub> and D<sub>2</sub> in decalin which has fewer reaction pathways and constant reaction order in H<sub>2</sub> in comparison to water. By measuring the rates of the reactions, hydrogenolysis and hydrogenation, under an atmosphere of D<sub>2</sub> rather than H<sub>2</sub>, the kinetic isotope effects were found to be 5.7 and 4.8 (Table 4-3), respectively. These values agree with the hydrogen dependences of rates on the pressure of H<sub>2</sub> and indicate that hydrogen addition is involved during the rate-determining step. In addition, the diffusion and activation of H<sub>2</sub> on the metal surface were tested by mixing H<sub>2</sub> and D<sub>2</sub> under the same reaction conditions (see Figure 4-15 in Appendix), they are not limiting the reaction rates because the H/D exchange between H<sub>2</sub> and D<sub>2</sub> reached the equilibrium instantly.

Figure 4-4 and Figure 4-5 show the yields of the products of diphenyl ether over Ni catalyst under 5 bar of H<sub>2</sub> and D<sub>2</sub>, respectively. The products distributions and the selectivity of the reaction routes are very close in both atmospheres, which implies that the reaction mechanism does not change when we switch the gas from H<sub>2</sub> to D<sub>2</sub>. Because D-labeled diphenyl ether was observed after the reaction, and the rate of the H/D exchange between D<sub>2</sub> and ether was found to be comparable to the total conversion of diphenyl ether (Figure 4-5), decrease of the abundance of D in the gas phase during the reaction should be noted when we analyze the isotopic effect of the reaction rates and trace the deuterium in the products.

**Table 4-3. Kinetic isotopic experiments of diphenyl ether.<sup>[a]</sup>**

		Ni/SiO <sub>2</sub> , D <sub>2</sub>		further hydrogenation	
		decalin			
		TOF / h <sup>-1</sup>		Selectivity of	
Ether	Gas	Hydrogenolysis	Hydrogenation	hydrogenolysis	
	H <sub>2</sub>	68 ± 5	95 ± 5	42 %	
	D <sub>2</sub>	12 ± 3	20 ± 4	38 %	
<i>KIE<sub>H/D</sub></i>		5.7	4.8		

<sup>[a]</sup> Reaction conditions: diphenyl ether (1.70 g), 64 wt. % Ni/SiO<sub>2</sub> catalyst (10 mg), decalin 40 ml, 150 °C, gas pressure is 5 bar at room temperature, stirring at 700 rpm. TOFs were calculated at < 20 % conversion.



**Figure 4-4. Time-yield plots from the reaction of diphenyl ether over Ni catalyst under H<sub>2</sub> in decalin.** Reaction conditions: ether (5.1 g), 64 wt. % Ni/SiO<sub>2</sub> catalyst (10 mg), decalin 40 ml, 150 °C and 5 bar of hydrogen at room temperature, stirring at 700 rpm.

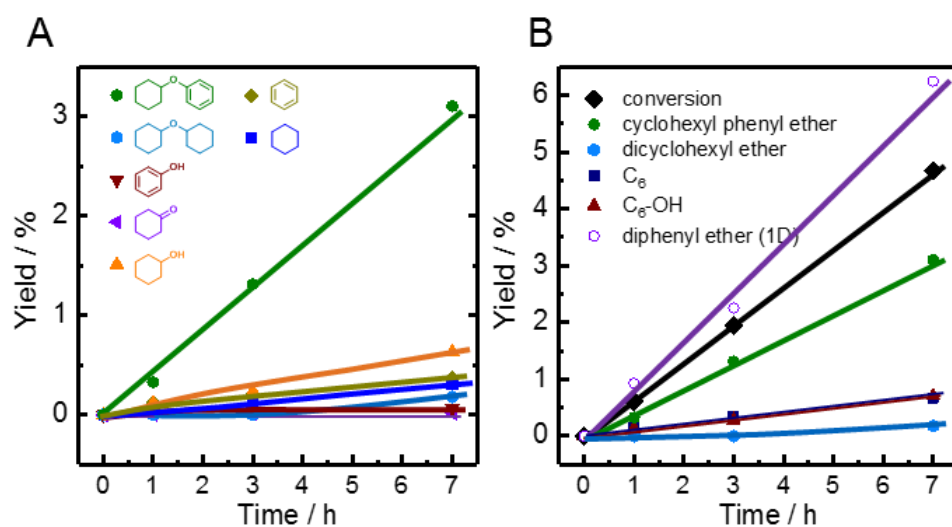


**Figure 4-5. Time-yield plots from the reaction of diphenyl ether over Ni catalyst under D<sub>2</sub> in decalin.** Reaction conditions: ether (5.1 g), 64 wt. % Ni/SiO<sub>2</sub> catalyst (10 mg), decalin 40 ml, 150 °C and 5 bar of deuterium at room temperature, stirring at 700 rpm.

As shown in Figure 4-6A, in D<sub>2</sub>, the rates of the consumptions of diphenyl ether (calculated from the recovered materials after the reaction) and D<sub>2</sub> (calculated from the readouts of D<sub>2</sub> pressure) are 32 h<sup>-1</sup> and 100 h<sup>-1</sup>, respectively. About three D<sub>2</sub> molecules were consumed when one ether molecule was converted to one cyclohexyl phenyl ether or one benzene and one cyclohexanol. Trace amount of phenol was detected under this reaction condition. The H/D exchange rate between diphenyl ether and D<sub>2</sub> was



$35 \text{ h}^{-1}$ , this relatively slow rate ensured the high abundance of D in gas phase which allowed us to analyze the deuterium distribution in the primary products from hydrogenolysis. The abundance of D in gas phase has been measured by sampling the gas after the reaction and analyzing by mass spectroscopy, it was 100 % at 0 h and 82 % at 7 h (Figure 4-6B).

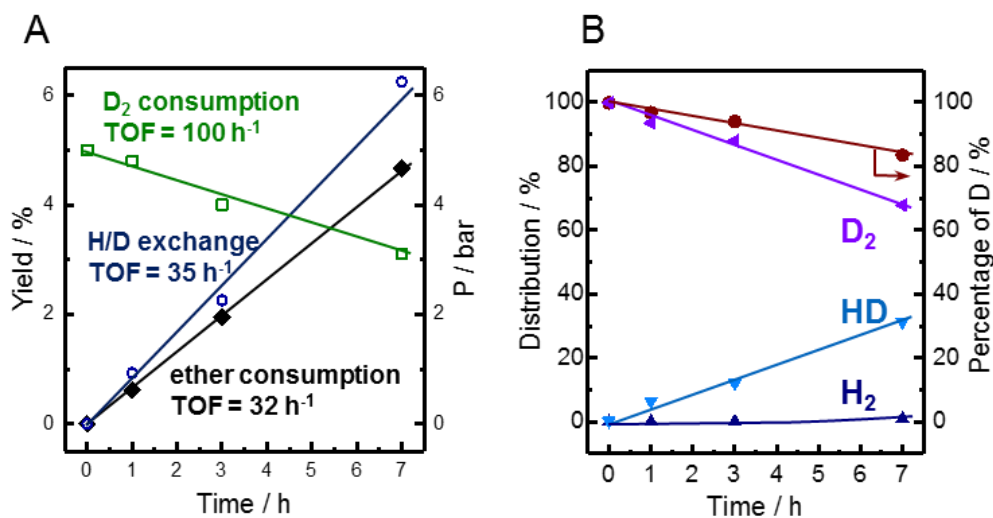


**Figure 4-6.** Reactions of aryl ether in  $\text{D}_2$ . (A) Comparison of the rates of ether consumption,  $\text{D}_2$  consumption and H/D exchange between  $\text{D}_2$  and ether. (B) The distribution of  $\text{H}_2$ , HD and  $\text{D}_2$  in gas phase.

The contents of deuterium in the primary products of hydrogenolysis of diphenyl ether, benzene and phenol, were determined by GC-mass spectroscopy. Because the D from the hydroxyl group in phenol can exchange with the H in GC column, the hydroxyl group in phenol was exchanged to OH via several wash steps by water prior to the GC measurement. Figure 4-7 shows the deuterium incorporation on the aromatic rings of benzene and phenol. One D was found in benzene (> 90 %) and no D was found in the aromatic ring of phenol (> 90 %) at 1h, the decrease of the distribution of  $\text{C}_6\text{H}_5\text{D}$  and  $\text{C}_6\text{H}_5\text{-OH}$  at longer reaction time was the result of the decrease of the D abundance and the H/D exchange. Since one phenol and one benzene are generated from one diphenyl ether and one  $\text{D}_2$  over nickel catalyst, the products from  $\text{D}_2$  are  $\text{C}_6\text{H}_5\text{D}$  and  $\text{C}_6\text{H}_5\text{-OD}$ . The details of the reactions of diphenyl ether in  $\text{D}_2$  are summarized in Figure 4-8.

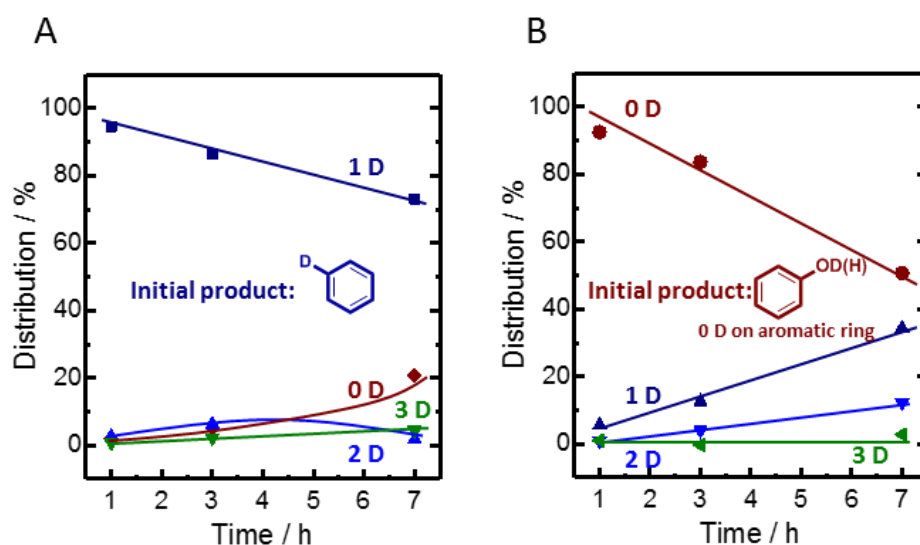


Figure 4-7. For the reaction of aryl ether in  $D_2$ , the D incorporation into primary products (A for benzene and B for phenol) from hydrogenolysis.

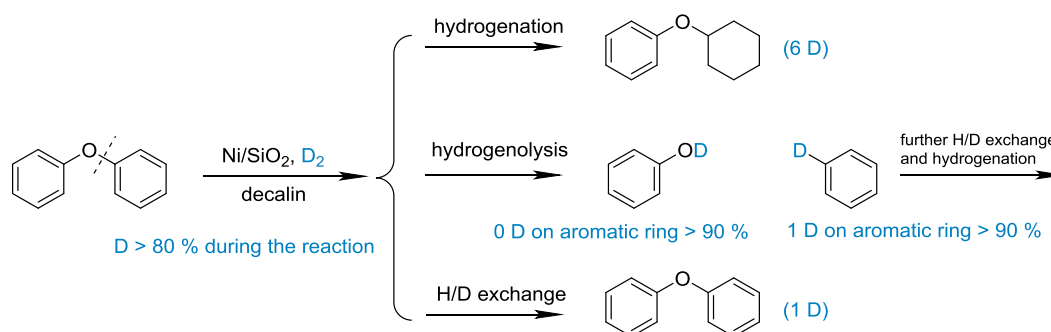
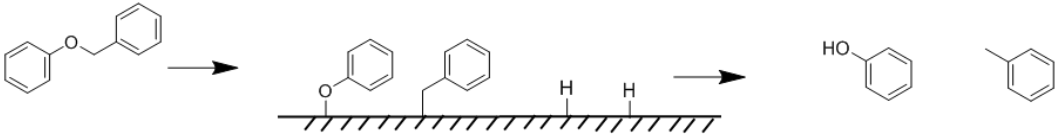


Figure 4-8. Summary of reactions of diphenyl ether under  $D_2$ .

### 4.3.3 Comparison between diphenyl ether and benzyl phenyl ether

Because of the primary kinetic isotope effect ( $K_H/K_D > 5$ ) and reaction order (half) in  $H_2$  pressure for the hydrogenolysis of diphenyl ether in decalin, the first hydrogen addition has to be considered in the mechanism of C-O bond cleavage. For the hydrogenolysis of a weaker C-O bond, benzyl phenyl ether, experimental and theoretical work showed the C-O bond breaks on the metal surface to form adsorbed benzyl and phenoxy radicals first, then the recombination between surface H and the radicals will generate toluene and phenol, respectively. The rate determining step is the cleavage of C-O bond, and hydrogen addition is not involved.<sup>15</sup> The comparison between diphenyl ether and benzyl phenyl ether has been made to verify that the mechanism of hydrogenolysis of diphenyl ether is initiated by one hydrogen addition rather than C-O bond scission.

Table 4-4. Detailed information of the reactions of benzyl phenyl ether on Ni catalyst.



Gas	TOF / h <sup>-1</sup>	molar selectivity / %								
		hydrocarbons			oxygenates		hydrogenation		isomerization	
12 bar H <sub>2</sub>	370	49	<1	32	5	11	1		<1	
5 bar H <sub>2</sub>	460	53	<1	22	5	18	1		<1	
5 bar D <sub>2</sub>	240	51	<1	37	3	8	1		<1	
<i>KIE<sub>H/D</sub></i>	1.9									

<sup>[a]</sup> Reaction conditions: benzyl phenyl ether (1.00 g), 64 wt. % Ni/SiO<sub>2</sub> catalyst (10 mg), decalin 40 ml, 150 °C, stirring at 700 rpm. TOFs were calculated at < 20 % conversion.

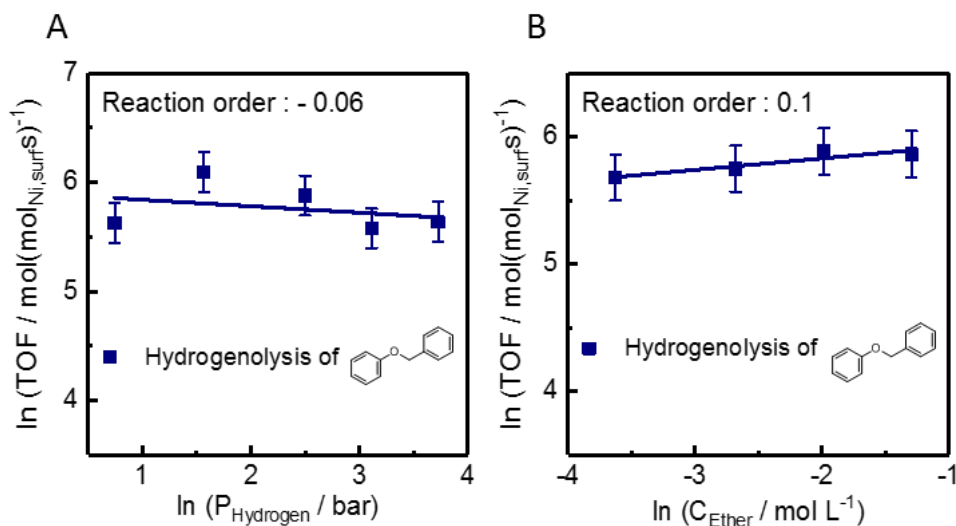
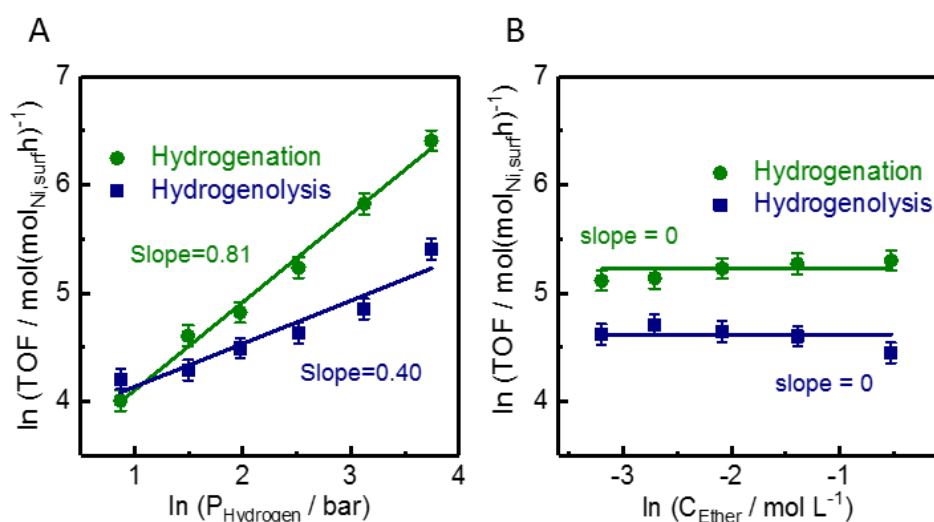


Figure 4-9. Reaction orders in H<sub>2</sub> pressure (A) and ether concentration (B) of hydrogenolysis of benzyl phenyl ether on Ni catalyst in decalin.

Reaction conditions: 64 wt. % Ni/SiO<sub>2</sub> catalyst (10 mg), decalin 40 ml, 150 °C, stirring at 700 rpm. H<sub>2</sub> pressure varies from 2.1 to 42 bar. Ether concentration varies from 0.027 to 0.27 M. TOFs were calculated at < 20 % conversion.

Table 4-4 shows the reaction rates and products distribution of the conversion of benzyl phenyl ether over nickel catalyst under the same reaction conditions compared to diphenyl ether. Comparing to diphenyl ether, hydrogenolysis of benzyl phenyl ether showed higher rates and selectivity (> 96 %) in the reaction conditions we have measured, this can be explained by the weaker bond dissociation energy of the C-O bond. Relatively indistinctive kinetic isotopic effect ( $KIE_{HD} = 1.9$ ) and inconspicuous hydrogen dependence were observed. This agrees with the mechanism showing in Table 4-4 while the rate-determining step is the cleavage of C-O bond. The rate dependences of  $H_2$  pressure and ether concentration were measured by varying  $H_2$  pressure from 2.1 to 42 bar and ether concentration from 0.027 to 0.27 M, respectively (Figure 4-9). The approximate zero (-0.06) reaction order in  $H_2$  pressure and zero (0.1) reaction order in ether concentration are consistent with the mechanism that the rate-determining step is the cleavage of C-O bond when the surface coverage of ether is relatively high (see details in Appendix).

For diphenyl ether, as shown in Figure 4-10, reaction orders for hydrogenolysis and hydrogenation are both zero order in ether concentration which also agree with the high surface coverage of ether. The positive reaction order in  $H_2$  pressure for hydrogenolysis (0.40) indicates a mechanistic scenario which is not initiated with C-O bond breaking. Most likely, the hydrogenolysis of diphenyl ether starts from one hydrogen addition.



**Figure 4-10. Reaction orders in  $H_2$  pressure (A) and ether concentration (B) of reactions of diphenyl ether on Ni catalyst in decalin.**

Reaction conditions: 64 wt. % Ni/SiO<sub>2</sub> catalyst (10 mg), decalin 40 ml, 150 °C, stirring at 700 rpm.  $H_2$  pressure varies from 2.4 to 42 bar. Ether concentration varies from 0.04 to 0.60 M. TOFs were calculated at < 20 % conversion.

### 4.3.4 Hypothesis for reaction mechanism of hydrogenolysis and DFT calculations

Considering the hydrogen dependence, isotope effect and initial products in  $D_2$  ( $C_6H_5D$  and  $C_6H_5-OD$ ) of hydrogenolysis of diphenyl ether, four mechanisms (Figure 4-11B and C) which could potentially occur on the metal surface were proposed. For the concerted C-O bond breaking mechanisms (Figure 4-11B), the C-O bond breaks with the assistant of hydrogen attack on the O or C to form phenol or benzene at first, then the recombination between the remaining fragment and surface hydrogen generates the other initial product. The first hydrogen addition mechanistic scenarios (Figure 4-11C) start with one hydrogen addition to the ipso or ortho position of the left, adsorbed, aromatic ring, then the disturbed C-O bonds are weakened and cleaved on the metal surface to form  $C_6H_6$  and phenoxy group. Another mechanism, C-O bond breaking (Figure 4-11A) is also listed for comparison, the rate-determining step in this mechanism is C-O scission was proved in homogeneous system by the zero reaction order in  $H_2$  pressure and non-isotope effect from  $H_2$  and  $D_2$ .<sup>15</sup>

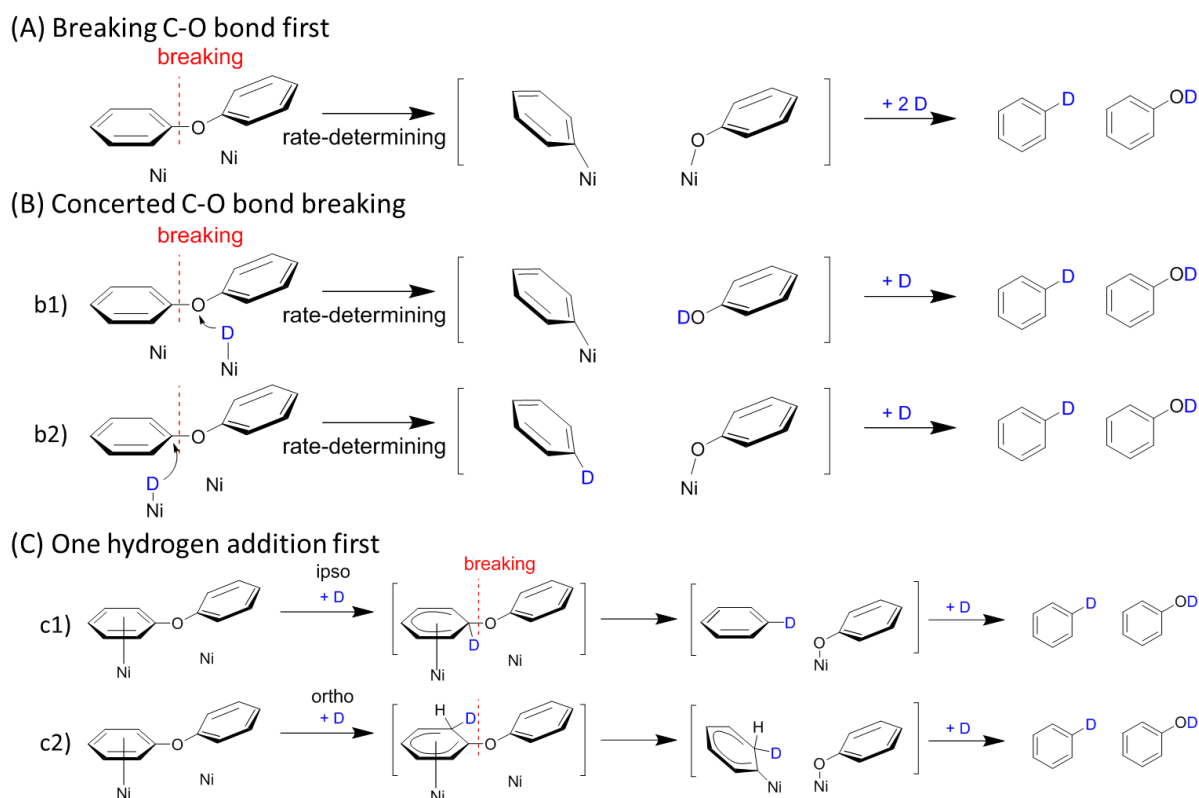


Figure 4-11. Hypothesis of reaction mechanism of hydrogenolysis of diphenyl ether over Nickel catalyst.

To gain mechanistic insights into the hydrogen assisted C-O bond cleavage mechanism and more importantly, as the rate-determining step in hydrogenolysis reaction of diphenyl ether over nickel based catalysts, density functional theory calculations were performed to study both hydrogenation and hydrogenolysis (C-O bond scission) routes shown in Figure 4-11. Carbon attacking (path b2 in Figure 4-11) was found for concerted mechanism and ortho addition (path c2) was found for advanced hydrogen addition. The concerted C-O bond breaking pathway (path b2) is unlikely due to the high activation barrier of 200 kJ/mol. While the addition of first hydrogen at the ortho C position on the aromatic ring is 108 kJ/mol (path c2) is favorable over the direct C-O bond cleavage step with a barrier of 158 kJ/mol (path a). Upon the first hydrogenation step, our calculations showed that the second hydrogenation (103 kJ/mol) is still kinetically easier than the C-O bond scission (137 kJ/mol). While the third consecutive hydrogenation step is feasible with much lower barrier of 69 kJ/mol. This is consistent with the experimental observation of first order in H<sub>2</sub> pressure for hydrogenation and high hydrogenation product selectivity. We note that the addition of first hydrogen atom at the aromatic ring would facilitate the C-O bond scission of the adsorbed ether. In terms of kinetical barrier, the C-O bond scission of first hydrogen-added diphenyl ether and the second hydrogenation are concurrent competitive although the latter one is more competitive shown in Figure 4-12. As a result, the hydrogenolysis route is half order in H<sub>2</sub> pressure as observed in our experiments.

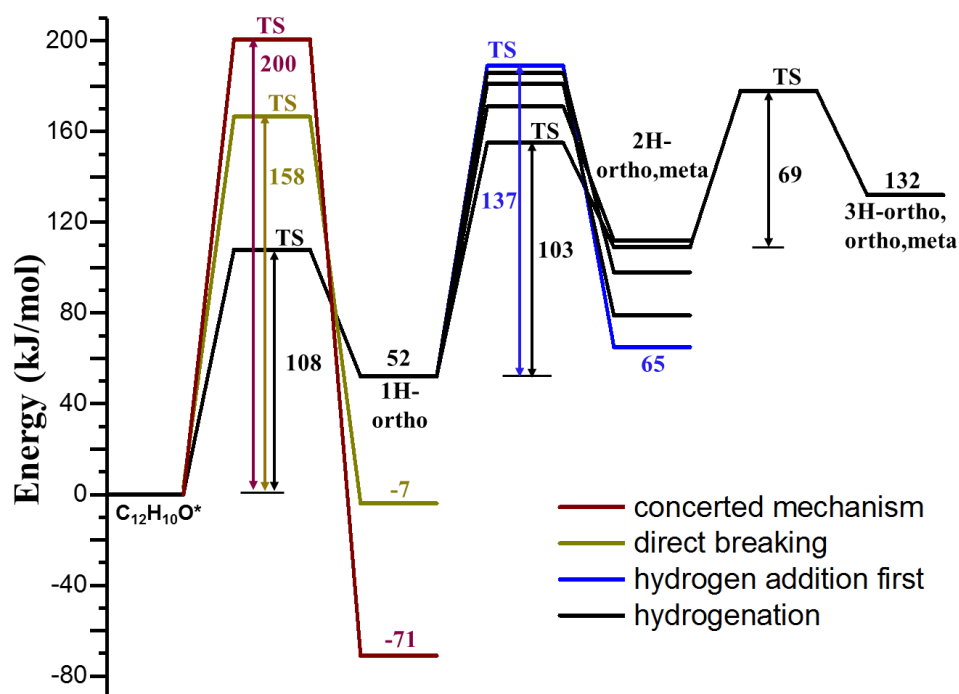
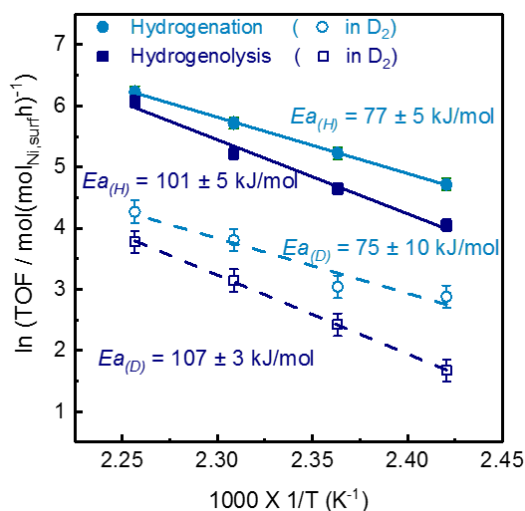


Figure 4-12. DFT calculated energy profile of diphenyl ether conversion.

The apparent reaction energies of hydrogenolysis and hydrogenation in decalin were measured to be 101 and 77 kJ/mol, respectively (Figure 4-13). The relatively lower activation energy for hydrogenation is consistent with the DFT calculations. Similar activation energies have been observed for the reactions of diphenyl ether in  $D_2$ . In aqueous phase, lower reaction rates and lower reaction energies were found (Figure 4-14).



**Figure 4-13.** Arrhenius plots [ $\ln(\text{TOF})$  vs  $1/T$ ] for the conversion of diphenyl ether under  $H_2$  and  $D_2$  in decalin.

Reaction conditions: ether (1.70 g), decalin (40 mL), 64 wt.% Ni/SiO<sub>2</sub> (10.0 mg), 413–443 K, 12 bar for hydrogen and 5 bar for deuterium, stirring at 700 rpm.

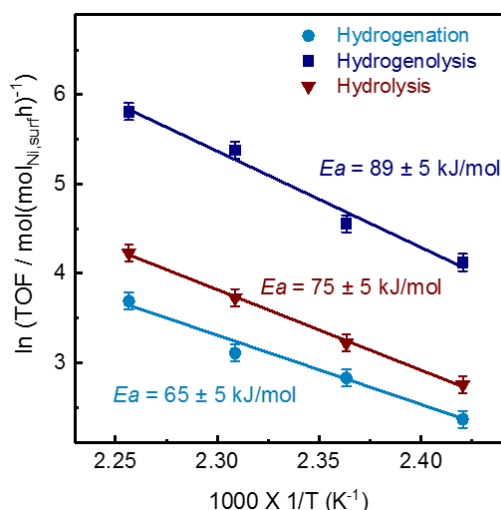


**Figure 4-14.** Arrhenius plots [ $\ln(\text{TOF})$  vs  $1/T$ ] for the conversion of diphenyl ether under  $H_2$  in water.

Reaction conditions: ether (1.70 g), water (80 mL), 64 wt.% Ni/SiO<sub>2</sub> (20.0 mg), 413–443 K, 40 bar of hydrogen, stirring at 700 rpm.

## 4.4 Conclusions

In conclusion, we have demonstrated a detailed mechanistic study of hydrogenolysis of diphenyl ether which is highly selective in apolar and polar phases over heterogeneous Ni catalyst. Kinetic, isotopic and theoretical investigations were undertaken to illustrate the mechanism which was initiated by first hydrogen addition to the ortho position in the aromatic ring, then underwent C-O bond breaking. In contrast to the homogeneous Ni catalysts,<sup>15</sup> hydrogen is involved in the rate-determining step because positive reaction order in H<sub>2</sub> and primary isotopic effect was observed.

## 4.5 Acknowledgements

This work was supported by the U.S. Department of Energy, Office of Science, Office of Basic Energy Sciences, Division of Chemical Sciences, Geosciences, and Biosciences. Portions of the work were performed at the William R. Wiley Environmental Molecular Science Laboratory, a national scientific user facility sponsored by the DOE's Office of Biological and Environmental Research located at Pacific Northwest National Laboratory, a multiprogram national laboratory operated for DOE by Battelle Memorial Institute.

## 4.6 Appendix

### 4.6.1 Analysis of D incorporation in the chemicals by MS

The D content in recovered diphenyl ether and the initial products from hydrogenolysis of diphenyl ether, benzene and phenol, were carefully analyzed by GC-MS, i.e., an Agilent 7890A GC equipped with a HP-5MS 25 m × 0.25 μm (i.d.) column and coupled with Agilent 5975C MS. Because the D from the hydroxyl group in phenol can exchange with the H in GC column, the hydroxyl group in phenol was exchanged to OH via several wash steps by water prior to the GC measurement. For each compound, the base peak is the m/z value equivalent to mass itself, i.e. diphenyl ether is 170, benzene is 78 and phenol is 94. Because undetectable intensities for the m/z ≥ M + 4 were observed for these chemicals, we calculated the distribution functions of 0D, 1D, 2D and 3D labeled compounds ( $x_{0D}$ ,  $x_{1D}$ ,  $x_{2D}$  and  $x_{3D}$ ) via the equation listed below from the MS result.  $I_{[i]}$  is the peak intensity of m/z = i from measurement and  $ref_{[i]}$  is the peak intensity of m/z = i from unlabeled material.

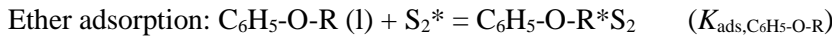
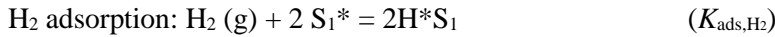


$$\begin{pmatrix} ref_{[M]} & ref_{[M-1]} & ref_{[M-2]} & ref_{[M-3]} \\ ref_{[M+1]} & ref_{[M]} & ref_{[M-1]} & ref_{[M-2]} \\ ref_{[M+2]} & ref_{[M+1]} & ref_{[M]} & ref_{[M-1]} \\ ref_{[M+3]} & ref_{[M+2]} & ref_{[M+1]} & ref_{[M]} \end{pmatrix} \begin{pmatrix} x_{0D} \\ x_{1D} \\ x_{2D} \\ x_{3D} \end{pmatrix} = \begin{pmatrix} I_{[M]} \\ I_{[M+1]} \\ I_{[M+2]} \\ I_{[M+3]} \end{pmatrix}$$

#### 4.6.2 Derivation of rate equations

We derive the kinetic expressions for the proposed mechanisms of hydrogenolysis in the main text based on the conventional Langmuir–Hinshelwood model with the following assumptions: (i) hydrogen adsorbs dissociatively on the metal site ( $S_1$ ), but it does not compete for the same sites ( $S_2$ ) with the ether and ether derived molecules (intermediates and products); (ii) the coverage of reaction intermediates and products are negligible at low conversions, so the most abundant chemical on the active site ( $S_2$ ) is the reactant. Some expressions are consistent with the observed rate dependencies on  $H_2$  pressure (half order for hydrogenolysis, Figure 4-1) and ether concentration (zero order, Figure 4-10). The constant reaction order in  $H_2$  despite 18-fold variation in  $H_2$  pressure indicates that the surface coverage of H is relatively low under the reaction conditions.

1) Within the mechanistic framework proposed in Figure 4-11 (main text), we first assume adsorption for reactants ( $H_2$  on  $S_1$  and ether on  $S_2$ ) are quasi-equilibrated:



Assuming any of the above steps to be rate-determining does not lead to rate expressions consistent with the observed reaction orders.

2) Applying site balance to all surface species, we have:

$$S_1: [S_1^*]_0 = [S_1^*] + [H^*S_1]$$

$$S_2: [S_2^*]_0 = [S_2^*] + [C_6H_5-O-R^*S_2] + \Sigma[\text{Derivatives}^*S_2]$$

where  $[^*]_0$  is the total number of sites available at the surface, and  $\Sigma[\text{Derivatives}^*S_2]$  is the sum of the coverage of reaction intermediates and products.

The rate of the reaction equals to the rate of the rate-determining step (RDS):  $r = r_{rds}$

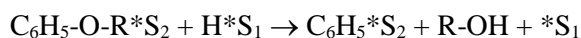
3a) C-O bond breaking mechanism,



$$r_a = \frac{k_{rds\_a} K_{ads,C_6H_5OR} [C_6H_5OR]}{(1 + K_{ads,C_6H_5OR} [C_6H_5OR])^2} \quad (\text{Eq. 4-1})$$

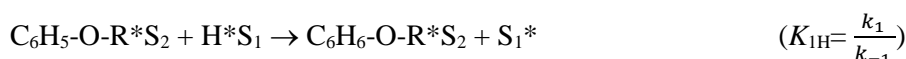
where  $k_{rds\_a}$  is the rate constant for the RDS.

3b) Concerted C-O bond breaking mechanism, the rate determining step is the H assisted C-O cleavage:



$$r_b = \frac{k_{rds\_b} K_{ads, C_6H_5OR} [C_6H_5OR] (K_{ads, H_2} [H_2])^{0.5}}{(1 + K_{ads, C_6H_5OR} [C_6H_5OR]) (1 + (K_{ads, H_2} [H_2])^{0.5})} \quad (\text{Eq. 4-2})$$

3c) First hydrogen addition mechanism,

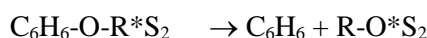


where  $k_1$  and  $k_{-1}$  are the forward and reverse rate constants for the first H addition step. It could be quasi-equilibrated, kinetically relevant or rate-determining.

If the rate-determining step is the hydrogen addition:

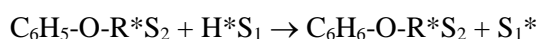
$$r_c = \frac{K_{1H} K_{ads, C_6H_5OR} [C_6H_5OR] (K_{ads, H_2} [H_2])^{0.5}}{(1 + K_{ads, C_6H_5OR} [C_6H_5OR]) (1 + (K_{ads, H_2} [H_2])^{0.5})} \quad (\text{Eq. 4-3})$$

If the first hydrogen addition is quasi-equilibrated, then the rate-determining step is the C-O cleavage:

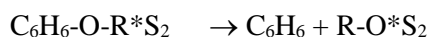


$$r_c = \frac{k_{rds\_c} K_{1H} K_{ads, C_6H_5OR} [C_6H_5OR] (K_{ads, H_2} [H_2])^{0.5}}{(1 + K_{ads, C_6H_5OR} [C_6H_5OR]) (1 + (K_{ads, H_2} [H_2])^{0.5})} \quad (\text{Eq. 4-4})$$

From the reactions under D<sub>2</sub>, we observed comparable reaction rates of C-O bond cleavage (12h<sup>-1</sup>, Table 4-3) and H/D exchange between ether and D<sub>2</sub> (35 h<sup>-1</sup>, Figure 4-6). It indicates that first hydrogen addition step should be kinetically relevant. So we use the steady-state approximation to derive the rate law by assuming that the rate of production of C<sub>6</sub>H<sub>6</sub>-O-R (first H addition product) is equal to the rate of its consumption.



where  $k_1$  and  $k_{-1}$  are the forward and reverse rate constants,



where  $k_c$  is the forward rate constant,

$$r_c = k' [C_6H_5-O-R^*S_2] [H^*S_1] = \frac{k' K_{ads, C_6H_5OR} [C_6H_5OR] (K_{ads, H_2} [H_2])^{0.5}}{(1 + K_{ads, C_6H_5OR} [C_6H_5OR]) (1 + (K_{ads, H_2} [H_2])^{0.5})} \quad (\text{Eq. 4-5})$$

where  $k' = k_1 k_c / (k_{-1} + k_c)$ .

4) The measured reaction order in  $H_2$  was close to half order (0.4) for hydrogenolysis, and the reaction order in concentration of ether reactant was zero. According to Eq. 4-1, non-hydrogen dependency should be observed. For Eq. 4-2 and 4-5, when the surface coverage of ether is high and hydrogen is low, we should observe the reaction orders are zero order in ether concentration and half order in  $H_2$  pressure. These two expressions are consistent with the measured reaction orders.

### 4.6.3 Discussion about diffusion limitation

The complicated heterogeneous reaction system is constituted by liquid solvent, solid catalyst, organic reactant and products, and the high pressure  $H_2$  gas. For kinetic measurements, all experiments must be performed in the kinetic regime without mass transport limitations. The reaction rates should not be limited by the mass transport phenomena between liquid-solid, liquid-liquid, or liquid-gas phases. H/D exchange experiments were obtained to test the mass transfer of  $H_2$  and  $D_2$  from gas phase to metal catalyst surface (Figure 4-15). The exchange reached equilibrium instantly when reaction temperature (150 °C) was achieved, it indicates that the mass transfer and activation of  $H_2$  do not limit the reaction rates.

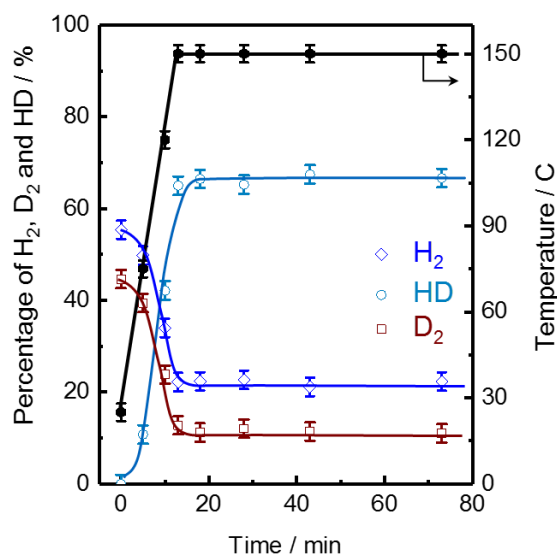


**Figure 4-15. H/D exchange between  $H_2$  and  $D_2$  in Parr reactor.**

Reaction conditions: decalin (40 mL), 64 wt.% Ni/SiO<sub>2</sub> (10.0 mg), pressure of the gas is 12 bar (45 % of  $D_2$  and 55 % of  $H_2$ ), the reactor needs 13 mins to achieve 150 °C, stirring at 700 rpm.

The experiments with varying stirring speeds were also performed to gain insights into possible mass transfer effects for the condense phase, Figure 4-16, mass transfer limitations do exist when the stirring speed is less than 300 rpm. All systematic experiments have been performed with a stirring speed of 700 rpm to exclude mass transfer effects.

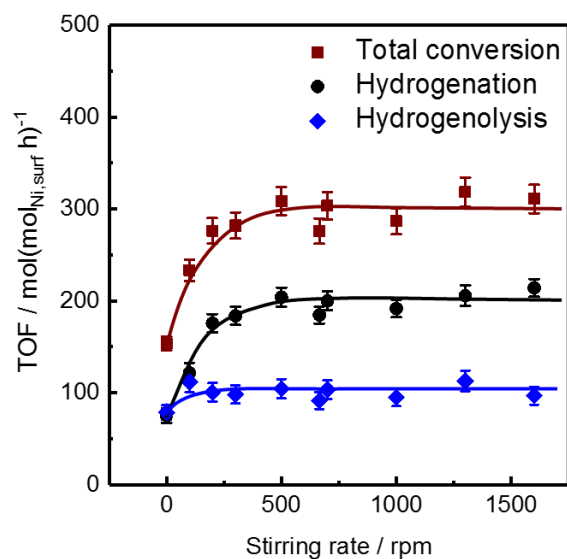


**Figure 4-16. Stirring dependency.**

Reaction conditions: ether (1.70 g), decalin (40 mL), 64 wt.% Ni/SiO<sub>2</sub> (10.0 mg), 12 bar of H<sub>2</sub>, 150 °C, stirring speed varies from 0 to 1600 rpm.

## 4.7 References

1. Zakzeski, J.; Bruijninx, P. C. A.; Jongerius, A. L.; Weckhuysen, B. M., *Chemical Reviews* **2010**, *110* (6), 3552-3599.
2. Alonso, D. M.; Wettstein, S. G.; Dumesic, J. A., *Chemical Society Reviews* **2012**, *41* (24), 8075-98.
3. Besson, M.; Gallezot, P.; Pinel, C., *Chemical Reviews* **2014**, *114* (3), 1827-1870.
4. Li, C.; Zhao, X.; Wang, A.; Huber, G. W.; Zhang, T., *Chemical Reviews* **2015**, *115* (21), 11559-624.
5. Rosen, B. M.; Quasdorf, K. W.; Wilson, D. A.; Zhang, N.; Resmerita, A.-M.; Garg, N. K.; Percec, V., *Chemical Reviews* **2011**, *111* (3), 1346-1416.
6. Cornella, J.; Zarate, C.; Martin, R., *Chemical Society Reviews* **2014**, *43* (23), 8081-8097.
7. Duzee, E. M. v.; Adkins, H., *Journal of the American Chemical Society* **1935**, *57* (1), 147-151.
8. Marshall, A. L.; Alaimo, P. J., *Chemistry – A European Journal* **2010**, *16* (17), 4970-4980.
9. Wang, X.; Rinaldi, R., *ChemSusChem* **2012**, *5* (8), 1455-1466.
10. Sergeev, A. G.; Hartwig, J. F., *Science* **2011**, *332* (6028), 439-443.
11. Kelley, P.; Lin, S.; Edouard, G.; Day, M. W.; Agapie, T., *Journal of the American Chemical Society* **2012**, *134* (12), 5480-3.
12. Cornella, J.; Gómez-Bengoa, E.; Martin, R., *Journal of the American Chemical Society* **2013**, *135* (5), 1997-2009.
13. Gao, F.; Webb, J. D.; Hartwig, J. F., *Angewandte Chemie International Edition* **2016**, *55* (4), 1474-8.
14. Meng, Q.; Hou, M.; Liu, H.; Song, J.; Han, B., *Nature Communications* **2017**, *8*, 14190.
15. Saper, N. I.; Hartwig, J. F., *Journal of the American Chemical Society* **2017**, *139* (48), 17667-17676.
16. Wang, M.; Shi, H.; Camaioni, D. M.; Lercher, J. A., *Angewandte Chemie International Edition* **2017**, *56* (8), 2110-2114.
17. Wang, M.; Gutiérrez Oliver, Y.; Camaioni Donald, M.; Lercher Johannes, A., *Angewandte Chemie International Edition* **2018**, *57* (14), 3747-3751.
18. Nguyen, J. D.; Matsuura, B. S.; Stephenson, C. R. J., *Journal of the American Chemical Society* **2014**, *136* (4), 1218-1221.
19. Rahimi, A.; Ulbrich, A.; Coon, J. J.; Stahl, S. S., *Nature* **2014**, *515*, 249.
20. Tobisu, M.; Chatani, N., *Accounts of Chemical Research* **2015**, *48* (6), 1717-1726.
21. Son, S.; Toste, F. D., *Angewandte Chemie International Edition* **2010**, *49* (22), 3791-3794.
22. Parsell, T. H.; Owen, B. C.; Klein, I.; Jarrell, T. M.; Marcum, C. L.; Hauptert, L. J.; Amundson, L. M.; Kenttämä, H. I.; Ribeiro, F.; Miller, J. T.; Abu-Omar, M. M., *Chemical Science* **2013**, *4* (2), 806-813.
23. Barta, K.; Ford, P. C., *Accounts of Chemical Research* **2014**, *47* (5), 1503-1512.
24. Chatterjee, M.; Chatterjee, A.; Ishizaka, T.; Kawanami, H., *Catalysis Science & Technology* **2015**, *5* (3), 1532-1539.

25. Chen, L.; Koranyi, T. I.; Hensen, E. J., *Chemical Communications* **2016**, 52 (60), 9375-8.
26. Shao, Y.; Xia, Q.; Dong, L.; Liu, X.; Han, X.; Parker, S. F.; Cheng, Y.; Daemen, L. L.; Ramirez-Cuesta, A. J.; Yang, S.; Wang, Y., *Nature Communications* **2017**, 8, 16104.
27. Haibach, M. C.; Lease, N.; Goldman, A. S., *Angewandte Chemie International Edition* **2014**, 53 (38), 10160-3.
28. Álvarez-Bercedo, P.; Martín, R., *Journal of the American Chemical Society* **2010**, 132 (49), 17352-17353.
29. Song, Q.; Wang, F.; Cai, J.; Wang, Y.; Zhang, J.; Yu, W.; Xu, J., *Energy & Environmental Science* **2013**, 6 (3), 994.
30. Zaheer, M.; Kempe, R., *ACS Catalysis* **2015**, 5 (3), 1675-1684.
31. He, J.; Zhao, C.; Lercher, J. A., *Journal of the American Chemical Society* **2012**, 134 (51), 20768-20775.
32. Sawatlon, B.; Wititsuwannakul, T.; Tantirungrotechai, Y.; Surawatanawong, P., *Dalton Transactions* **2014**, 43 (48), 18123-18133.
33. Xu, L.; Chung, L. W.; Wu, Y.-D., *ACS Catalysis* **2016**, 6 (1), 483-493.
34. Sergeev, A. G.; Webb, J. D.; Hartwig, J. F., *Journal of the American Chemical Society* **2012**, 134 (50), 20226-20229.
35. He, J.; Zhao, C.; Mei, D.; Lercher, J. A., *Journal of Catalysis* **2014**, 309, 280-290.
36. Molinari, V.; Giordano, C.; Antonietti, M.; Esposito, D., *Journal of the American Chemical Society* **2014**, 136 (5), 1758-1761.
37. Zaheer, M.; Hermannsdörfer, J.; Kretschmer, W. P.; Motz, G.; Kempe, R., *ChemCatChem* **2014**, 6 (1), 91-95.
38. Zhang, J.; Teo, J.; Chen, X.; Asakura, H.; Tanaka, T.; Teramura, K.; Yan, N., *ACS Catalysis* **2014**, 4 (5), 1574-1583.
39. Kresse, G.; Furthmüller, J., *Physical Review B* **1996**, 54 (16), 11169-11186.
40. Kresse, G.; Hafner, J., *Physical Review B* **1993**, 48 (17), 13115-13118.
41. Blöchl, P. E., *Physical Review B* **1994**, 50 (24), 17953-17979.
42. Kresse, G.; Joubert, D., *Physical Review B* **1999**, 59 (3), 1758-1775.
43. Perdew, J. P.; Burke, K.; Ernzerhof, M., *Physical Review Letters* **1996**, 77 (18), 3865-3868.

## Chapter 5 Catalytic Reductive Cleavage of Diphenyl Ether over Noble Metal Catalysts

*The catalytic cleavage of C-O bond in diphenyl ether can be controlled by the choice of the noble metal catalysts (Ru, Pt, Rh and Pd) and different solvents. The aromatic C-O bond is cleaved hydrogenolytically and/or hydrolytically, while in parallel the aromatic rings can be hydrogenated without changing the molecular backbone. The preference to hydrogenolysis of the C-O bond over hydrogenation of the aromatic ring increases in the order Pd/C < Rh/C < Pt/C  $\approx$  Ru/C both in decalin and water, it is due to the difference of oxophilicity of different metal catalysts. For hydrolysis in water, a reverse trend was observed. Because the reductive hydrolysis occurs via partial hydrogenation (two hydrogen addition), more reductive hydrolysis is obtained when the selectivity of hydrogenation is higher.*

## 5.1 Introduction

As we discussed in the previous chapters, selective catalytic cleavage of aryl ethers and other types of C–O bonds is highly challenging because of their relatively high bond dissociation energies and the competition with alternative hydrogenation reactions.<sup>1-6</sup> This is one of the central challenges for the valorization of the lignin component of biomass.<sup>7-9</sup> The depolymerization can occur *via* selective oxidation of lignin followed by a redox-neutral cleavage<sup>9</sup> or *via* a reductive pathway using metal/acid catalyzed hydrolysis and hydrogenolysis.<sup>10</sup> Both pathways should be able to lead to successfully complete deconstruction of lignin, the rates and complexity of the operating conditions make it mandatory to find more active catalysts. For fundamental investigation of the principal relation between active catalysts and the reactivity of the C–O ether bond cleavage, model compounds of lignin, i.e.  $\alpha$ -O-4,  $\beta$ -O-4 and 4-O-5 linkages, were widely used.<sup>11-12</sup> Meanwhile, a wide range of heterogeneous noble metal<sup>12-23</sup>, non-noble metal<sup>11, 24-31</sup> acid,<sup>32-37</sup> and multifunctional<sup>10, 38-40</sup> catalysts have been reported for the selective cleavage of these model compounds. Most of these catalysts tend to operate under reductive conditions and elevated temperatures.

Under reductive conditions, the reaction pathways for the conversion of aryl ethers are broadly classified into hydrogenation, hydrogenolysis and hydrolysis (reductive). Here, “hydrogenation” is limited to reactions which saturate the aromatic rings without breaking the molecular backbone. For diphenyl ether which contains one of the strongest common structural link (4-O-5 linkage) and has been systematically studied from chapter 2 to chapter 4, hydrogenation generates cyclohexyl phenyl ether and dicyclohexyl ether, hydrogenolysis generates benzene and phenol (1:1) and reductive hydrolysis generates cyclohexanone and phenol (1:1). These three pathways were observed in aqueous phase over Ni/SiO<sub>2</sub> and Pd/C catalysts under hydrogen with different selectivities, and only hydrogenolysis and hydrogenation were found in decalin (Figure 5-1).

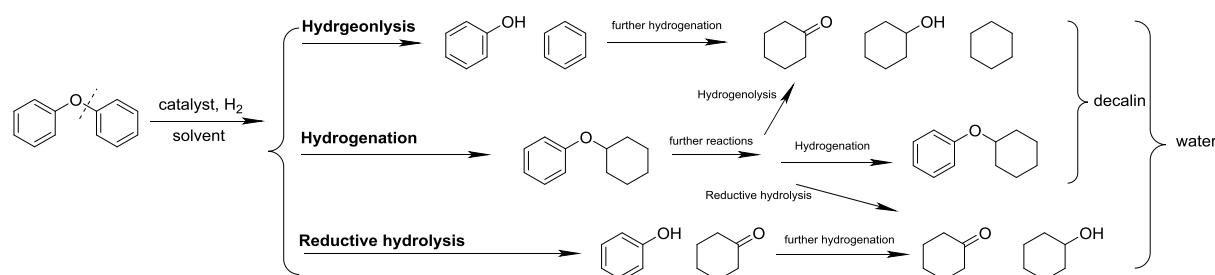


**Figure 5-1.** Reaction pathways and secondary reactions of diphenyl ether over metal catalyst under hydrogen in decalin and water.



Due to our previous mechanistic studies for hydrogenolysis on Ni/SiO<sub>2</sub> catalyst and reductive hydrolysis on Pd/C catalysts, we established the mechanisms for these individual C-O cleavage pathways. As shown in Figure 5-2, for supported nickel catalysts, the hydrogenolysis is initiated by one hydrogen addition to the aromatic ring, the C-O bond breaks on the metal surface afterward. On supported palladium catalysts in water, partial hydrogenation of diphenyl ether forms an enol ether intermediate, the intermediate rapidly adds water to form hemiacetal which then eliminates the phenol to form cyclohexanone.

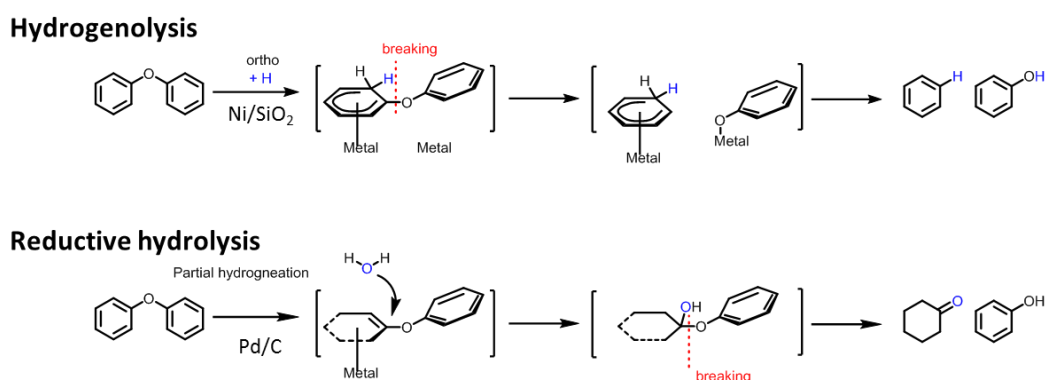


**Figure 5-2. Reaction mechanisms for hydrogenolysis and reductive hydrolysis.**

Based on the investigations of the mechanism for C-O cleavage reactions, a development of catalysts to understand activity and selectivity along the individual pathways could be achieved. Here, we evaluated four carbon supported noble metal catalysts (Ru, Pt, Rh and Pd) on reductive conversion of diphenyl ether along specific reaction pathways, i.e., hydrogenation and selective C-O bond cleavage *via* hydrogenolysis or reductive hydrolysis in polar (water) and apolar (decalin) solvents. In decalin, only hydrogenolysis was observed for C-O cleavage and the selectivity varied from 2 % to 21 % by changing the catalysts from Ru to Pd. For each metal catalyst, the selectivity of hydrogenolysis didn't change dramatically in water comparing to decalin. The preference to hydrogenolysis of the C-O bond over hydrogenation of the aromatic ring increases in the order Pd/C < Rh/C < Pt/C  $\approx$  Ru/C. We believe this is due to the difference of oxophilicity of different metal catalysts. For reductive hydrolysis in water on different metal catalysts, a reverse trend was observed. Because the reductive hydrolysis occurs via partial hydrogenation (two hydrogen addition) and the mechanism is in parallel with hydrogenation, more reductive hydrolysis is obtained when the selectivity of hydrogenation is higher.

## 5.2 Experimental

### 5.2.1 Chemicals and commercial catalysts

The chemicals were purchased from commercial suppliers and used as provided: diphenyl ether (Sigma-Aldrich, >99% GC assay), cyclohexyl phenyl ether (Sigma-Aldrich, >95% GC assay), benzene (Sigma-Aldrich, >99.5% GC assay), phenol (Sigma-Aldrich, >99% GC assay), cyclohexanone (Sigma-Aldrich, >99% GC assay), cyclohexanol (Sigma-Aldrich, >99% GC assay), dichloromethane (Sigma-Aldrich, >99.5% GC assay), decahydronaphthalene, mixture of cis + trans (Sigma-Aldrich, anhydrous,  $\geq 99\%$ ), 5 wt. % Ru/C (Sigma-Aldrich), 5 wt. % Rh/C (Sigma-Aldrich), 5 wt. % Pd/C (Sigma-Aldrich), 5 wt. % Pt/C (Sigma-Aldrich), H<sub>2</sub> (>99.999%), N<sub>2</sub> (> 99.999%), D<sub>2</sub> (Sigma-Aldrich, 99.9 atom % D) and normal H<sub>2</sub>O (Milli-Q, ultrapure water dispenser system). The lower metal loading catalysts, 0.25 wt. % Ru/C, 0.25 wt. % Pt/C and 0.25 wt. % Rh/C, were obtained by physically mixing original catalysts with activated carbon.

### 5.2.2 Catalyst tests

The detailed reaction conditions are described in the figure captions and table footnotes. Typically, the reactions were carried out in Parr autoclave reactors (Series 4848, 300 mL reactor for aqueous phase reactions and 100 mL reactor for decalin) in the presence of H<sub>2</sub>. Firstly, the ether, catalyst and solvent (water or decalin, 80 mL) were added into the Parr reactor at room temperature. After the reactor was flushed with H<sub>2</sub> three times, the autoclave was pressurized with H<sub>2</sub>, and the reaction was conducted at a certain temperature with a stirring speed of 700 rpm.

After the reaction, the reactor was quenched to ambient temperature by an ice/water mixture, and the contents in the reactor from aqueous phase were extracted using dichloromethane and analyzed by GC-MS, i.e., an Agilent 7890A GC equipped with a HP-5MS 25 m  $\times$  0.25  $\mu$ m (i.d.) column and coupled with Agilent 5975C MS. Products from reactions in decalin were directly measured after the dilution by dichloromethane. 1,3-Dimethoxybenzene was used as an internal standard for quantification purposes. The carbon balances for all the reported experiments were  $90 \pm 5\%$ . The turnover frequency (TOF) was calculated from conversion < 20 % and based on the number of surface metal atoms measured by H<sub>2</sub> chemisorption.

Because benzene and cyclohexane are generated only by hydrogenolysis (no cleavage of aromatic and aliphatic C-OH), the C-based selectivity of hydrogenolysis is twice the summed selectivity of benzene and cyclohexane. The selectivity of hydrolysis is calculated by subtracting the selectivities of hydrogenolysis and hydrogenation from 100%.

### 5.2.3 Catalyst characterizations

**Transmission electron micrographs (TEM)** were measured on a JEM-2010 Jeol transmission microscope operated at 120 kV. Before TEM measurement, the samples were dispersed in methanol on a carbon-coated Cu grid for TEM measurement.

**H<sub>2</sub> chemisorption measurement.** The catalysts were pretreated with a reduction under 0.1 MPa H<sub>2</sub> at 473 K for 4 h. Then the samples were activated in vacuum at 473 K for 1 h. The H<sub>2</sub> adsorption isotherms (chemisorption and physisorption) were recorded at 0.7 to 60 kPa at 308 K, following the first isotherms the samples were outgassed for 1 h in order to remove the physisorbed H<sub>2</sub>, which was followed by another adsorption isotherm (physisorption). The metal dispersions were obtained from the difference between extrapolated intercepts of the first and second isotherms with the assumption of H : metal atomic ratio = 1.

## 5.3 Result and discussion

### 5.3.1 Reactions in decalin

The reactions of diphenyl ether were measured in decalin first because hydrogenolysis is the only C-O cleavage reaction pathway which competes with hydrogenation. Table 5-1 shows the comparison of the selectivities of hydrogenolysis and hydrogenation at full conversion of diphenyl ether over four commercial supported noble metal catalysts (5 wt. % Ru/C, 5 wt. % Pt/C, 5 wt. % Rh/C and 5 wt. % Pd/C) at the same reaction conditions. The selectivities of hydrogenolysis of the metals scale as Ru > Pt > Rh > Pd. Pt and Rh catalysts showed higher reactivities than Ru and Pd catalysts. Cyclohexyl phenol ether, the product from hydrogenation of diphenyl ether, can be further hydrogenated or cleaved by hydrogen, it could change the overall selectivities of different reaction pathways during the reaction.

**Table 5-1. Selectivities of different reaction routes of diphenyl ether over different metal catalysts in decalin at full conversions.**

Catalyst	Time/min	Conversion	Selectivity	
			Hydrogenolysis	Hydrogenation
5 wt. % Ru/C	180	100%	21%	79%
5 wt. % Pt/C	60	98%	19%	81%
5 wt. % Rh/C	60	99%	11%	89%
5 wt. % Pd/C	360	98%	2%	98%

Reaction conditions: 10 mmol ether, 10 mg catalyst, 40 ml decalin, 40 bar of hydrogen at room temperature, 150 °C, stirring at 700 rpm.

In order to focus on the primary reactions of diphenyl ether, the conversions of diphenyl ether were controlled under 20 % by varying the reaction time and catalyst loading. Interestingly, the selectivities barely changed comparing to the selectivities at full conversion for each metal, it points to the fact that reaction of cyclohexyl phenyl ether is almost hydrogenation which generates dicyclohexyl ether. And the general reactivity of the metals scale as  $Rh > Pt > Ru > Pd$ . The TOFs were calculated based on the number of surface metal atoms measured by  $H_2$  chemisorption, the dispersions for the metal catalysts are comparable (Ru/C is 23 %, Pt/C is 57 %, Rh/C is 27 % and Pd/C is 31 %). The dispersions were also calculated from nanoparticle sizes measured by TEM (see details in Appendix).

**Table 5-2. Selectivities of different reaction routes and TOFs of diphenyl ether over different metal catalysts in decalin at low conversions.**

	TOF / s <sup>-1</sup>	Selectivity	
		Hydrogenolysis	Hydrogenation
Ru/C	2.0	21%	79%
Pt/C	5.5	20%	80%
Rh/C	7.4	9%	91%
Pd/C	0.70	2%	98%

Reaction conditions: 10 mmol ether, 10 mg 5 wt. % Ru/C, 20 mg 0.25 wt. % Rh/C, 20 mg 0.25 wt. % Pt/C or 10 mg 5 wt. % Pd/C catalyst, 40 ml decalin, 40 bar of hydrogen at room temperature, 150 °C, stirring at 700 ppm. TOFs were calculated at < 20 % conversion.

Product distribution from the reactions of diphenyl ether over different catalysts were carefully measured at different reaction times (Time-Yield plots in Appendix). The major products count for hydrogenolysis are cyclohexanol and cyclohexane even at conversions lower than 5 % for all the catalysts, it indicates that the primary products, benzene and phenol, are rapidly hydrogenated. The ratio between  $C_6$  (benzene, cyclohexene and cyclohexane) and  $C_6$ -OH (phenol, cyclohexanone and cyclohexanol) was constantly 1:1 across the reaction times and catalysts, which means hydrogenolysis was the only pathway for C-O cleavage of diphenyl ether and cyclohexyl phenyl ether and deoxygenation of  $C_6$ -OH was not observed under the reaction conditions. Figure 5-3 shows the summary of the product ( $C_6$ ,  $C_6$ -OH, cyclohexyl phenyl ether and dicyclohexyl ether) yields as a function of conversion. The yields of  $C_6$  and  $C_6$ -OH increased linearly up to 100 % of conversion over these four metals, it indicates that there is no contribution to hydrogenolysis from the secondary reactions of hydrogenation products (cyclohexyl phenyl ether and dicyclohexyl ether).

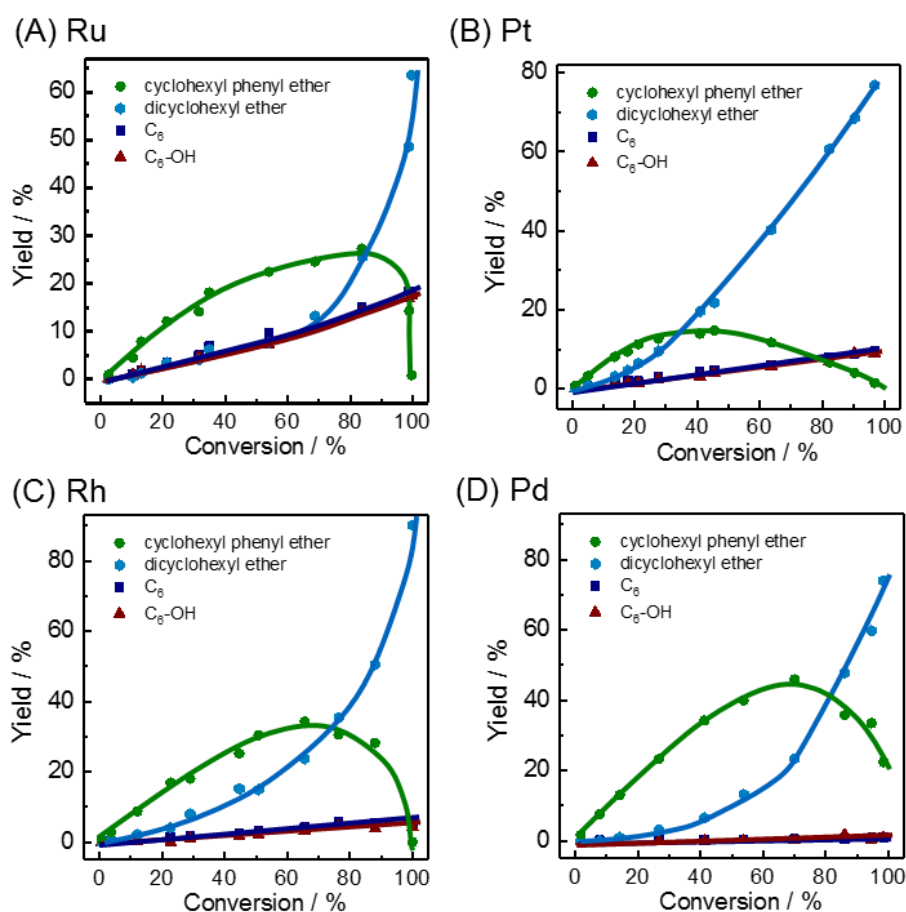


**Figure 5-3. Conversion-Yield plots of reactions of diphenyl ether on metal catalysts in decalin. (A) Ru, (B) Pt, (C) Rh and (D) Pd.**

$C_6$  represents benzene, cyclohexene and cyclohexane,  $C_6$ -OH represents phenol, cyclohexanone and cyclohexanol. Reaction conditions: 10 mmol ether, 40 ml decalin, 10 mg 5 wt. % Ru/C, 20 mg 0.25 wt. % Pt/C, 20 mg 0.25 wt. % Rh/C or 10 mg 5 wt. % Pd/C catalyst, 40 bar of  $H_2$ , 150 °C.

Comparing the four metal catalysts, dicyclohexyl phenyl ether was generated with different selectivities as primary product from hydrogenation of diphenyl ether and the secondary reaction of cyclohexyl phenyl ether dominated the overall reaction at different conversions over different catalysts. At conversions lower than 20 %, the yields of dicyclohexyl ether increased linearly and the selectivities were 22 %, 25 %, 17 % and 2 % from Ru, Pt, Rh and Pd, respectively. Diphenyl ether can be directly hydrogenated to dicyclohexyl ether, it implies that the two aromatic rings can be both adsorbed on the metal surface. Due to the high hydrogenation reactivity of noble metals, the double ring adsorption model decreases the possibility of C-O bond cleavage. Hydrogenation of cyclohexyl phenyl ether started to obviously change the selectivity of dicyclohexyl ether at conversions higher than 30 % on all catalysts. But for different catalysts, the highest yield of cyclohexyl phenyl ether were different and occurred at different conversions. The yield of cyclohexyl phenyl ether only achieved 15 % and started

to decrease at 45 % of conversion on Pt catalyst. For other catalysts, the highest yields (23 % for Ru, 34 % for Rh and 45 % for Pd) occurred at approximately 70 % of conversion. This is because of the competitive adsorption and different reactivity between diphenyl ether and cyclohexyl phenyl ether. In general, C-O cleavage (via hydrogenolysis) and hydrogenation of diphenyl ether were observed with different selectivities on noble metal catalysts, and secondary reactions are relatively simple to analyze because insignificant C-O cleavage of the intermediate and final products were detected.

As we demonstrated the reaction mechanism of hydrogenolysis in Chapter 4 by kinetic measurements (hydrogen dependency and isotopic effect) and DFT calculations. The reaction orders in H<sub>2</sub> pressure for hydrogenolysis and hydrogenation were determined (Figure 5-4), while the reaction orders in H<sub>2</sub> pressure for hydrogenolysis were approximately half order (Ru was 0.79, Pt was 0.39, Rh was 0.55 and Pd was 0.40) and reaction orders for hydrogenation were approximately first order (Ru was 1.4, Pt was 0.77, Rh was 0.84 and Pd was 0.79). These are consistent with the reaction orders that we measured from Ni/SiO<sub>2</sub> catalysts in decalin in Chapter 4. The constant reaction orders in H<sub>2</sub> pressure indicate that the reaction mechanisms over these five different metal catalysts (Ni/SiO<sub>2</sub>, Ru/C, Pt/C, Rh/C and Pd/C) are the same. For hydrogenation, the second hydrogen addition is the rate-determining step. Hydrogenolysis is initiated by one hydrogen addition to one ortho position of the aromatic ring, then the weakened C-O bond breaks on the metal surface (Figure 5-2).

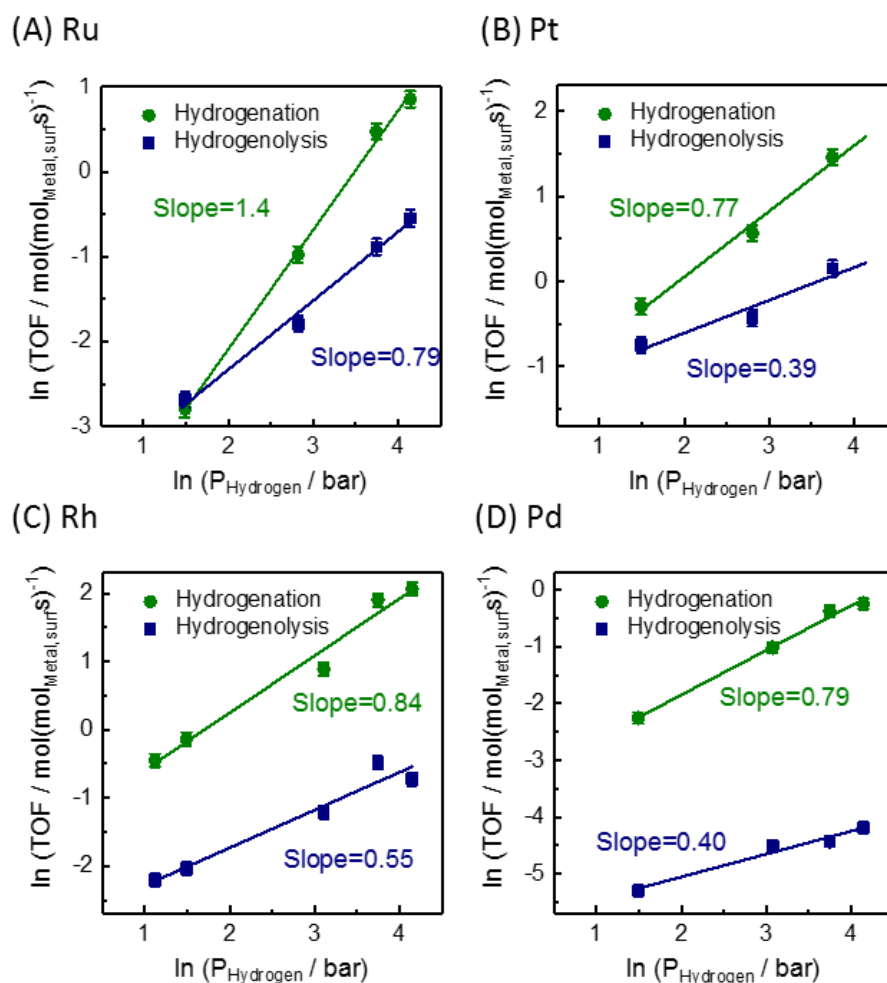


**Figure 5-4. Reaction orders in H<sub>2</sub> pressure of reactions, hydrogenation and hydrogenolysis, of diphenyl ether on metal catalysts in decalin. (A) Ru, (B) Pt, (C) Rh and (D) Pd.**

Reaction conditions: metal catalyst (10 mg 5 wt. % Ru/C, 20 mg 0.25 wt. % Pt/C, 20 mg 0.25 wt. % Rh/C or 10 mg 5 wt. % Pd/C), 10 mmol ether, 40 ml decalin, 150 °C, stirring at 700 rpm. H<sub>2</sub> pressure varies from 3 to 63 bar at room temperature. TOFs were calculated at < 20 % conversion.

In order to gain deeper understanding of the reaction mechanism, reactions of diphenyl ether over four noble metal catalyst were compared under the same pressure of H<sub>2</sub> and D<sub>2</sub>. TOFs and selectivities of hydrogenolysis and hydrogenation are shown in Table 5-3. Unlike the results from Ni/SiO<sub>2</sub> catalysts, insignificant isotopic effect were observed from these catalysts ( $R_{\text{H}}/R_{\text{D}}$  was 1.4 for Ru/C, 1.0 for Pt, 0.7 for Rh and 0.6 for Pd). This might be because the first hydrogen addition is kinetically irrelevant over noble metal catalysts. Comparing to Ni, these noble metals are better catalysts for hydrogenation of aromatics<sup>41-43</sup> and the oxophilicity of these noble metals are weaker<sup>44-45</sup>. The oxophilicity of a metal symbolizes the interaction between oxygen and the metal. Stronger interaction between oxygen and the metal may lead to easier C-O bond cleavage to form a metal-oxygen bond.<sup>45</sup> On noble metal catalysts, if the rate of first hydrogen addition step gets extremely faster than the following C-O bond breaking

step, the first hydrogen addition would be kinetically irrelevant. Insignificant isotopic effect is reasonable when bond breaking is the rate-determining step.

**Table 5-3. Kinetic isotopic experiments of diphenyl ether over different metal catalysts in decalin.**

Catalyst	Gas	TOF / s <sup>-1</sup>			Selectivity	
		Total	Hydrogenolysis	Hydrogenation	Hydrogenolysis	Hydrogenation
Ru/C	H <sub>2</sub>	0.13	0.069	0.060	53%	47%
	D <sub>2</sub>	0.091	0.041	0.050	45%	55%
<i>R<sub>H</sub>/R<sub>D</sub></i>		1.4	1.7	1.2		
Pt/C	H <sub>2</sub>	1.2	0.48	0.74	39%	61%
	D <sub>2</sub>	1.3	0.48	0.79	38%	62%
<i>R<sub>H</sub>/R<sub>D</sub></i>		1.0	1.0	0.9		
Rh/C	H <sub>2</sub>	0.75	0.11	0.64	15%	85%
	D <sub>2</sub>	1.0	0.15	0.88	15%	85%
<i>R<sub>H</sub>/R<sub>D</sub></i>		0.7	0.7	0.7		
Pd/C	H <sub>2</sub>	0.11	0.005	0.10	5%	95%
	D <sub>2</sub>	0.18	0.006	0.18	3%	97%
<i>R<sub>H</sub>/R<sub>D</sub></i>		0.6	0.8	0.6		

Reaction conditions: 10 mmol ether, 10 mg 5 wt. % Ru/C, 20 mg 0.25 wt. % Pt/C, 20 mg 0.25 wt. % Rh/C or 10 mg 5 wt. % Pd/C catalyst, 40 ml decalin, 5 bar of H<sub>2</sub> or D<sub>2</sub> at room temperature, 150 °C, stirring at 700 ppm. TOFs were calculated at < 20 % conversion.

### 5.3.2 Reactions in water

Decalin was used as model system for apolar solvent because of the inert property of the solvent and easy analysis for the products and secondary reactions. Since very little is known about the metal catalyzed hydrolysis except Pd as we discussed in Chapter 2 and water is ubiquitously presented when converting molecules derived from renewable carbon resources, water was chosen as the next solvent. Table 5-4 shows the comparison of the selectivities of hydrogenolysis, hydrogenation and hydrolysis at full conversion of diphenyl ether over the four noble metal catalysts (Ru/C, Pt/C, Rh/C and Pd/C) under the same reaction conditions. The selectivities of hydrogenolysis of the metals scale as Pt > Ru > Rh > Pd, this is a little bit different compared with the reactions in decalin (Ru > Pt > Rh > Pd). Hydrolysis was detected from these four catalysts. Just as we discussed in Chapter 2, hydrolysis dominated the reaction of diphenyl ether on Pd in water. While considerable selectivities of hydrolysis were also observed from Pt (18 %), Ru (42 %) and Rh (42 %) catalysts. In contrast to the reactions in decalin



(selectivities of hydrogenation were higher than 79 %), hydrogenation products yield were 50 % or lower at full conversion of diphenyl ether from all these metals in water. Furthermore, the selectivity of C-O cleavage products from cyclohexyl phenyl ether on Pd/C was 87 % at 190 °C in water (Chapter 2). Secondary reactions could change overall selectivities of the reaction pathways dramatically at different conversions of diphenyl ether.

**Table 5-4. Selectivities of different reaction routes of diphenyl ether over different metal catalysts in water at full conversions.**

Catalyst	Time/min	Conversion	Selectivity		
			Hydrogenolysis	Hydrolysis	Hydrogenation
5 wt. % Ru/C	60	99%	22%	42%	36%
5 wt. % Pt/C	60	99%	31%	18%	50%
5 wt. % Rh/C	60	100%	8%	42%	50%
5 wt. % Pd/C	360	100%	1%	84%	15%

Reaction conditions: 10 mmol ether, 10 mg catalyst, 80 ml water, 40 bar of hydrogen at room temperature, 150 °C, stirring at 700 ppm.

Then the conversions of diphenyl ether were controlled under 20 % to focus on the initial reactions (Table 5-5). Significant differences were found from the reaction pathway selectivities compare to the reactions at full conversion, this is due to the secondary reactions of cyclohexyl phenyl ether, and detailed analysis will be made next. For each metal catalyst, the selectivity of hydrogenolysis was close to the reactions in decalin, and the sum of the selectivities of hydrolysis and hydrogenation was equal to the selectivity of hydrogenation in decalin. Since higher selectivity of hydrolysis was observed with higher selectivity of hydrogenation on these metal catalysts in water, the mechanism of hydrolysis could fall in line with hydrogenation as we proposed in Chapter 2. Comparing the general reactivity of the metal catalysts in water with the reactions in decalin, the trend is exactly the same (Rh > Pt > Ru > Pd) and relatively higher rates were obtained for each metal catalyst except Pd. These comparable selectivities of reaction pathways and increased reaction rates indicate that the overall chemistry of the conversion of diphenyl ether over this metal catalysts stayed the same when different solvents (decalin and water) were used.

**Table 5-5. Selectivities of different reaction routes and TOFs of diphenyl ether over different metal catalysts in water at low conversions.**

	TOF / s <sup>-1</sup>	Selectivity		
		Hydrogenolysis	Hydrolysis	Hydrogenation
Ru/C	5.7	20%	11%	69%
Pt/C	12	22%	11%	67%
Rh/C	29	5%	13%	82%
Pd/C	0.64	2%	17%	81%

Reaction conditions: 10 mmol ether, 10 mg 5 wt. % Ru/C, 20 mg 0.25 wt. % Rh/C, 20 mg 0.25 wt. % Pt/C or 10 mg 5 wt. % Pd/C catalyst, 80 ml water, 40 bar of hydrogen at room temperature, 150 °C, stirring at 700 ppm. TOFs were calculated at < 20 % conversion.

Since the secondary reactions are important for the cleavage of C-O bond in the ethers, product distribution from the reactions of diphenyl ether over different catalysts were carefully measured at different conversions (Figure 5-5). For Ru/C catalyst, the yield of C<sub>6</sub> products (sum of benzene, cyclohexene and cyclohexane) increased almost linearly in the whole range of conversion and the selectivity was 10 % at low conversion and 11 % at full conversion, meanwhile, the selectivity of C<sub>6</sub>-OH products (phenol, cyclohexanone and cyclohexanol) increased from 21 % (at low conversion) to 53 % (at full conversion). So the major reactions of cyclohexyl phenyl ether are hydrogenation and hydrolysis on Ru/C in water. For Pt/C catalyst, unlike the other three catalysts, dicyclohexyl ether was directly generated at low conversions and cyclohexyl phenyl ether was not detected as a major products at conversions higher than 30 %. Therefore, the contribution for the C-O cleavage reactions from secondary reactions was less on Pt comparing to other metal catalysts. Pt catalyst showed relatively minimal changes of selectivities of reaction pathways when the conversion of diphenyl ether was changed. In general, Ru and Pt catalysts were favorable for hydrogenolysis of diphenyl ether while Pt showed higher performance on hydrogenation and Ru was better for the hydrolysis of intermediate product, so more C-O cleavage products were obtained on Ru catalyst at high conversions.

For Rh/C and Pd/C catalysts, hydrogenolysis was the minor reaction pathway for diphenyl ether and cyclohexyl phenyl ether, so the yield of C<sub>6</sub> products remained low during the reaction. Even though dicyclohexyl ether was not directly formed from diphenyl ether on Rh, it was the major products in the end of the reaction because cyclohexyl phenyl ether was mainly converted via hydrogenation on Rh. Since hydrolysis of cyclohexyl phenyl ether also occurred on Rh, the selectivity of hydrolysis increased from 13 % at low conversion to 42 % at full conversion. Pd/C showed the highest selectivity of hydrolysis of diphenyl ether and cyclohexyl phenyl ether among these catalysts. Because hydrolysis dominated the reaction of cyclohexyl phenyl ether on Pd, the overall selectivities of reaction pathways

dramatically changed during the reaction. Detailed changes of the selectivities of different reaction routes according to conversions over different catalysts are shown in Appendix.

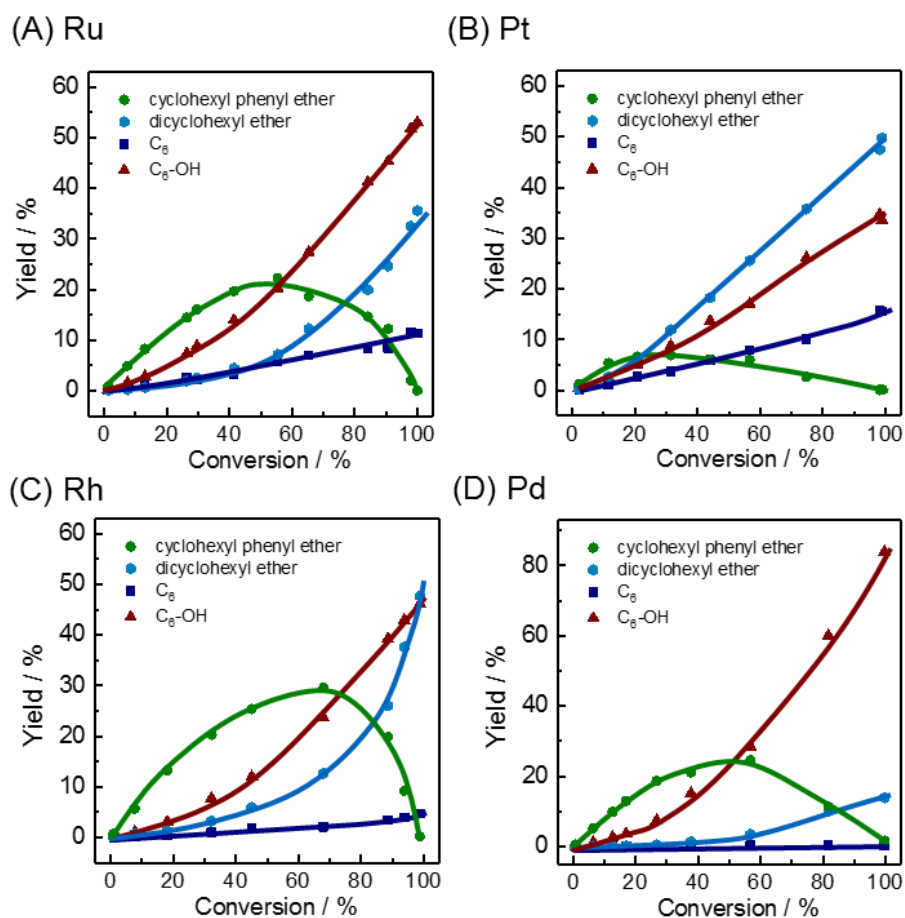


**Figure 5-5. Conversion-Yield plots of reactions of diphenyl ether on metal catalysts in water. (A) Ru, (B) Pt, (C) Rh and (D) Pd.**

C<sub>6</sub> represents benzene, cyclohexene and cyclohexane, C<sub>6</sub>-OH represents phenol, cyclohexanone and cyclohexanol. Reaction conditions: 10 mmol ether, 80 ml water, 20 mg 0.25 wt. % Ru/C, 20 mg 0.25 wt. % Pt/C, 10 mg 0.25 wt. % Rh/C or 10 mg 5 wt. % Pd/C catalyst, 40 bar of H<sub>2</sub>, 150 °C.

The reaction orders in H<sub>2</sub> pressure for the hydrogenolysis, hydrogenation and hydrolysis were measured over these four metal catalysts (Figure 5-6). The reaction orders in H<sub>2</sub> pressure for hydrogenolysis were approximately half order (Ru was 0.6, Pt was 0.5, Rh was 0.4 and Pd was 0.4) and reaction orders for hydrogenation were approximately first order (Ru was 1.1, Pt was 1.1, Rh was 1.1 and Pd was 1.0). These reaction orders are consistent to the reaction orders that we observed previously in decalin. Hydrolysis showed similar reaction order in H<sub>2</sub> pressure comparing to hydrogenation, i.e. Ru was 1.1, Pt was 1.6, Rh was 1.3 and Pd was 1.1. As we detected a similar hydrogen dependencies between hydrolysis and hydrogenation on Pd, which can be explained by the mechanism that we proposed in Figure 5-2. No matter which metal catalyst was used, the hydrolysis of diphenyl ether is initiated via

partial hydrogenation to form an enol ether, then the enol ether will react with water to form a hemiacetal which will easily result in the C-O bond cleavage.

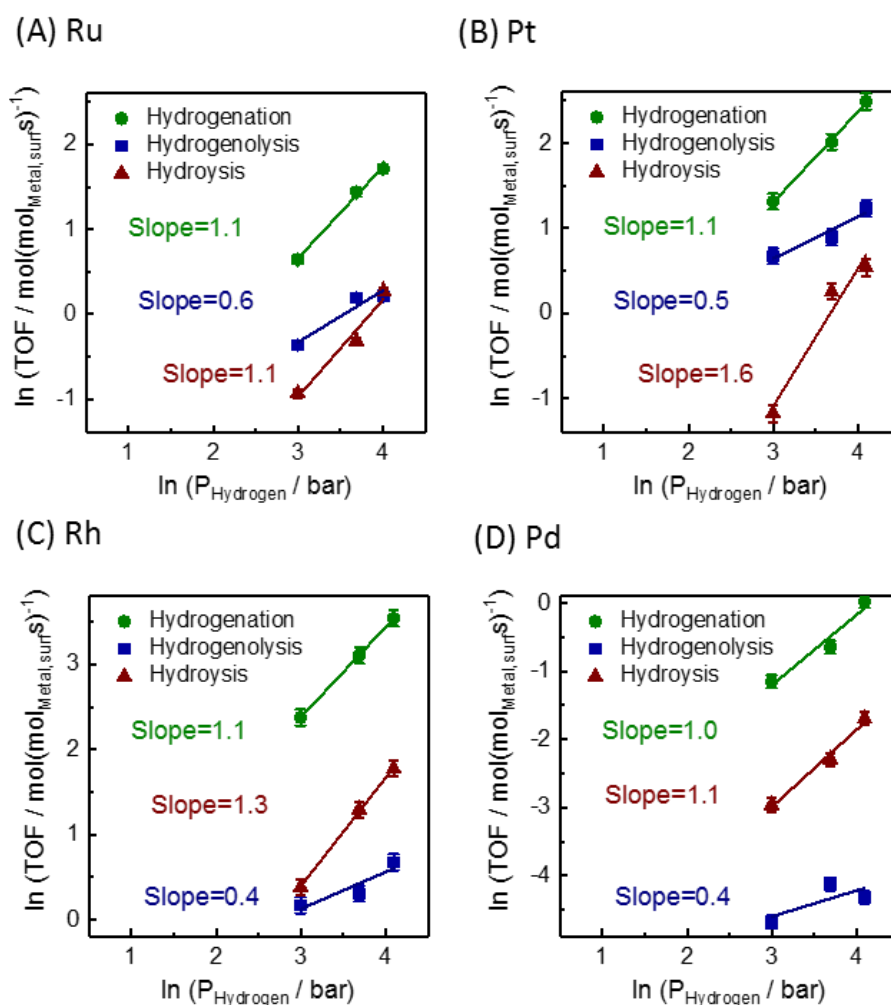


**Figure 5-6. Reaction orders in  $H_2$  pressure of reactions, hydrogenation, hydrogenolysis and hydrolysis, of diphenyl ether on metal catalysts in water. (A) Ru, (B) Pt, (C) Rh and (D) Pd.**

Reaction conditions: metal catalyst (20 mg 0.25 wt. % Ru/C, 20 mg 0.25 wt. % Pt/C, 10 mg 0.25 wt. % Rh/C or 10 mg 5 wt. % Pd/C), 10 mmol ether, 80 ml water, 150 °C, stirring at 700 rpm.  $H_2$  pressure varies from 20 to 60 bar at room temperature. TOFs were calculated at < 20 % conversion.

### 5.3.3 Discussion

Because an enol ether has to be generated and reacts with a water molecule to produce reductive hydrolysis products, the difference in the possibility of forming the enol ether and the desorption property of the ether from the metal surface between these metals may cause the difference in the selectivity of hydrolysis. DFT calculations are being undertaken to gain more fundamental insights.

For hydrogenolysis, the C-O bond scission on metal surface after one hydrogen addition forms a benzene molecule and a phenoxy group on the metal surface. The strong interaction between metal and oxygen may lead to favorable formation of phenoxy group on the metal. Correlations between the energy barrier for direct deoxygenation of anisole<sup>45</sup> and phenol<sup>46</sup>, and the oxophilicity of metal surfaces have been reported. We could compare the effect of oxophilicity (heat of dissociative adsorption of O<sub>2</sub> on the metal surface)<sup>47</sup> on the selectivities of hydrogenolysis over different metals under the same reaction condition. As summarized in Figure 5-7, an unclear trend was observed. Generally, the selectivity of hydrogenolysis decreases when the oxophilicity decreases except Pt. The inconsistency of Pt may be due to the different bonding energy of H comparing to other metals<sup>47</sup>.

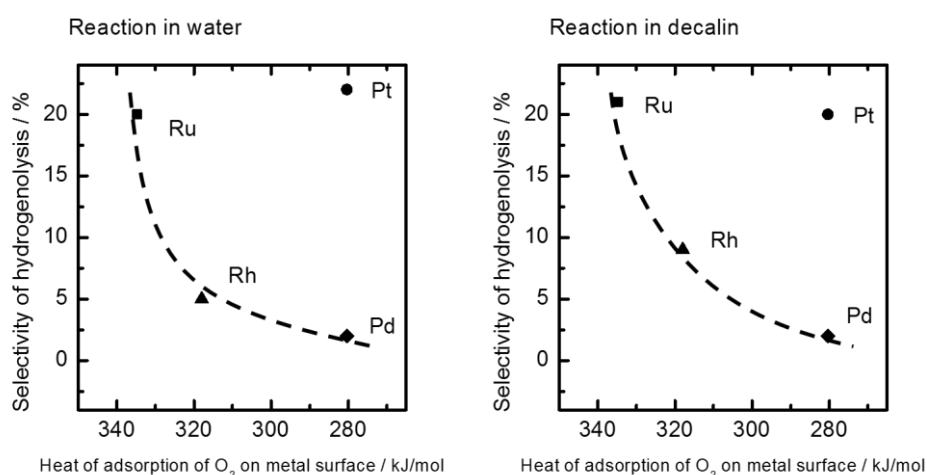


**Figure 5-7. Correlation between the selectivity of hydrogenolysis of diphenyl ether on metal catalysts surfaces and the heat of adsorption of O<sub>2</sub> on metal surfaces<sup>48-49</sup>.**

## 5.4 Conclusions

Herein, we completed the comparison of the reactivities and selectivities of the reactions of diphenyl ether over four noble metal catalysts, Ru/C, Pt/C, Rh/C and Pd/C, in polar (water) and apolar (decalin) solvents. The aromatic C-O bond is cleaved hydrogenolytically and/or hydrolytically, while in parallel the aromatic rings can be hydrogenated without changing the molecular backbone. In decalin, only hydrogenolysis was observed for C-O cleavage and the selectivity varied from 2 % to 21 %. The preference to hydrogenolysis of the C-O bond over hydrogenation of the aromatic ring increases in the order Pd/C < Rh/C < Pt/C ≈ Ru/C in decalin and water, which might be due to the difference of oxophilicity of different metal catalysts. For hydrolysis in water, a reverse trend was observed. Because the reductive hydrolysis occurs via partial hydrogenation (two hydrogen additions) and the mechanism is in parallel with hydrogenation, more reductive hydrolysis is obtained when the selectivity of

hydrogenation is higher. We concluded that the reaction mechanisms of reductive hydrolysis and hydrogenolysis remained the same over these metal catalysts in different solvents (water and decalin).

## 5.5 Acknowledgements

This work was supported by the U.S. Department of Energy, Office of Science, Office of Basic Energy Sciences, Division of Chemical Sciences, Geosciences, and Biosciences. Portions of the work were performed at the William R. Wiley Environmental Molecular Science Laboratory, a national scientific user facility sponsored by the DOE's Office of Biological and Environmental Research located at Pacific Northwest National Laboratory, a multi-program national laboratory operated for DOE by Battelle Memorial Institute.

## 5.6 Appendix

### 5.6.1 Particle size and dispersion of supported metal nanoparticles

The TEM images of four metals are shown in Figure 5-8. The averaged four metal (Ru, Pt, Rh, Pd) particle sizes are 5.2, 3.2, 5.8, and 3.1 nm, respectively (Table 5-6). By assuming that the crystal structure of these noble metal nanoparticles is face-centered cubic (fcc) and the atom density on the surface ( $n_s$ ) is the average of the atom densities of (111), (110) and (100) planes, the dispersion was calculated through a relation as listed below<sup>50</sup>,

$$\phi = \frac{6Mn_s}{\rho N_A d}$$

where  $M$  is atomic mass,  $\rho$  is the density,  $N_A$  is Avogadro constant and  $d$  is the diameter of the nanoparticle.

**Table 5-6. Particle sizes and dispersions calculated from particle size and H<sub>2</sub> chemisorption of noble metal catalysts.**

Catalyst	Particle size / nm	Dispersion (TEM)	Dispersion (chemisorption)
5 wt. % Ru/C	5.2	20%	23%
5 wt. % Pt/C	3.2	35%	57%
5 wt. % Rh/C	5.8	19%	27%
5 wt. % Pd/C	3.1	34%	31%

The dispersions from H<sub>2</sub> chemisorption measurements are slightly higher than the dispersions calculated from particles size except Pd. This might be caused by small nanoparticles which were invisible in the TEM measurements. So the turnover frequency (TOF) was calculated based on the number of surface metal atoms measured by H<sub>2</sub> chemisorption.

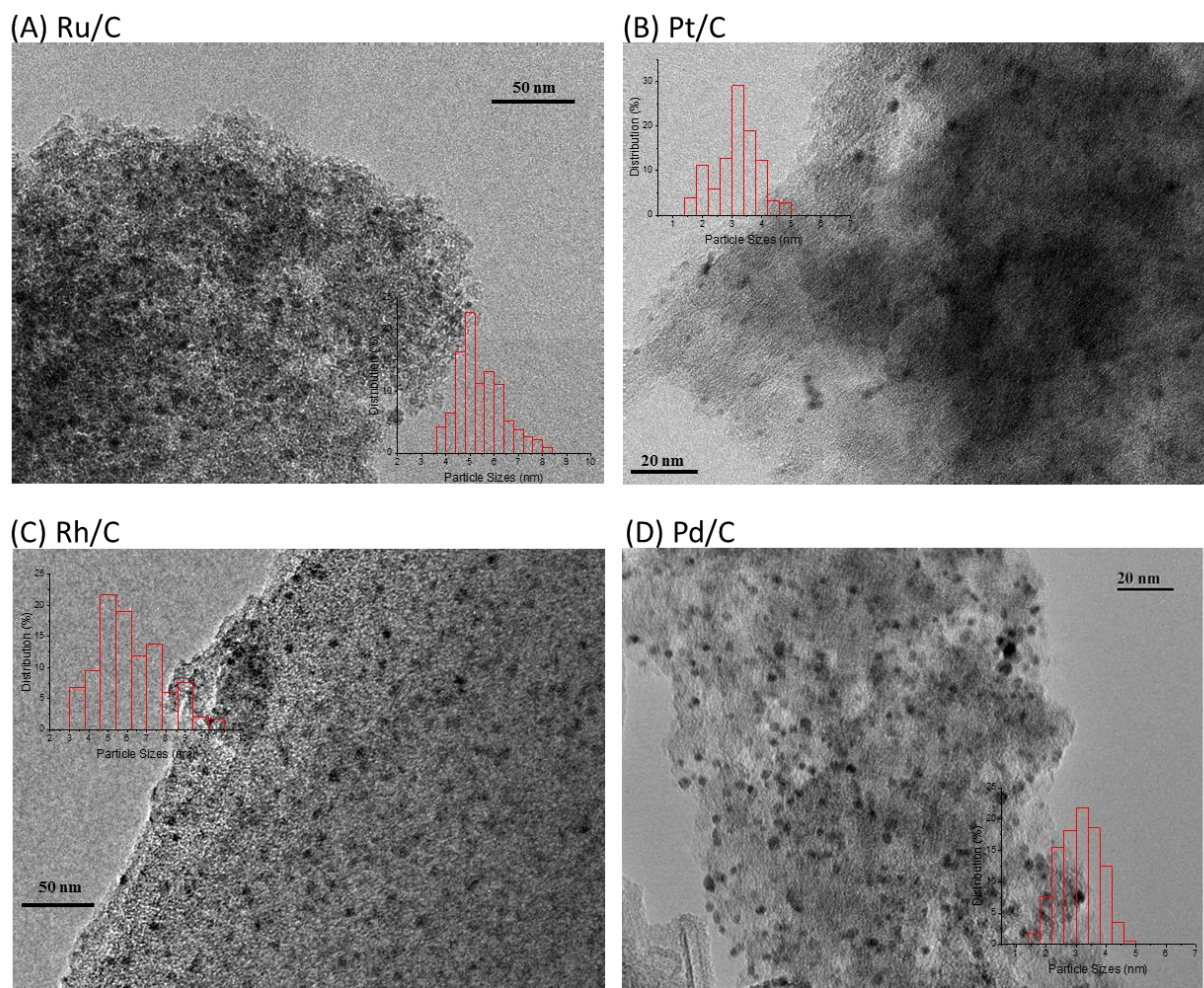


**Figure 5-8. TEM images of the metal catalysts. (A) Ru, (B) Pt, (C) Rh and (D) Pd. (more than 500 particle areas were counted for the TEM measurement)**

## 5.6.2 Reaction details in decalin

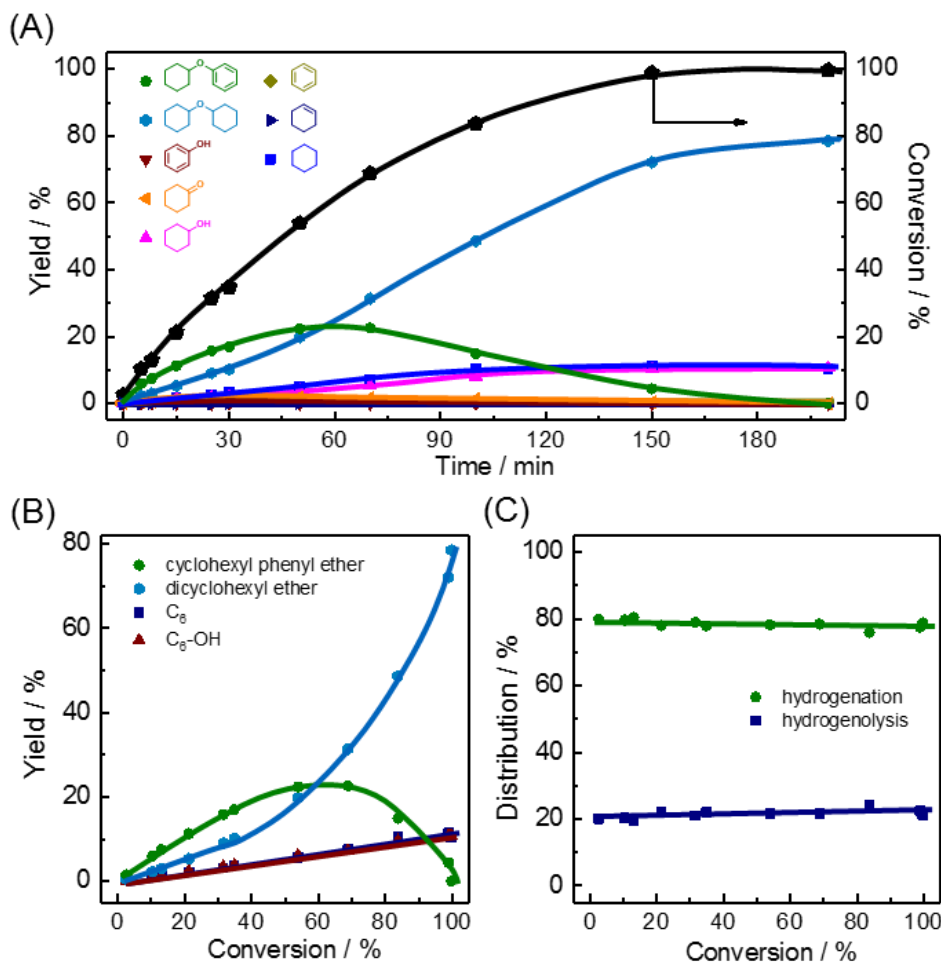


**Figure 5-9. Time-yield plots (A), conversion-yield plots (B) and distributions of the reaction pathways plots (C) for the reaction of diphenyl ether on Ru catalyst in decalin.**

In figure B, C<sub>6</sub> represents benzene, cyclohexene and cyclohexane, C<sub>6</sub>-OH represents phenol, cyclohexanone and cyclohexanol. Reaction conditions: 10 mmol ether, 40 ml decalin, 10 mg 5 wt. % Ru/C, 40 bar of H<sub>2</sub>, 150 °C.



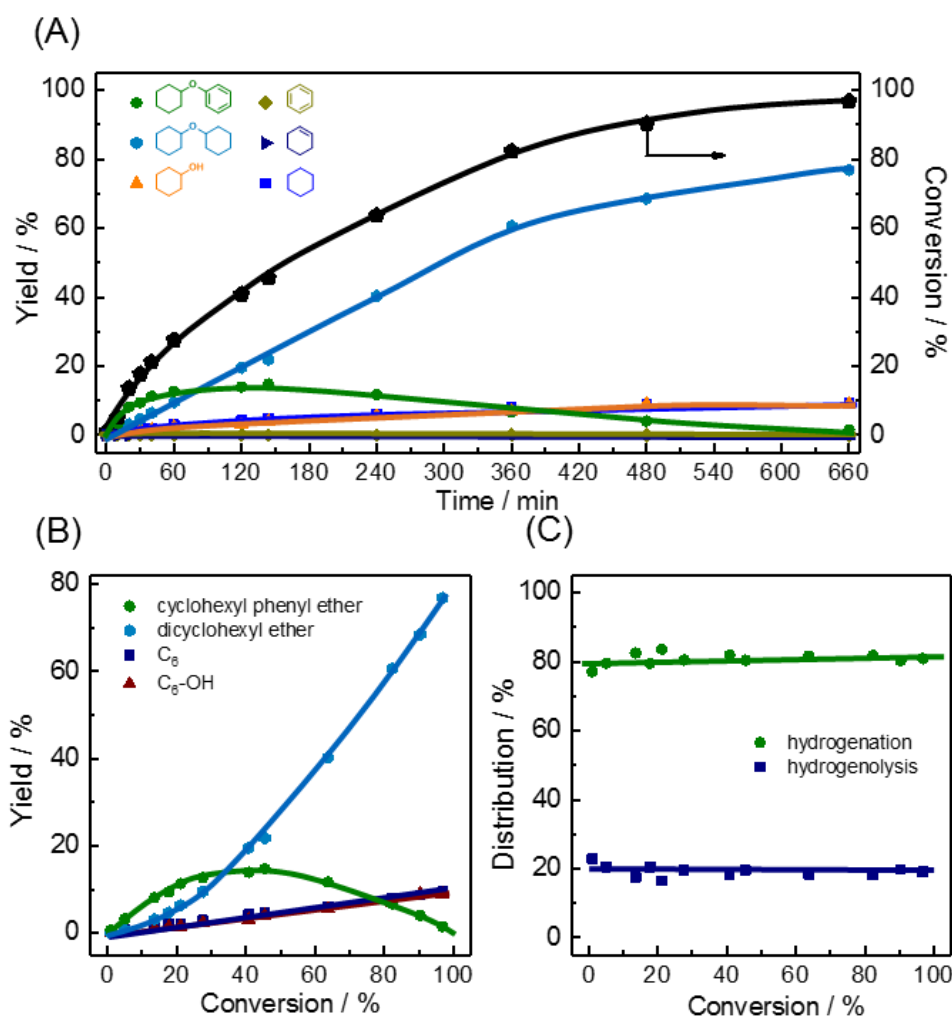


**Figure 5-10. Time-yield plots (A), conversion-yield plots (B) and distributions of the reaction pathways plots (C) for the reaction of diphenyl ether on Pt catalyst in decalin.**

In figure B, C<sub>6</sub> represents benzene, cyclohexene and cyclohexane, C<sub>6</sub>-OH represents phenol, cyclohexanone and cyclohexanol. Reaction conditions: 10 mmol ether, 40 ml decalin, 20 mg 0.25 wt. % Pt/C, 40 bar of H<sub>2</sub>, 150 °C.

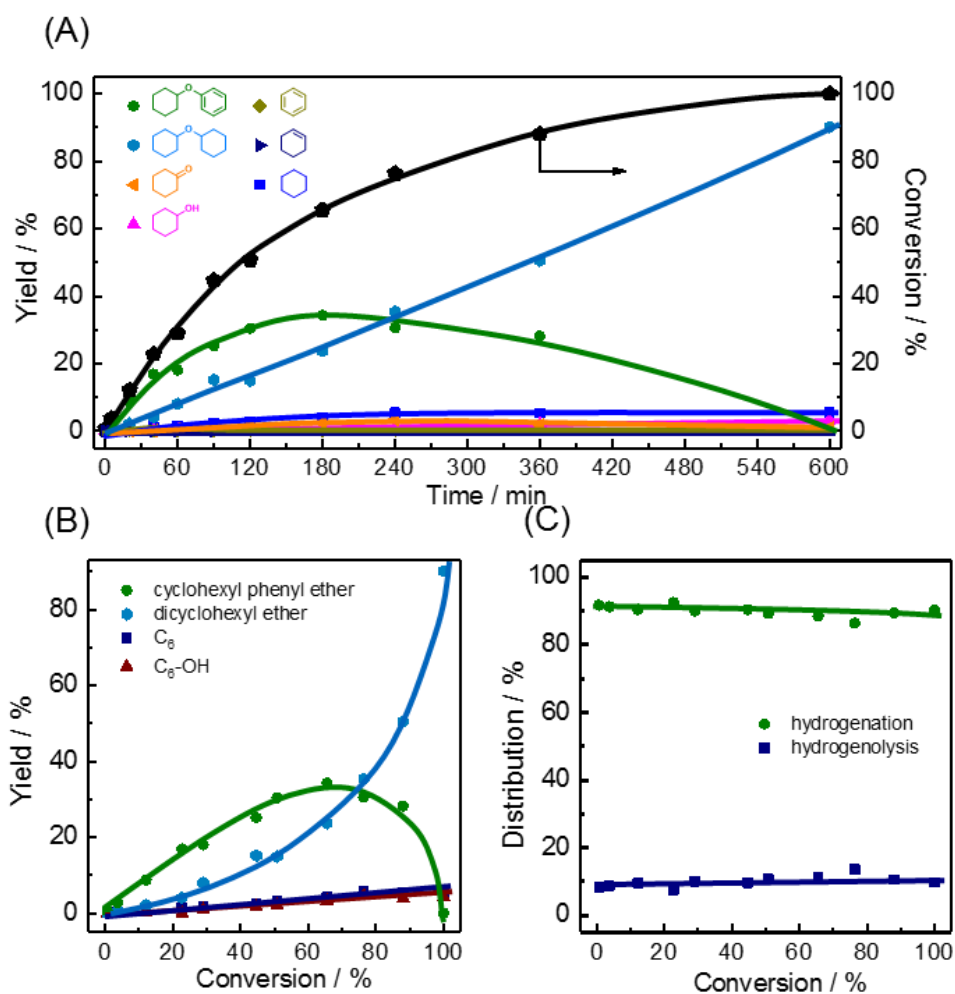


**Figure 5-11. Time-yield plots (A), conversion-yield plots (B) and distributions of the reaction pathways plots (C) for the reaction of diphenyl ether on Rh catalyst in decalin.**

In figure B, C<sub>6</sub> represents benzene, cyclohexene and cyclohexane, C<sub>6</sub>-OH represents phenol, cyclohexanone and cyclohexanol. Reaction conditions: 10 mmol ether, 40 ml decalin, 20 mg 0.25 wt. % Rh/C, 40 bar of H<sub>2</sub>, 150 °C.

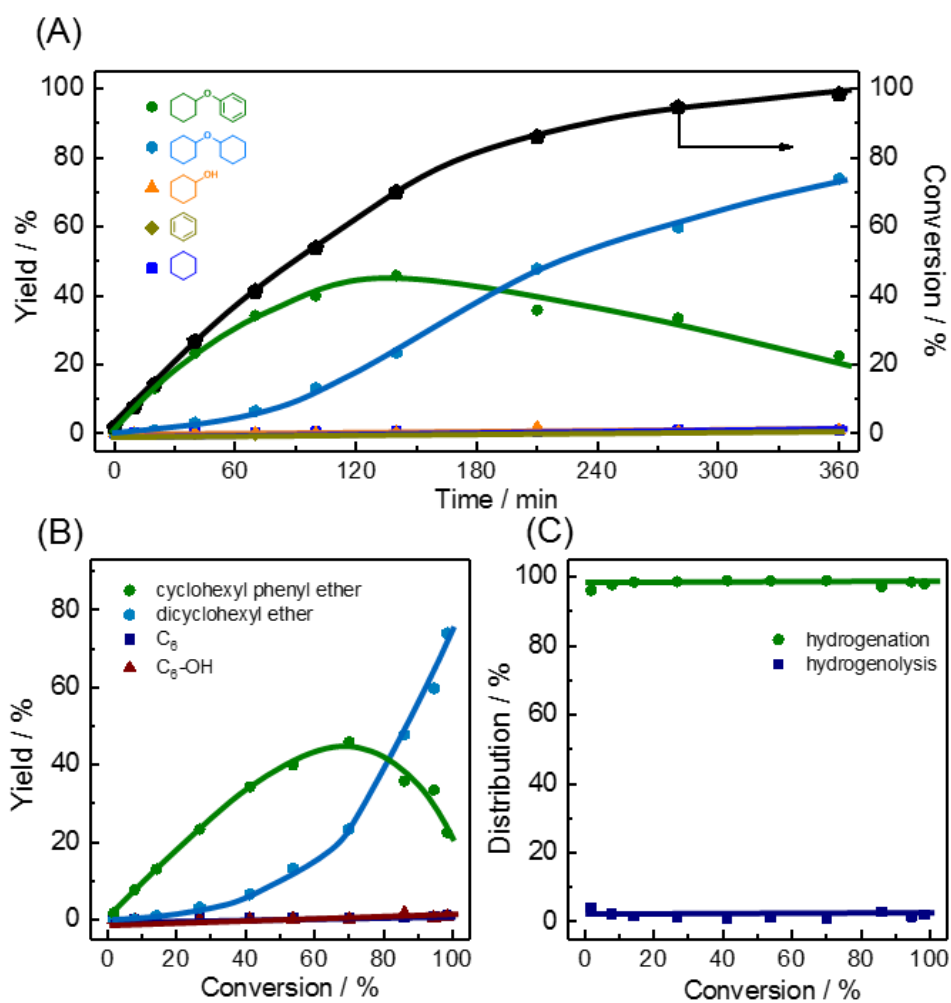


**Figure 5-12. Time-yield plots (A), conversion-yield plots (B) and distributions of the reaction pathways plots (C) for the reaction of diphenyl ether on Pd catalyst in decalin.**

In figure B, C<sub>6</sub> represents benzene, cyclohexene and cyclohexane, C<sub>6</sub>-OH represents phenol, cyclohexanone and cyclohexanol. Reaction conditions: 10 mmol ether, 40 ml decalin, 10 mg 5 wt. % Pd/C, 40 bar of H<sub>2</sub>, 150 °C.

## 5.6.2 Reaction details in water

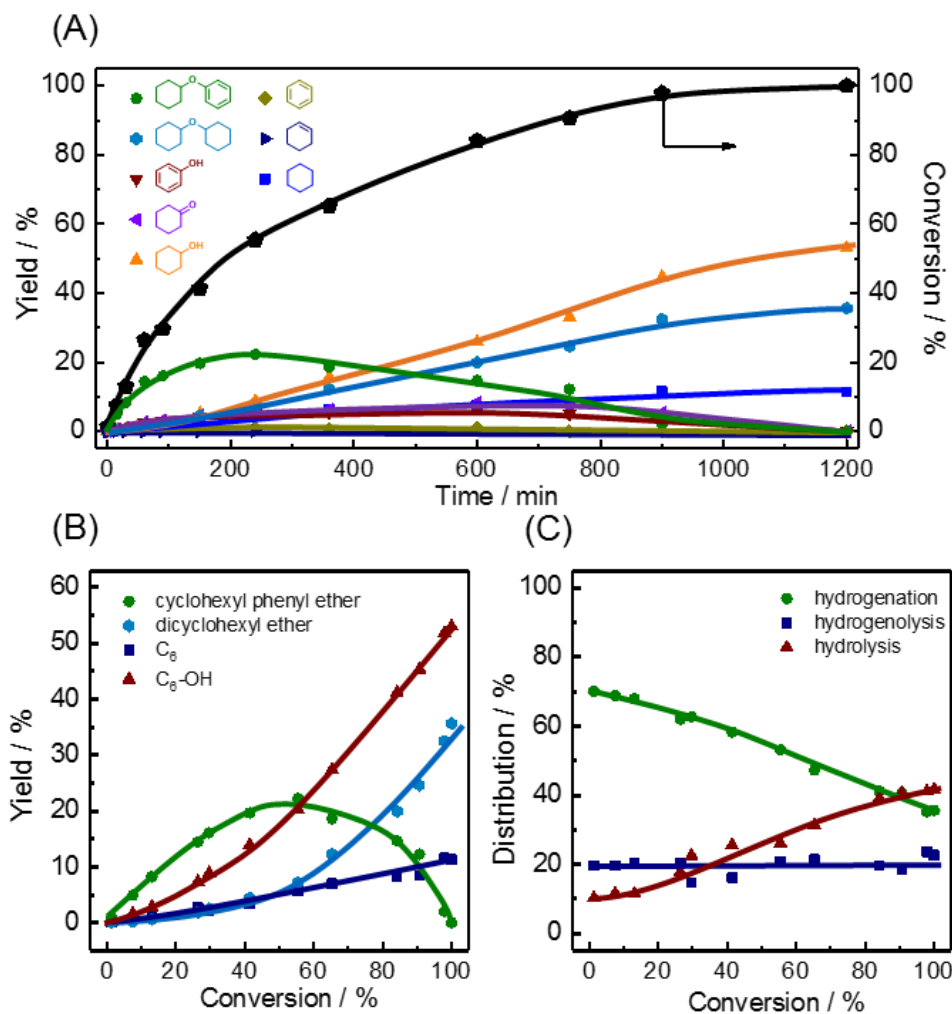


**Figure 5-13. Time-yield plots (A), conversion-yield plots (B) and distributions of the reaction pathways plots (C) for the reaction of diphenyl ether on Ru catalyst in water.**

In figure B, C<sub>6</sub> represents benzene, cyclohexene and cyclohexane, C<sub>6</sub>-OH represents phenol, cyclohexanone and cyclohexanol. Reaction conditions: 10 mmol ether, 80 ml water, 20 mg 0.25 wt. % Ru/C, 40 bar of H<sub>2</sub>, 150 °C.

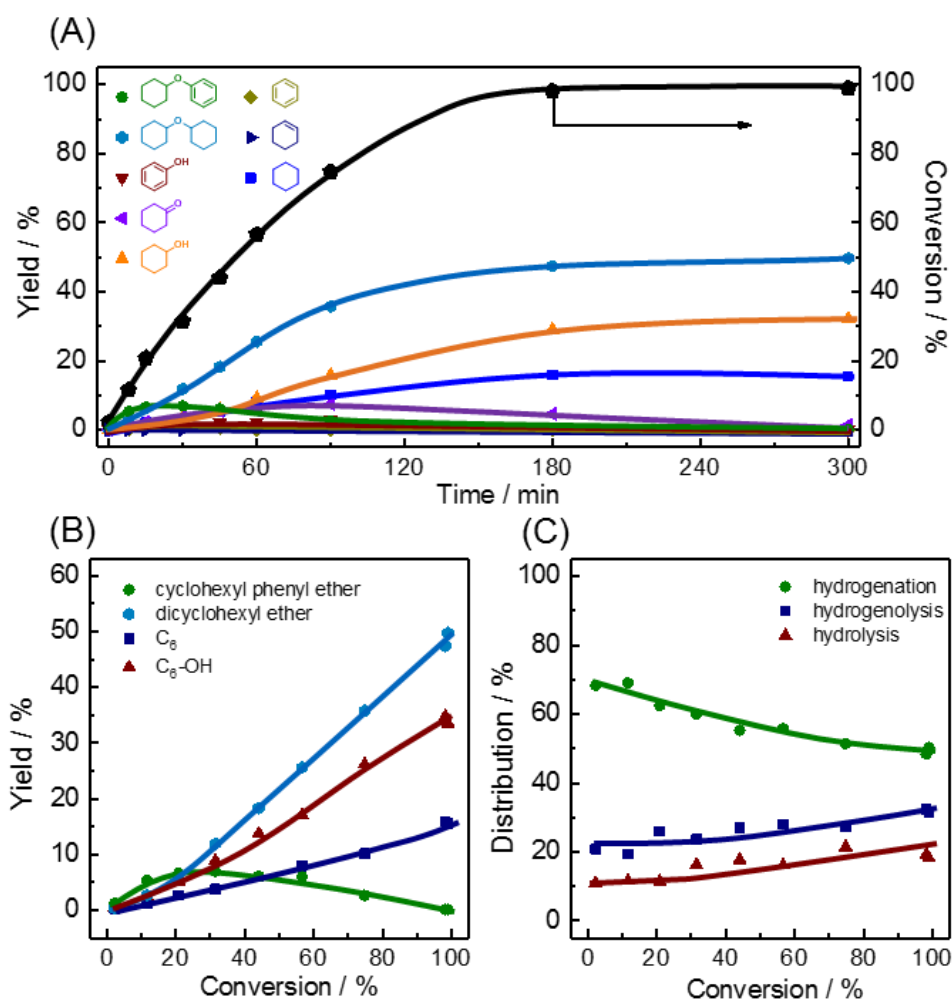


**Figure 5-14. Time-yield plots (A), conversion-yield plots (B) and distributions of the reaction pathways plots (C) for the reaction of diphenyl ether on Pt catalyst in water.**

In figure B, C<sub>6</sub> represents benzene, cyclohexene and cyclohexane, C<sub>6</sub>-OH represents phenol, cyclohexanone and cyclohexanol. Reaction conditions: 10 mmol ether, 80 ml water, 20 mg 0.25 wt. % Pt/C, 40 bar of H<sub>2</sub>, 150 °C.

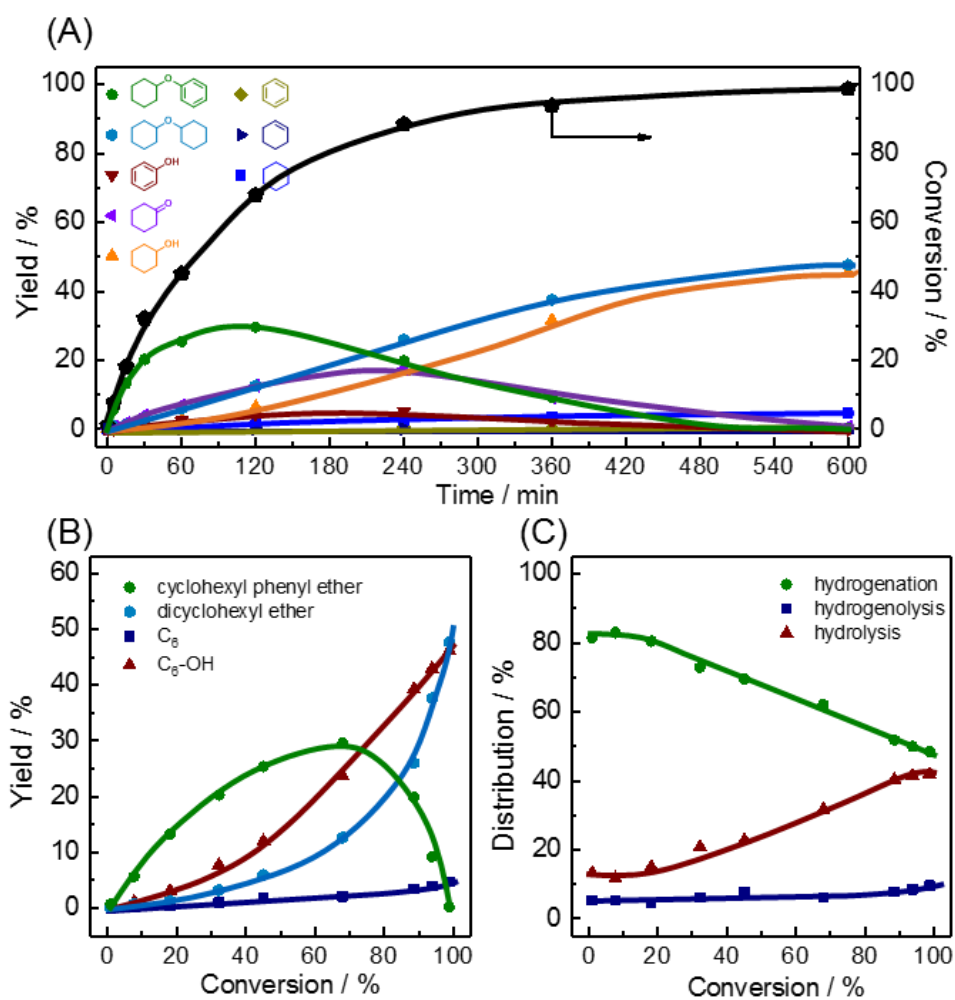


**Figure 5-15. Time-yield plots (A), conversion-yield plots (B) and distributions of the reaction pathways plots (C) for the reaction of diphenyl ether on Rh catalyst in water.**

In figure B, C<sub>6</sub> represents benzene, cyclohexene and cyclohexane, C<sub>6</sub>-OH represents phenol, cyclohexanone and cyclohexanol. Reaction conditions: 10 mmol ether, 80 ml water, 10 mg 0.25 wt. % Rh/C, 40 bar of H<sub>2</sub>, 150 °C.

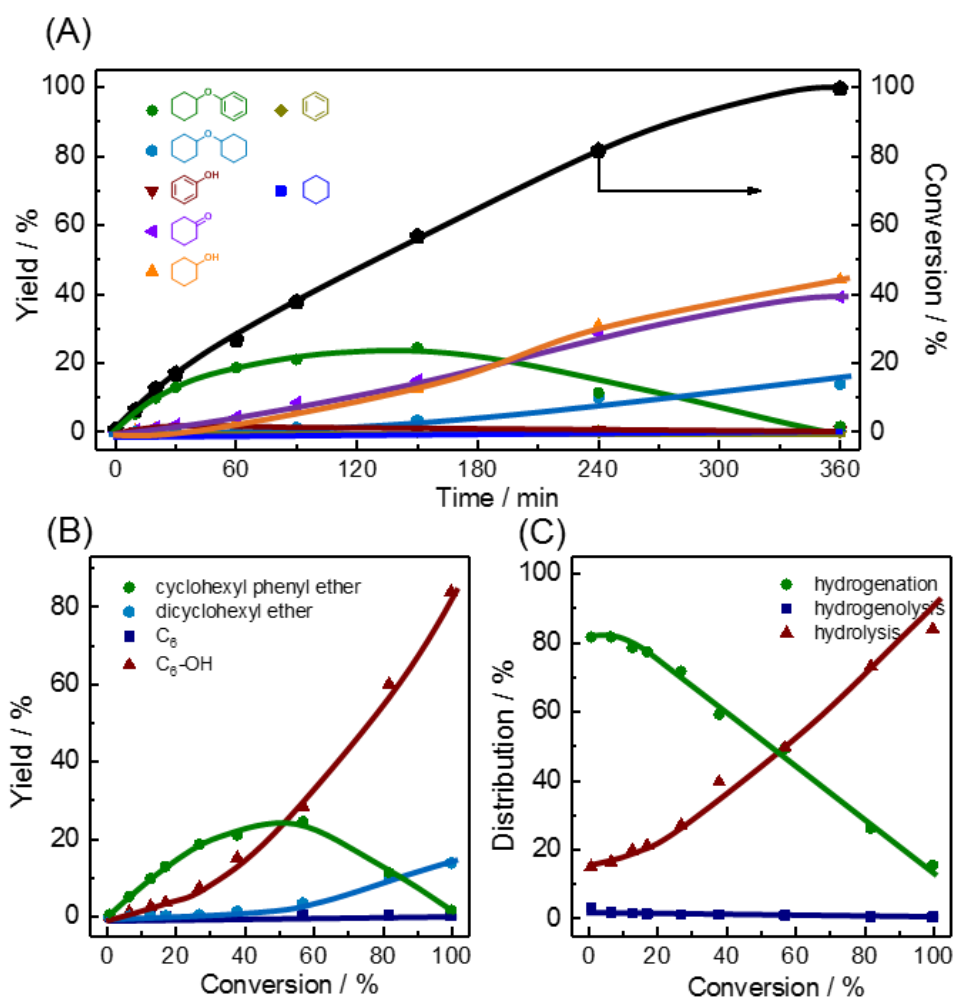


**Figure 5-16. Time-yield plots (A), conversion-yield plots (B) and distributions of the reaction pathways plots (C) for the reaction of diphenyl ether on Pd catalyst in water.**

In figure B, C<sub>6</sub> represents benzene and cyclohexane, C<sub>6</sub>-OH represents phenol, cyclohexanone and cyclohexanol. Reaction conditions: 10 mmol ether, 80 ml water, 10 mg 5 wt. % Pd/C, 40 bar of H<sub>2</sub>, 150 °C.

## 5.7 References

1. Deuss, P. J.; Barta, K., *Coordination Chemistry Reviews* **2016**, *306*, 510-532.
2. Li, C.; Zhao, X.; Wang, A.; Huber, G. W.; Zhang, T., *Chemical Reviews* **2015**, *115* (21), 11559-11624.
3. Zaheer, M.; Kempe, R., *ACS Catalysis* **2015**, *5* (3), 1675-1684.
4. Ruppert, A. M.; Weinberg, K.; Palkovits, R., *Angewandte Chemie International Edition* **2012**, *51* (11), 2564-2601.
5. Zakzeski, J.; Bruijninx, P. C. A.; Jongerius, A. L.; Weckhuysen, B. M., *Chemical Reviews* **2010**, *110* (6), 3552-3599.
6. Gasser, C. A.; Hommes, G.; Schäffer, A.; Corvini, P. F.-X., *Applied Microbiology and Biotechnology* **2012**, *95* (5), 1115-1134.
7. Corma, A.; Iborra, S.; Velty, A., *Chemical Reviews* **2007**, *107* (6), 2411-2502.
8. Kobayashi, H.; Komanoya, T.; Guha, S. K.; Hara, K.; Fukuoka, A., *Applied Catalysis A: General* **2011**, *409-410*, 13-20.
9. Rahimi, A.; Ulbrich, A.; Coon, J. J.; Stahl, S. S., *Nature* **2014**, *515* (7526), 249-252.
10. Kasakov, S.; Shi, H.; Camaioni, D. M.; Zhao, C.; Baráth, E.; Jentys, A.; Lercher, J. A., *Green Chemistry* **2015**, *17* (11), 5079-5090.
11. He, J.; Zhao, C.; Lercher, J. A., *Journal of the American Chemical Society* **2012**, *134* (51), 20768-20775.
12. Zhang, J.; Teo, J.; Chen, X.; Asakura, H.; Tanaka, T.; Teramura, K.; Yan, N., *ACS Catalysis* **2014**, *4* (5), 1574-1583.
13. Lin, Y.-C.; Li, C.-L.; Wan, H.-P.; Lee, H.-T.; Liu, C.-F., *Energy & Fuels* **2011**, *25* (3), 890-896.
14. Lee, C. R.; Yoon, J. S.; Suh, Y.-W.; Choi, J.-W.; Ha, J.-M.; Suh, D. J.; Park, Y.-K., *Catalysis Communications* **2012**, *17*, 54-58.
15. Parsell, T. H.; Owen, B. C.; Klein, I.; Jarrell, T. M.; Marcum, C. L.; Hauptert, L. J.; Amundson, L. M.; Kenttämä, H. I.; Ribeiro, F.; Miller, J. T.; Abu-Omar, M. M., *Chemical Science* **2013**, *4* (2), 806-813.
16. Güvenatam, B.; Kurşun, O.; Heeres, E. H. J.; Pidko, E. A.; Hensen, E. J. M., *Catalysis Today* **2014**, *233*, 83-91.
17. Li, Z.; Assary, R. S.; Atesin, A. C.; Curtiss, L. A.; Marks, T. J., *Journal of the American Chemical Society* **2014**, *136* (1), 104-107.
18. Kim, J. K.; Lee, J. K.; Kang, K. H.; Lee, J. W.; Song, I. K., *Journal of Molecular Catalysis A: Chemical* **2015**, *410*, 184-192.
19. Lu, J.; Wang, M.; Zhang, X.; Heyden, A.; Wang, F., *ACS Catalysis* **2016**, *6* (8), 5589-5598.
20. Xia, Q.; Chen, Z.; Shao, Y.; Gong, X.; Wang, H.; Liu, X.; Parker, S. F.; Han, X.; Yang, S.; Wang, Y., *Nature Communications* **2016**, *7*, 11162.
21. Zhang, J.; Ibrahim, M.; Collière, V.; Asakura, H.; Tanaka, T.; Teramura, K.; Philippot, K.; Yan, N., *Journal of Molecular Catalysis A: Chemical* **2016**, *422*, 188-197.
22. Wang, M.; Shi, H.; Camaioni, D. M.; Lercher, J. A., *Angewandte Chemie International Edition* **2017**, *56* (8), 2110-2114.



23. Wang, M.; Gutiérrez Oliver, Y.; Camaioni Donald, M.; Lercher Johannes, A., *Angewandte Chemie International Edition* **2018**, *57* (14), 3747-3751.
24. He, J.; Lu, L.; Zhao, C.; Mei, D.; Lercher, J. A., *Journal of Catalysis* **2014**, *311*, 41-51.
25. He, J.; Zhao, C.; Mei, D.; Lercher, J. A., *Journal of Catalysis* **2014**, *309*, 280-290.
26. Prasomsri, T.; Shetty, M.; Murugappan, K.; Román-Leshkov, Y., *Energy & Environmental Science* **2014**, *7* (8), 2660-2669.
27. Ma, R.; Hao, W.; Ma, X.; Tian, Y.; Li, Y., *Angewandte Chemie International Edition* **2014**, *53* (28), 7310-7315.
28. Kärkäs, M. D.; Matsuura, B. S.; Monos, T. M.; Magallanes, G.; Stephenson, C. R. J., *Organic & Biomolecular Chemistry* **2016**, *14* (6), 1853-1914.
29. Molinari, V.; Clavel, G.; Graglia, M.; Antonietti, M.; Esposito, D., *ACS Catalysis* **2016**, *6* (3), 1663-1670.
30. Wang, Y.-Y.; Ling, L.-L.; Jiang, H., *Green Chemistry* **2016**, *18* (14), 4032-4041.
31. Cui, X.; Yuan, H.; Junge, K.; Topf, C.; Beller, M.; Shi, F., *Green Chemistry* **2017**, *19* (1), 305-310.
32. Singh, S. K.; Ekhe, J. D., *RSC Advances* **2014**, *4* (53), 27971-27978.
33. Deepa, A. K.; Dhepe, P. L., *ACS Catalysis* **2015**, *5* (1), 365-379.
34. Deuss, P. J.; Scott, M.; Tran, F.; Westwood, N. J.; de Vries, J. G.; Barta, K., *Journal of the American Chemical Society* **2015**, *137* (23), 7456-7467.
35. Siskin, M.; Katritzky, A. R.; Balasubramanian, M., *Energy & Fuels* **1991**, *5* (5), 770-771.
36. Katritzky, A. R.; Barcock, R. A.; Balasubramanian, M.; Greenhill, J. V.; Siskin, M.; Olmstead, W. N., *Energy & Fuels* **1994**, *8* (2), 487-497.
37. Roberts, V. M.; Knapp, R. T.; Li, X.; Lercher, J. A., *ChemCatChem* **2010**, *2* (11), 1407-1410.
38. Huang, X.; Atay, C.; Korányi, T. I.; Boot, M. D.; Hensen, E. J. M., *ACS Catalysis* **2015**, *5* (12), 7359-7370.
39. Song, W.; Liu, Y.; Baráth, E.; Zhao, C.; Lercher, J. A., *Green Chemistry* **2015**, *17* (2), 1204-1218.
40. Wang, X.; Rinaldi, R., *Catalysis Today* **2016**, *269*, 48-55.
41. Mu, W.; Ben, H.; Du, X.; Zhang, X.; Hu, F.; Liu, W.; Ragauskas, A. J.; Deng, Y., *Bioresource Technology* **2014**, *173*, 6-10.
42. Teles, C. A.; Rabelo-Neto, R. C.; de Lima, J. R.; Mattos, L. V.; Resasco, D. E.; Noronha, F. B., *Catalysis Letters* **2016**, *146* (10), 1848-1857.
43. Zang, W.; Li, G.; Wang, L.; Zhang, X., *Catalysis Science & Technology* **2015**, *5* (5), 2532-2553.
44. Liu, X.; An, W.; Turner, C. H.; Resasco, D. E., *Journal of Catalysis* **2018**, *359*, 272-286.
45. Tan, Q.; Wang, G.; Long, A.; Dinse, A.; Buda, C.; Shabaker, J.; Resasco, D. E., *Journal of Catalysis* **2017**, *347*, 102-115.
46. Hensley, A. J. R.; Wang, Y.; McEwen, J.-S., *ACS Catalysis* **2015**, *5* (2), 523-536.
47. Toyoshima, I.; Somorjai, G. A., *Catalysis Reviews Science and Engineering* **1979**, *19*, 105-159.

48. Madey, T. E.; Engelhardt, H. A.; Menzel, D., *Surface Science* **1975**, 48, 304-328.
49. Brennan, D.; Hayward, D. O.; Trapnell, B. M. W., *Proceedings of the Royal Society of London. Series A. Mathematical and Physical Sciences* **1960**, 256 (1284), 81-105.
50. Pérez, O.-L.; Romeu, D.; Yacamán, M. J., *Journal of Catalysis* **1983**, 79 (1), 240-241.

## Chapter 6 Summary

The aim of this thesis is to gain fundamental insights into the catalytic reductive cleavage of aromatic C-O bonds in aryl ethers over supported metal catalysts. Due to the high activation barrier for effective aromatic C-O bond cleavage, the site selectivity in the presence of multiple C-O bonds and the competing hydrogenation of the aromatic rings, this cleavage is still a difficult problem relevant to depolymerization of lignin and C-O bond activation in synthetic chemistry. Mechanistic details of the cleavage of aromatic C-O bonds over heterogeneous metal catalysts have been rarely reported. To gain high reactivity and selectivity to C-O bond cleavage in aryl ethers catalyzed by metal catalysts and explore the mechanisms, different metal catalysts were evaluated in polar and apolar solvents under H<sub>2</sub> via kinetic and isotopic measurements. The results are summarized in Figure 6-1, Pd and Ni catalysts were found to be highly selective toward reductive hydrolysis and hydrogenolysis, respectively.

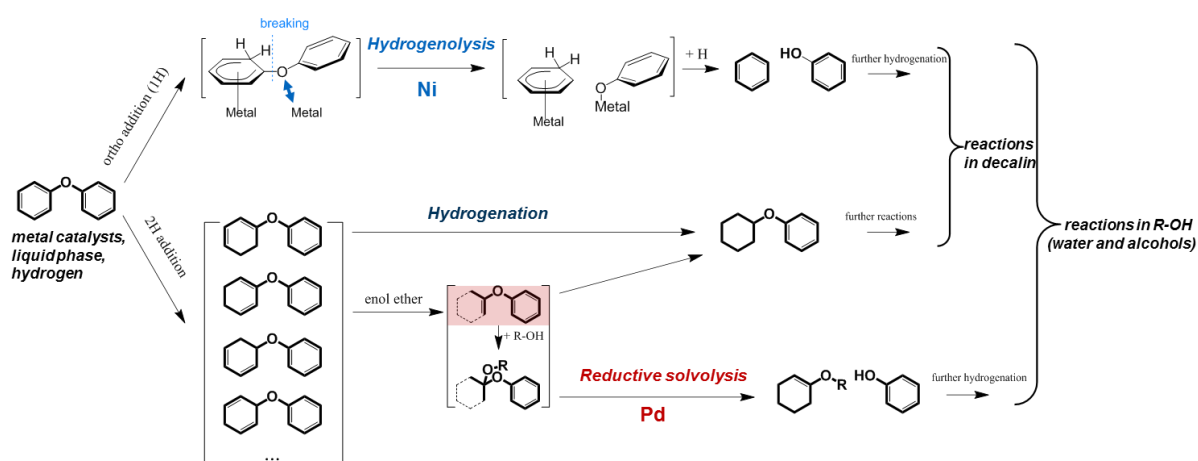


**Figure 6-1.** Summary of reaction pathways of diphenyl ether catalyzed by metal in liquid phase under H<sub>2</sub>.

Metallic Pd surfaces are highly selective in promoting the reductive hydrolysis of aromatic ethers in aqueous phase at relatively mild temperatures and pressures of H<sub>2</sub>. At quantitative conversions, the selectivity to hydrolysis products of Ph-O-R ethers was observed to range from 50 % (R = Ph) to greater than 90% (R = n-C<sub>4</sub>H<sub>9</sub>, c-C<sub>6</sub>H<sub>11</sub> and PhCH<sub>2</sub>CH<sub>2</sub>). By the analysis of the evolution of products with and without incorporation of H<sub>2</sub><sup>18</sup>O, the pathway is concluded to be initiated by Pd metal-catalyzed partial hydrogenation of the phenyl group to an enol ether that rapidly adds water to form a hemiacetal which then undergoes elimination to cyclohexanone and phenol/alkanol products. A remarkable feature of the reaction is that the stronger Ph-O bond is cleaved, rather than the weaker aliphatic O-R bond. Then alcohols (R-OH) were tested as solvent which could react with the enol ether. The aromatic C-O bond is cleaved by reductive solvolysis over Pd catalyst, which is initiated by Pd-catalyzed partial hydrogenation of one phenyl ring to form the enol ether. The enol ether reacts rapidly with R-OH to

form a ketal which generates methoxycyclohexene by eliminating phenol or an alkanol. Subsequent hydrogenation leads to methoxycyclohexane.

Ni-catalyzed hydrogenolysis was observed as the major reaction route of the conversion of diphenyl ether in polar (water) and apolar (decalin) solvents, which initially generates benzene and phenol.  $H_2$  dependence (half order) and isotopic experiments ( $K_H/K_D = 5.7$ ) showed that the first hydrogen addition is kinetically involved in the hydrogenolytic step. By the comparison between hydrogenolysis of aliphatic C-O bond (benzyl phenyl ether) and aromatic C-O bond (diphenyl ether) and theoretical calculations, the reaction mechanism was concluded to be initiated by one hydrogen addition to the aromatic ring, then the weakened C-O bond cleaves on the metal surface afterward.

Different metal catalysts (Ru/C, Pt/C, Rh/C and Pd/C) can be used to control the catalytic chemistry of the cleavage of C-O bonds in aryl ethers. The aromatic C-O bond is cleaved hydrogenolytically and/or hydrolytically, while in parallel the aromatic rings can be hydrogenated. In decalin, only hydrogenolysis was observed for C-O cleavage and the selectivity varied from 2 % to 21 % by changing the catalyst from Pd to Ru. For each metal catalyst, the selectivity of hydrogenolysis did not change dramatically in water compared to decalin. The preference to hydrogenolysis of the C-O bond over hydrogenation of the aromatic ring increases in the order Pd/C < Rh/C < Pt/C  $\approx$  Ru/C, it is due to the difference of oxophilicity of different metal catalysts. For hydrolysis in water, a reverse trend was observed. Because the reductive hydrolysis occurs via partial hydrogenation (two hydrogen addition), more reductive hydrolysis is obtained when the selectivity of hydrogenation is higher. Based on the kinetic measurements of the reactions on different metal catalysts, we concluded that the reaction mechanisms of reductive hydrolysis and hydrogenolysis remained the same over these catalysts in different solvents (water and decalin).

Understanding the above factors gives us the possibility to manage the reactivity of selective C-O cleavage of aryl ethers by designing catalysts and tuning reaction conditions for the targeted transformation of the complex ether oligomers.

## **Curriculum Vitae**

Meng Wang was born on October 2<sup>nd</sup>, 1990 in Hubei, China. Growing up in Yichang (Hubei, China), he later was matriculated into the Department of Chemistry at Nanjing University (Jiangsu, China) in September 2008, where he received his bachelor's degree of Science in chemistry in July 2012. He continued his education at Nanjing University as a master student and obtained his master's degree of Science in Physical Chemistry under the supervision of Prof. Luming Peng in July 2015, with the thesis titled "Solid-State NMR Studies of Oxide Catalytic Materials". In August 2015, he was enrolled as Ph.D. student at Technische Universität München (Germany) in the group of Prof. Dr. Johannes A. Lercher and employed at the Pacific Northwest National Laboratory (Richland, WA, USA) performing the experimental work for this Ph.D. thesis. Recent research is focused on fundamental understanding of reductive cleavage of aromatic ethers over different metal catalysts.

## List of Publications

1. **Wang, Meng**; Gutiérrez, Oliver Y.; Camaioni, Donald M.; Lercher, Johannes A. Palladium-Catalyzed Reductive Insertion of Alcohols into Aryl Ether Bonds. *Angewandte Chemie International Edition* 2018, 57 (14), 3747-3751.
2. **Wang, Meng**; Shi, Hui; Camaioni, Donald M.; Lercher, Johannes A. Palladium-Catalyzed Hydrolytic Cleavage of Aromatic C–O Bonds. *Angewandte Chemie International Edition* 2017, 56 (8), 2110-2114.
3. **Wang, Meng**; Mei, Donghai, Gutiérrez, Oliver Y.; Camaioni, Donald M.; Lercher, Johannes A. Mechanistic Studies of Hydrogenolysis of Aryl Ethers Catalyzed by Heterogeneous Nickel Catalyst. Prepared for submission.
4. **Wang, Meng**; Gutiérrez, Oliver Y.; Camaioni, Donald M.; Lercher, Johannes A. Reductive catalytic cleavage of diphenyl ether over noble metal catalysts. Prepared for submission.
5. **Wang, Meng**; Jaegers, Nicholas; Wan, Chuan; Hu, Jianzhi; Shi, Hui; Camaioni, Donald M.; Gutierrez, Oliver Y.; Lercher, Johannes A. Genesis and Stability of Hydronium Ion in Zeolite Channels. Prepared for submission.
6. Vjunov, Aleksei\*; **Wang, Meng**\*; Govind, Niranjana; Huthwelker, Thomas; Shi, Hui; Mei, Donghai; Fulton, John L.; Lercher, Johannes A., Tracking the Chemical Transformations at the Brønsted Acid Site upon Water-Induced Deprotonation in a Zeolite Pore. *Chemistry of Materials* 2017, 29 (21), 9030-9042. (\* contributed equally)
7. Hu, Jian Zhi; Wan, Chuan; Vjunov, Aleksei; **Wang, Meng**; Zhao, Zhenchao; Hu, Mary Y.; Camaioni, Donald M.; Lercher, Johannes A.,  $^{27}\text{Al}$  MAS NMR Studies of HBEA Zeolite at Low to High Magnetic Fields. *The Journal of Physical Chemistry C* 2017, 121 (23), 12849-12854.
8. Nie, L.; Mei, D. H.; Xiong, H. F.; Peng, B.; Ken, Z. B.; Hernandez, X. I. P.; DeLariva, A.; **Wang, M.**; Engelhard, M. H.; Kovarik, L.; Datye, A. K.; Wang, Y., Activation of surface lattice oxygen in single-atom Pt/CeO(2) for low-temperature CO oxidation. *Science* 2017, 358 (6369), 1419-+.
9. **Wang, Meng**; Wu, Xin-Ping; Zheng, Sujuan; Zhao, Li; Li, Lei; Shen, Li; Gao, Yuxian; Xue, Nianhua; Guo, Xuefeng; Huang, Weixin; Gan, Zhehong; Blanc, Frédéric; Yu, Zhiwu; Ke, Xiaokang; Ding, Weiping; Gong, Xue-Qing; Grey, Clare P.; Peng, Luming, Identification of different oxygen species in oxide nanostructures with  $^{17}\text{O}$  solid-state NMR spectroscopy. *Science Advances* 2015, 1 (1), e1400133.

10. **Wang, Meng**; Yu, Guiyun; Ji, Wenxu; Li, Lei; Ding, Weiping; Peng, Luming, Identification of intrinsic hydrogen impurities in ZnO with H-1 solid-state nuclear magnetic resonance spectroscopy. *Chemical Physics Letters* 2015, 627, 7-12.
11. **Wang, Meng\***; Xia, Yifen\*; Zhao, Li; Song, Chenhai; Peng, Luming; Guo, Xuefeng; Xue, Nianhua; Ding, Weiping, Remarkable acceleration of the fructose dehydration over the adjacent Bronsted acid sites contained in an MFI-type zeolite channel. *Journal of Catalysis* 2014, 319, 150-154. (\* contributed equally)
12. Zhou, Yu\*; Jin, Yanhua\*; **Wang, Meng\***; Zhang, Wei\*; Xie, Jingyan; Gu, Jing; Wen, Haimeng; Wang, Jun; Peng, Luming, One-Pot Synthesis of Zeolitic Strong Solid Bases: A Family of Alkaline-Earth Metal-Containing Silicalite-1. *Chemistry-a European Journal* 2015, 21 (43), 15412-15420. (\* contributed equally)
13. Zhang, Xiaoning; Deng, Chao; **Wang, Meng**; Liu, Xin; Lin, Chen; Peng, Luming; Wang, Leyong, Topochemical polymerisation of assembled diacetylene macrocycle bearing dibenzylphosphine oxide in solid state. *Supramolecular Chemistry* 2017, 29 (2), 94-101.
14. Song, Chenhai; Chu, Yueying; **Wang, Meng**; Shi, Hui; Zhao, Li; Guo, Xuefeng; Yang, Weimin; Shen, Jianyi; Xue, Nianhua; Peng, Luming; Ding, Weiping, Cooperativity of adjacent Brønsted acid sites in MFI zeolite channel leads to enhanced polarization and cracking of alkanes. *Journal of Catalysis* 2017, 349, 163-174.
15. Li, Y. H.; Wu, X. P.; Jiang, N. X.; Lin, M.; Shen, L.; Sun, H. C.; Wang, Y. Z.; **Wang, Meng**; Ke, X. K.; Yu, Z. W.; Gao, F.; Dong, L.; Guo, X. F.; Hou, W. H.; Ding, W. P.; Gong, X. Q.; Grey, C. P.; Peng, L. M., Distinguishing faceted oxide nanocrystals with O-17 solid-state NMR spectroscopy. *Nature Communications* 2017, 8, 6.
16. Yu, Guiyun; Zhou, Yahui; Yang, Rong; **Wang, Meng**; Shen, Li; Li, Yuhong; Xue, Nianhua; Guo, Xuefeng; Ding, Weiping; Peng, Luming, Dehydration and Dehydroxylation of Layered Double Hydroxides: New Insights from Solid-State NMR and FT-IR Studies of Deuterated Samples. *Journal of Physical Chemistry C* 2015, 119 (22), 12325-12334.
17. Ding, Jian; **Wang, Meng**; Peng, Luming; Xue, Nianhua; Wang, Yimeng; He, Ming-Yuan, Combined desilication and phosphorus modification for high-silica ZSM-5 zeolite with related study of hydrocarbon cracking performance. *Applied Catalysis a-General* 2015, 503, 147-155.
18. Zhao, Li; Qi, Zhe; Blanc, Frederic; Yu, Guiyun; **Wang, Meng**; Xue, Nianhua; Ke, Xiaokang; Guo, Xuefeng; Ding, Weiping; Grey, Clare P.; Peng, Luming, Investigating Local Structure in Layered



Double Hydroxides with O-17 NMR Spectroscopy. *Advanced Functional Materials* 2014, 24 (12), 1696-1702.

19. Yu, Guiyun; Shen, Ming; **Wang, Meng**; Shen, Li; Dong, Wenhao; Tang, Sheng; Zhao, Li; Qi, Zhe; Xue, Nianhua; Guo, Xuefeng; Ding, Weiping; Hu, Bingwen; Peng, Luming, Probing Local Structure of Layered Double Hydroxides with H-1 Solid-State NMR Spectroscopy on Deuterated Samples. *Journal of Physical Chemistry Letters* 2014, 5 (2), 363-369.

20. Li, Jing; Zhou, Yu; Mao, Dan; Chen, Guojian; Wang, Xiaochen; Yang, Xiaoning; **Wang, Meng**; Peng, Luming; Wang, Jun, Heteropolyanion-based ionic liquid-functionalized mesoporous copolymer catalyst for Friedel-Crafts benzylation of arenes with benzyl alcohol. *Chemical Engineering Journal* 2014, 254, 54-62.

21. Fu, Teng; **Wang, Meng**; Cai, Weimeng; Cui, Yuming; Gao, Fei; Peng, Luming; Chen, Wei; Ding, Weiping, Acid-Resistant Catalysis without Use of Noble Metals: Carbon Nitride with Underlying Nickel. *ACS Catalysis* 2014, 4 (8), 2536-2543.

22. Song, Chenhai; **Wang, Meng**; Zhao, Li; Xue, Nianhua; Peng, Luming; Guo, Xuefeng; Ding, Weiping; Yang, Weimin; Xie, Zaiku, Synergism between the Lewis and Bronsted acid sites on HZSM-5 zeolites in the conversion of methylcyclohexane. *Chinese Journal of Catalysis* 2013, 34 (11), 2153-2159.

## **List of Presentations**

- 1) **Palladium catalyzed aromatic C-O bond cleavage of aryl ethers**, abstract & oral presentation, 25th North American Meeting of the Catalysis Society, June 2017, Denver, CO, US
- 2) **Monitoring the formation and mobility of hydronium ions in zeolite channels by NMR**, abstract & poster, Gordon Research Seminar-Catalysis, June 2018, New London, NH, US
- 3) **Palladium-catalyzed reductive solvolysis of aryl ethers**, abstract & oral presentation, 256th ACS National Meeting, August 2018, Boston, MA, US

## **Contribution of collaborators**

Meng Wang and Donald M. Camaioni developed the concept and designed experiments for chapter 2 and 3, Meng Wang developed the concept and designed experiments for chapter 4 and 5. Meng Wang measured the experiments. Yuntao Zhao and Donghai Mei provided the DFT calculations for chapter 4. Meng Wang, Oliver Y. Gutierrez, Hui Shi, Donghai Mei, Donald M. Camaioni and Johannes A. Lercher are all involved in the discussion of the results and implications and contributed to the writing of the manuscript at all stages.